DESIGN OF NOVEL PRINTED MICROWAVE BAND-REJECT FILTERS USING SPLIT-RING RESONATOR AND COMPLEMENTARY SPLIT-RING RESONATOR

A THESIS

SUBMITTED TO THE DEPARTMENT OF ELECTRICAL AND ELECTRONICS ENGINEERING

AND THE INSTITUTE OF ENGINEERING AND SCIENCE

OF BİLKENT UNIVERSITY

IN PARTIAL FULFILLMENT OF THE REQUIREMENTS

FOR THE DEGREE OF

MASTER OF SCIENCE

By

Volkan Öznazlı

August 2008

I certify that I have read this thesis and that in my opinion it is fully adequate, in scope and in quality, as a thesis for the degree of Master of Science.

Assoc. Prof. Vakur B. Ertürk (Supervisor)

I certify that I have read this thesis and that in my opinion it is fully adequate, in scope and in quality, as a thesis for the degree of Master of Science.

Dr. Tarık Reyhan

I certify that I have read this thesis and that in my opinion it is fully adequate, in scope and in quality, as a thesis for the degree of Master of Science.

Assoc. Prof. Özlem Aydın Çivi

Approved for the Institute of Engineering and Science:

Prof. Dr. Mehmet Baray
Director of Institute of Engineering and Science

ABSTRACT

DESIGN OF NOVEL PRINTED MICROWAVE BAND-REJECT FILTERS USING SPLIT-RING RESONATOR AND COMPLEMENTARY SPLIT-RING RESONATOR

Volkan Öznazlı
M.S. in Electrical and Electronics Engineering
Supervisor: Assoc. Prof. Vakur B. Ertürk
August 2008

Filters are one of the fundamental microwave components used to prevent the transmission or emission of signals with unwanted frequency components. In general, they can be considered as an interconnection of resonator structures brought together to accomplish a desired frequency response. Up to GHz frequencies, these resonator structures are usually constructed using lumped elements such as discrete capacitors and inductors. At microwave frequencies, discrete components lose their normal charcteristics and resonators can be realized using distributed structures like quarter- or half-wavelength transmission line stubs. However, filters built using this approach are generally big, especially when high frequency selectivity is desired.

Recently, sub-wavelength structures, namely split-ring resonator (SRR) and complementary split-ring resonator (CSRR), have attracted the attention of many researchers. Interesting properties of the periodic arrangements of these structures have led to the realization of left-handed materials. Furthermore, high-Q characteristics of these structures enabled the design of highly frequency

selective devices in compact dimensions. In this thesis, these two resonator structures are investigated in detail. A deep exploration of their resonance mechanisms and transmission properties is provided along with a brief survey of related literature. However, the main focus of the thesis is the design of band-reject filters based on these resonator structures. Experimental results based on measuring the scattering paramaters of fabricated prototypes are supported with computer simulations. Band-reject filters based on SRR and CSRR are compared and discussed. It is observed that both filter types have some advantages and disadvantages which make them suitable for different applications. Finally, an electronically switchable split-ring resonator structure based on PIN diodes is presented. It is demonstrated that by employing microwave PIN diodes across the slits of an SRR, the magnetic response of a SRR particle can be eliminated. This leads to the design of filters whose rejection bands can be removed electronically.

Keywords: Split-Ring Resonator (SRR), Complementary Split-Ring Resonator (CSRR), Band-Reject Filters, Metamaterials, Single-Negative (SNG) Medium

ÖZET

YARIKLI HALKA REZONATÖRLER VE TÜMLER YARIKLI HALKA REZONATÖRLER KULLANILARAK BASKI DEVRE BANDI DURDURAN MİKRODALGA FİLTRELERİN TASARIMI

Volkan Öznazlı
Elektrik ve Elektronik Mühendisliği Bölümü Yüksek Lisans
Tez Yöneticisi: Doç. Dr. Vakur B. Ertürk
Ağustos 2008

Filtreler istenmeyen frekans içeriğine sahip işaretlerin iletim veya yayılımını engellemek amacıyla kullanılan temel mikrodalga elemanlardan biridir. Genel olarak bir filtre, istenen bir frekans cevabını gerçekleştirmek üzere bir araya getirilmiş rezonatörler topluluğu olarak düşünülebilir. GHz bölgesine kadar olan frekanslarda, bu rezonatör yapıları bobin ve kondansatör gibi toplu elemanlar kullanılarak oluşturulabilir. Ancak mikrodalga frekanslara çıkıldığında, bu elemanlar normal karakteristiklerini kaybederler. Bu yüzden rezonatörler çeyrek veya yarım dalga boyunda açık veya kapalı devre iletim hattı gibi dağıtılmış yapılar kullanılarak gerçeklenirler. Ancak, özellikle yüksek frekans seçiciliği hedefleniyorsa, bu yaklaşımla tasarlanan filtreler fiziksel olarak oldukça büyük olabilirler.

Son yıllarda yarıklı halka rezonatörü (YHR) ve tümler yarıklı halka rezonatörü (TYHR) olarak adlandırılan, dalga boyundan çok küçük yapılar birçok araştırmacının ilgisini çekmeye başladı. Bu rezonatörlerin periyodik düzenlemelerinin gösterdiği ilginç özellikler, solak materyallerin üretilmesine

giden yolu açtı. Öte yandan bu yapıların sahip olduğu yüksek kalite faktörü özellikleri, küçük boyutlara ve yüksek frekans seçiciliğine sahip mikrodalga elemanların üretimini mümkün kıldı. Bu tezde, bu rezonatör yapıları detaylı olarak incelenmiştir. Rezonans mekanizmaları ve iletim özellikleri literatürden ilgili örneklerle birlikte sunulmuştur. Ancak tezin esas odak noktası bu rezonatörler kullanılarak tasarlanan bandı durduran filtre yapılarıdır. Üretilen prototipler üzerinde yapılan ölçüm sonuçları bilgisayar benzetimleriyle desteklenmiştir. YHR ve TYHR kullanılarak üretilen fitre yapıları karşılaştırmalı olarak tartışılmıştır. Her iki filtre yapısının da onları farklı uygulamalar için uygun kılan avantaj ve dezavantajları olduğu gözlemlenmiştir. Son olarak da, PIN diyotlar kullanılarak tasarlanan, elektronik olarak anahtarlanabilen bir yarıklı halka rezonatör yapısı sunulmuştur. Rezonatörlerin yarıkları üzerine PIN diyotlar bağlanarak YHR'nün manyetik tepkisinin engellenebildiği görülmüştür. Bu sonuç, durdurma bantları elektronik olarak kontrol edilebilen filtre yapılarının tasarımını mümkün kılmıştır.

Anahtar Kelimeler: Yarıklı Halka Rezonatörü (YHR), Tümler Yarıklı Halka Rezonatörü (TYHR), Bandı Durduran Filtre, Metamalzemeler, Tek-Negatif Ortam

ACKNOWLEDGMENTS

I would like to express my gratitude and my endless thanks to my supervisor Assoc. Prof. Vakur B. Ertürk for his supervision and invaluable guidance during the development of this thesis.

I would like to thank Dr. Tarık Reyhan and Assoc. Prof. Özlem Aydın Çivi, the members of my jury, for reading and commenting on the thesis.

I would like to express my gratitude to my company, Aselsan Electronic Inc, for allowing me to pursue this degree and also to use their fabrication and measurement facilities.

I would also like to thank Turkish Scientific and Technological Research Council (TÜBİTAK) for their financial assistance during my graduate study.

Finally, I would like to thank my family, Nihan, and all my friends for their patience, sincere love, and endless support.

Contents

List of Figures

List of Tables

To Nihan and My Family...

Chapter 1

Introduction

The term *microwave* can be used to describe the electromagnetic (EM) waves having frequencies ranging from 300 MHz to 300 GHz. However, in modern electromagnetic theory, waves with wavelengths in the order of millimeters (*i.e.,* frequencies from 30 GHz to 300 GHz) are generally referred to as *millimeter waves*. In the microwave regime where circuit dimensions become comparable to signal wavelengths, voltages and currents significantly vary in phase at different points of the device. Therefore, standard lumped-element approximations of circuit theory start to fail. For the design of microwave circuits, a broader theory of electromagnetics as described by the Maxwell's equations is required. In that sense, voltages and currents are treated as waves which propagate over the device and get reflected at some discontinuities resulting in what is called standing waves [1].

A microwave system (*e.g.,* communication, radar, navigation, electronic warfare systems) is an interconnection of many fundamental microwave devices including filters, power divider/combiners, couplers, circulators, amplifiers, attenuators, mixers, oscillators, switches etc. Among them, filters play many important roles in the design of radio frequency (RF) and microwave systems.

A filter is a two-port network intended to control the frequency response of a microwave system by allowing the transmission of signals at frequencies over its passband and rejecting the signal flow over its rejection band. The electromagnetic spectrum is limited and has to be shared. Filters are used to prevent undesired harmonics and any spurious content from being transmitted between cascaded stages of a microwave system or from being radiated by an antenna. In other words, they confine RF/microwave signals within predetermined spectral limits [2].

Based on their frequency selectivity characteristics, filters are classified in four groups:

- *Lowpass Filters:* Allow transmission of signals with no or little attenuation at frequencies lower than a cut-off frequency and reject high frequency content [See Figure 1.1 (a)].
- *Highpass Filters:* Allow transmission of signals with no or little attenuation at frequencies higher than a cut-off frequency and reject low frequency content [See Figure 1.1 (b)].
- *Bandpass Filters:* Allow transmission of signals with frequencies over a band bounded by a lower and an upper cut-off frequency and reject signals out of this band [See Figure 1.1 (c)].
- *Band-Reject Filters:* Reject signals within a frequency band bounded by a lower and an upper limit and allow transmission at frequencies out of this band [See Figure 1.1 (d)].

Frequency responses of all filter types are illustrated in Figure 1.1. However, all of these frequency responses are ideal and can never be perfectly realized in practice. Practical filter responses have smoother passband-to-stopband

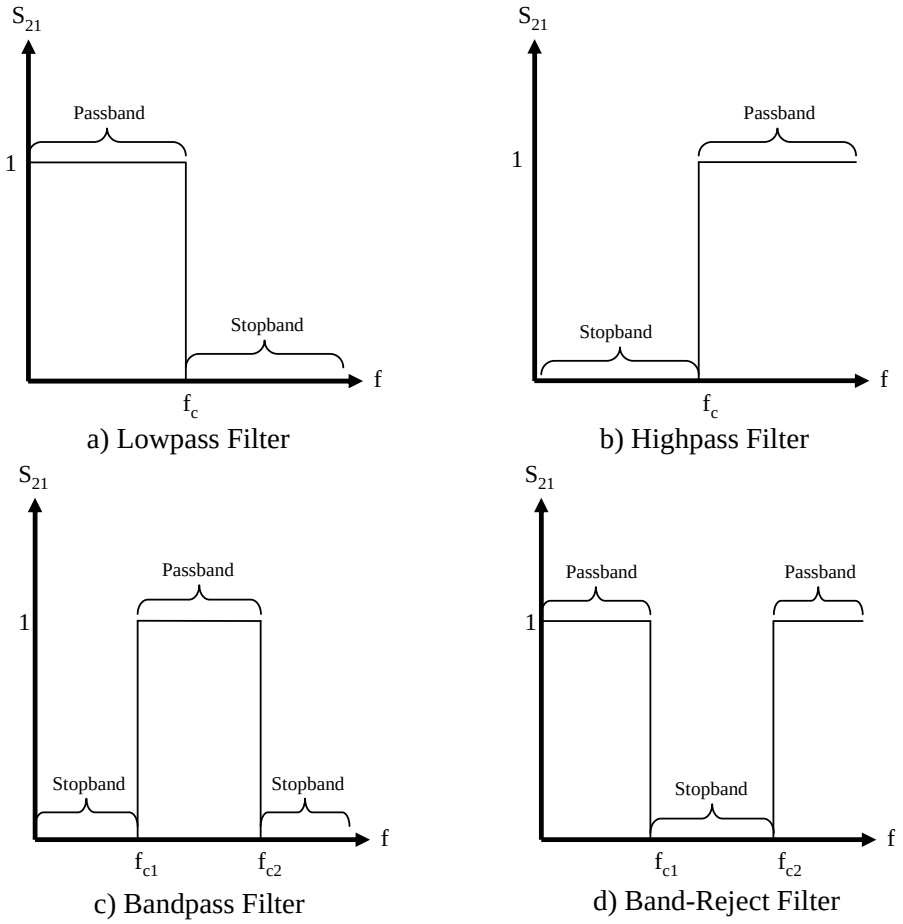

Figure 1.1: Filter types based on frequency selectivity characteristics

transitions. Passband insertion losses are desired to be as small as possible and stopband attenuations are desired to be as strong as possible.

In terms of their physical structures and operating frequencies, filters can be classified in two main groups:

- *Lumped Filters:* At frequencies up to lower MHz range, the phase change of a signal over the physical extent of a filter is negligible due to the wavelength being much longer than filter dimensions. At these frequencies, filters are usually implemented using lumped components such as discrete capacitors and inductors. There are two important methods for the design of lumped-element filters. In *image parameter method*, filters are implemented by cascading simpler two-port filter sections to obtain the

desired cutoff frequency and attenuation levels [1],[2]. Although this procedure looks simple, it may require many iterations to achieve the desired filter characteristics. The *insertion loss method* is a more modern procedure and uses more advanced network analysis techniques for filter design. Designs begin with simplified lowpass prototypes whose responses are normalized both in frequency and impedance. Transformations are then applied to obtain the desired cut-off frequency and attenuation [1],[2]. Using lumped elements, filters with relatively wide passband or stopbands can be designed. Furthermore, frequency responses obtained in lumped filters do not have spurious passbands which makes them superior to distributed filters.

- *Distributed Filters:* As the frequency of operation increases, lumped elements start to lose their normal characteristics. After a specific frequency called the parallel resonance frequency, inductors tend to behave like capacitors and vice versa. This effect is a result of package parasitics of discrete components. Therefore, at GHz frequencies distributed element technique is preferred for the design of filters. In this technique, transmission line pairs, open- and short-circuit stubs are employed as constituent filter elements. Using distributed approach, both waveguide and printed circuits can be implemented. Filters designed using both image parameter and insertion loss methods are lumped-element filters. For microwave applications, these filters are converted to distributed ones using the *Richard's transformation* and *Kuroda identities* [1],[2]. Due to the nature of transmission line sections which is periodic in frequency, the responses obtained in distributed filters are repetitive and spurious passbands are unavoidable.

As seen clearly, lumped and distributed filter designs have many advantages and disadvantages. Following a lumped-element approach, filters with good

selectivity and rejection can be designed in very compact dimensions. However, when the frequency of interest is in the microwave regime, employing a distributed element technique is inevitable. Another option is to construct printed inductor (*e.g.,* spiral inductor) and capacitors (*e.g.,* interdigital capacitor), then to implement the circuit using these discrete elements. Although it facilitates high-frequency operation, this technique causes physically increased device area.

A filter can be regarded as an interconnection of resonating elements arranged together to accomplish an overall frequency response. Conventional resonator structures used in distributed filters are generally quarter- or half-wavelength transmission line stubs. Especially in the lower GHz range, these stubs can occupy very large circuit area. Furthermore, if a filter response with sharp transition edges and very good stopband suppression is desired, one might have to employ many transmission line sections which will further increase the physical size of the filter.

The aim of this thesis is to present a relatively new technique for the design of printed microwave filters; in particular, microstrip band-reject filters. The idea is based on employing sub-wavelength resonators, namely, *split-ring resonator* (SRR) [4] and *complementary split-ring resonator* (CSRR) [5] as building blocks of filters. These two constituent particles are dual counter-parts of each other and have been extensively studied by many researchers since the beginning of the 21st century [4],[5],[7]-[14],[17]-[28],[32]-[40]. It has been found out that these electrically "tiny" (about one tenth of a wavelength) particles resonate with very high quality factors (widely denoted as Q) by exhibiting strong magnetic or electric response and provide good frequency selectivity as well as deep rejection in a few resonator stages. Many researchers have interpreted this behavior as being due to the strong current loops induced at resonance. This feature enables the design of very compact filters suitable for planar circuit technologies. Taking

the advantage of this property, many researchers have designed band-reject or band-pass filters based on stripline, microstrip, and coplanar waveguides. Moreover, it has been demonstrated that periodic arrangements of SRR and CSRR yield effective media with strange macroscopic properties like negative values of permittivity and permeability. In this thesis, band-reject filters based on SRRs and CSRRs are designed, simulated, fabricated, and tested. Frequency responses are examined in a comparative manner. Furthermore, a switching mechanism for these resonator structures is proposed.

In Chapter 2, a detailed investigation of SRR and CSRR including their resonance mechanisms, transmission properties, effective medium concept are provided along with a brief survey of the related literature. Chapter 3 presents the numerical and experimental filter characteristics of two fabricated filter prototypes, one for SRR and another for CSRR. Frequency responses of these prototypes are examined in detail and a comparative analysis of the filter performances of these structures is given. Chapter 4 offers an electronic control mechanism introduced to the SRR-based band-reject filter using microwave PIN diodes. Some modifications are made on the conventional SRR structure and finally single- and multi-stage band-reject prototypes are fabricated and tested. Effects of diode parasitics are also demonstrated both numerically and experimentally.

Chapter 2

Split-Ring Resonator and Its Complement

2.1 Introduction

In recent years, there has been a rapidly growing interest in designing artificial materials with extraordinary electromagnetic (EM) properties which are not possessed by naturally occurring materials. Macroscopically, the EM properties of a material can be described by its electric permittivity (ϵ) and magnetic permeability (μ). The *metamaterial* concept is based on reshaping ordinary conductors, which are almost non-magnetic, with some patterns and arranging these patterns in a periodic manner to give the overall structure some interesting electromagnetic properties such as negative values of effective permittivity and permeability.

Therefore, researchers have had to look for the means of obtaining negative effective values of ϵ and μ by microstructuring ordinary materials. This is why some authors call metamaterials *electrically engineered materials*.

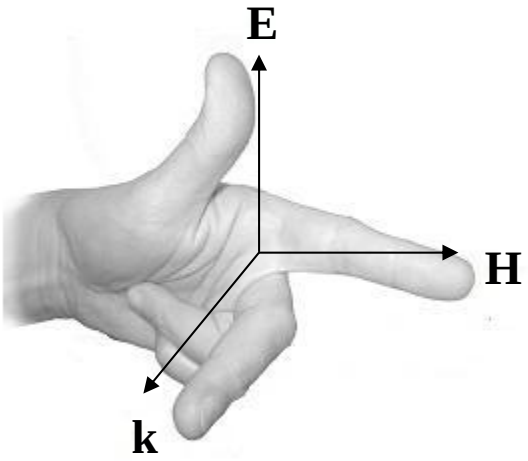

Figure 2.1: Left-Hand Rule

The idea of media with simultaneously negative permittivity and permeability was first reported in 1968 by Veselago [6]. He discovered that Maxwell's equations allow the existence of such a medium and that the wave propagation through this medium can be described by the electric field intensity vector **E**, magnetic field intensity vector **H**, and the wavenumber vector **k** forming a left-handed triplet as shown in Figure 2.1. This is why he called materials with negative effective ϵ and μ *left-handed materials* (LHMs). Veselago also predicted that such media could exhibit some unusual electromagnetic behavior like opposing phase velocity and Poynting vector, negative refractive index, and reversal of Doppler effect and Cherenkov radiation.

However, it was not until Pendry's introduction of *split-ring resonator* (SRR) that left handedness was experimentally possible [4]. After a while, Smith *et al.* experimentally demonstrated for the first time the feasibility of left-handed wave propagation in an artificial medium by combining SRRs with an array of metallic posts [7],[8].

In this chapter, two constituent structures for the design of metamaterials, the split-ring resonator (SRR) and its dual complementary split-ring resonator (CSRR) will be studied extensively. Section 2.2 and its subsections introduce the SRR, investigates its resonance mechanism and how a periodic arrangement

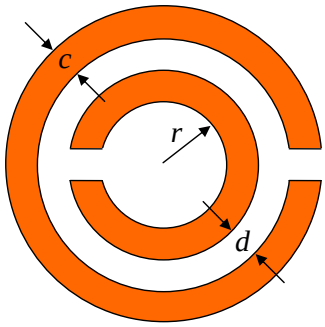

Figure 2.2: Originally proposed SRR topology

of this particle yields negative effective permeability. This section also contains a literature survey of the SRR including its applications to practical circuits. In Section 2.3, the counter-part of the SRR, namely the CSRR, will be introduced along with a brief survey of the related literature.

2.2 Split-Ring Resonator

A major step in the experimental realization of an LHM was the introduction of a novel particle called the *split-ring resonator* (SRR). In its original form as proposed by Pendry *et al.* [4], the SRR is composed of two concentric circular metallic rings each interrupted by a small gap, hence the name "split-ring". These gaps are located at the opposing sides of the inner and outer rings as illustrated in Figure 2.2.

The SRR is able to inhibit signal propagation in a narrow band in the vicinity of its resonant frequency when illuminated by a time-varying magnetic field with appreciable component parallel to its axis. Some authors have interpreted this behavior as being due to the extreme values of the effective permeability around the resonant frequency. Some others have claimed that SRRs can be modeled as parallel LC tank circuits and signal inhibition is facilitated by the induced current loops which are closed through the distributed capacitance between the concentric rings [11].

SRR-based applications are very appealing due to the sub-wavelength nature of the structure. This makes them highly preferable in a design where compactness is of primary interest. First remarkable applications of the SRR were achieved by placing arrays of them into rectangular waveguides [12],[13] facilitating the miniaturization of hollow waveguides. However, waveguide structures are generally preferred only in some high-power and very high frequency applications and today's microwave devices depend heavily on planar circuit technologies. Therefore many authors started working on possible printed circuit board (PCB) and monolithic microwave integrated circuit (MMIC)-compatible applications of the SRR.

2.2.1 The SRR as a Constituent Particle for Negative-μ Medium

As mentioned before, realization of left-handed electromagnetic behavior requires the accomplishment of a medium with a combination of negative permittivity and negative permeability over an overlapped frequency band. However, naturally occurring materials possess positive-valued permittivities and permeabilities. Moreover, although materials with a wide range permittivities can be found, most materials in nature have permeability values equal or close to that of free space, except for some ferromagnetic materials [3]. It was previously shown that a structure consisting of periodically arranged thin metallic wires could exhibit a plasma-like electric response and yield a negative effective permittivity below a plasma frequency [15],[16]. Such a structure itself constitutes a single-negative (SNG) medium that prohibits wave propagation.

Electric responses are induced by electric charges. Based on the principles of duality, it can be claimed that magnetic responses should be induced by magnetic charges. Also, if the thin metallic wires, which are made of good

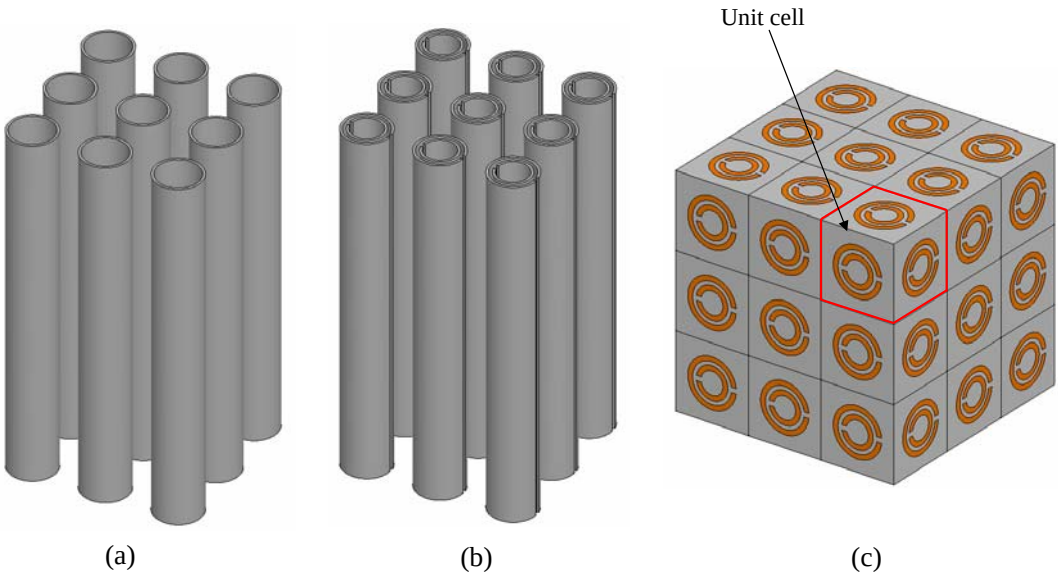

Figure 2.3: Different negative-μ structures proposed by Pendry *et al.*

electrical conductors, of the abovementioned structure [15],[16] are substituted by magnetic conductors (replacing electric charges with magnetic ones), a plasma-like structure with negative effective permeability can be obtained. However, due to the lack of magnetic charge and magnetic conductors, it is more challenging to obtain a magnetic response.

In their famous work, "*Magnetism from conductors and enhanced nonlinear phenomena*" [4], which has led to the experimental verification of left-handed wave propagation and negative refractive index, Pendry *et al.* replaced thin wires with cylindrically shaped metal sheets, again arranged in a periodic manner as illustrated in Figure 2.3 (a). The logic behind this arrangement was the equivalence between a magnetic dipole and an electric current loop. They showed that the array of cylindrical metal sheets displayed a rather limited magnetic effect and the resonant frequency seemed to be extremely high. As a next step, they incorporated some capacitative elements into their structure by using two concentric cylinders instead of one, each having slits at opposite sides in order to enhance the magnetic response. This structure is depicted in Figure 2.3 (b). The addition of these capacitances (inter-ring capacitance and slit capacitance)

strongly decreased the resonant frequency by balancing the inductance already present in the structure. Finally, an effective permeability (μ_{eff}) with a resonant form was obtained.

However, this structure was highly anisotropic because it displayed a magnetic response only if the magnetic field was directed along the axes of the cylinders and almost no magnetic response was displayed in other directions. In other words, it was acting as a one-dimensional plasma. Therefore, Pendry *et al.* replaced each cylinder with a series of flat split-ring structures. Furthermore, in order to provide the structure with some degree of isotropy, they employed split rings in all three directions forming what he called unit cells as illustrated in Figure 2.3 (c).

The split-ring resonator proposed by Pendry *et al.* consists of a pair of concentric rings with slits etched in opposite sides as illustrated in Figure 2.2. These slits prevent the current from flowing around any one ring; instead, current flows from one ring to the other due to the presence of the capacitance between the rings. The effective permeability of the medium containing a periodic arrangement of these SRRs was calculated based on the average magnetic field values induced when an incident H-field perpendicular to the rings is applied. This effective permeability is given by (2.1) [4]:

$$\mu_{eff} = 1 - \frac{\frac{\pi r^2}{a^2}}{1 + \frac{2l\sigma_1}{\omega r \mu_0} i - \frac{3l{c_0}^2}{\pi\omega^2 \ln\frac{2c}{d} r^3}} \tag{2.1}$$

In this equation, r, c, and d are the dimensions of an individual SRR as shown in Figure 2.2 and a is the distance between the centers of adjacent SRRs belonging to the same stack; l is the separation between two successive stacks, σ_1 is the per-unit-length resistance of each ring; μ_0 and c_0 are the permeability of free

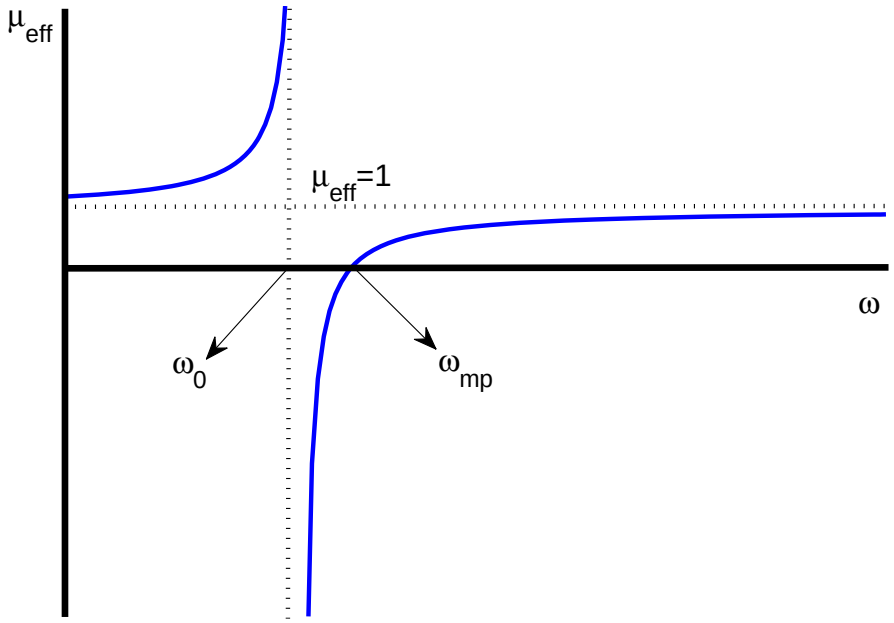

Figure 2.4: Effective permeability versus radial frequency for the SRR medium

space ($\approx 4\pi \times 10^{-7}$H/m) and the speed of light in free space ($\approx 3 \times 10^{8}$m/s), respectively.

The deficient aspects of (2.1) are that it does not take into account the effects of the type of dielectric material on which the SRRs are etched and also that the slit width, which introduces an important capacitive effect, does not appear in the effective μ expression.

When the SRRs are made of good conductors (*i.e.,* σ_1 is small), the imaginary part of effective permeability given in (2.1) can be ignored. Behavior of its real part versus radial frequency is plotted in Figure 2.4. There are two critical frequencies seen at this graph. ω_0, the frequency where the effective permeability diverges, is called the *resonant frequency* and ω_{mp}, the frequency where the effective permeability crosses the $\mu_{eff} = 0$ axis, is called the *magnetic plasma frequency* of the SRRs. These two critical frequencies can be calculated from (2.2) and (2.3) [4]:

$$\omega_0 = \sqrt{\frac{3l{c_0}^2}{\pi \ln \frac{2c}{d} r^3}} \tag{2.2}$$

$$\omega_{mp} = \sqrt{\frac{3l{c_0}^2}{\pi \ln \frac{2c}{d} r^3 \left(1 - \frac{\pi r^2}{a^2}\right)}} \tag{2.3}$$

As it is clearly seen from Figure 2.4, the effective permeability (μ_{eff}) exhibits an asymptotic behavior in its frequency response by taking extreme values around the resonant frequency. It is highly positive near the lower-frequency side of ω_0, whereas, most interestingly and strikingly, it is highly negative near the higher-frequency side of ω_0. Throughout a narrow frequency band which extends from ω_0 to ω_{mp}, the effective permeability possesses negative values. It becomes less negative as the frequency increases towards ω_{mp} and outside this negative-μ region, the effective permeability (relative to that of vacuum) becomes positive and quickly converges to unity.

It is noteworthy that the negative magnetic permeability which has been explained so far is not the permeability of the materials used. SRRs are made of ordinary, nonmagnetic conductors having a magnetic permeability of 1. Negative permeability is induced effectively by the overall response of the periodic arrangement of SRRs.

It can be verified using (2.2) that the resonances of SRRs occur at frequencies for which the wavelength is much larger than the diameter of the SRRs ($2r \approx \lambda/10$). This means that SRRs are sub-wavelength resonators with very compact dimensions compared to conventional resonator structures (*e.g.,* quarter-wavelength stubs).

2.2.2 The SRR as a Resonating Element

As mentioned in Section 2.2.1, the notion of negative permeability is valid for only the effective medium created by the periodically arranged SRRs. Nevertheless, a single SRR on its own is a sub-wavelength resonator and still possesses a strong magnetic response which must be explained by some other means.

Marqués *et al.* were the first to consider the individual SRR as an externally driven LC tank circuit [11]. They explained the response of the SRR to the excitation of a magnetic field along their axis using what they called a *local field* approach. Inner and outer split rings are coupled by means of a strong distributed capacitance in the region between the rings. When a time-harmonic magnetic field is externally applied in the direction parallel to the axes of the split rings, an electromotive force will appear around the rings if the angular frequency of the excitation is close to the resonant frequency (ω_0) of the SRR. This force will give rise to strong induced current loops. The induced current will flow between the rings in the form of a displacement current through the distributed capacitance. Therefore, the whole device behaves as an externally driven LC tank circuit.

The total capacitance of this LC circuit is the series capacitance of the upper and lower halves of the SRR with respect to the line containing the slits and the resonance frequency can be expressed as in (2.4) [11]:

$$\omega_0 = \sqrt{\frac{2}{\pi r_0 L C_{pul}}} \tag{2.4}$$

In the above equation, r_0 is the average radius of the SRR, L is the total inductance of the rings, and C_{pul} is the per-unit-length capacitance between the rings. This equation gives an important insight about the relationship between the resonant frequency and SRR dimensions:

- SRRs with shorter radii will have smaller inductance. Although C_{pul} will not be affected significantly by this change, the total capacitance between the rings will be reduced and higher resonant frequencies will result.

- Smaller separations between the inner and outer rings will increase C_{pul} and cause lower resonant frequencies.

Some important simulation-based observations regarding the relationships between SRR dimensions and resonant frequency will be presented in detail in Section 3.2.4. Although it is not seen in (2.4), the effect of slit capacitance on resonance will also be demonstrated. Furthermore, the induced loop currents around the split rings will be investigated in this section.

2.2.3 Transmission Properties of the SRR

Simultaneously negative values of ϵ and μ enhance backward wave propagation. However, if they have opposite signs, that is, either of them is negative, evanescent wave modes will be observed.

For any kind of electromagnetic wave, the wavenumber, k, is responsible for the propagation of the wave through the medium. This parameter depends on the electromagnetic properties of the medium, as well as the radial frequency of the wave. It appears in the phase-advance term ($e^{j\mathbf{k}.\mathbf{r}}$) of the time-harmonic solution and can be calculated from [1]:

$$k^2 = \omega^2 \mu_{eff} \epsilon_{eff} \tag{2.5}$$

This equation implies that for an ordinary, lossless medium, the wavenumber is a real positive number because ω, μ_{eff}, and ϵ_{eff} are all positive. However, if either effective permittivity or permeability takes on negative values, the

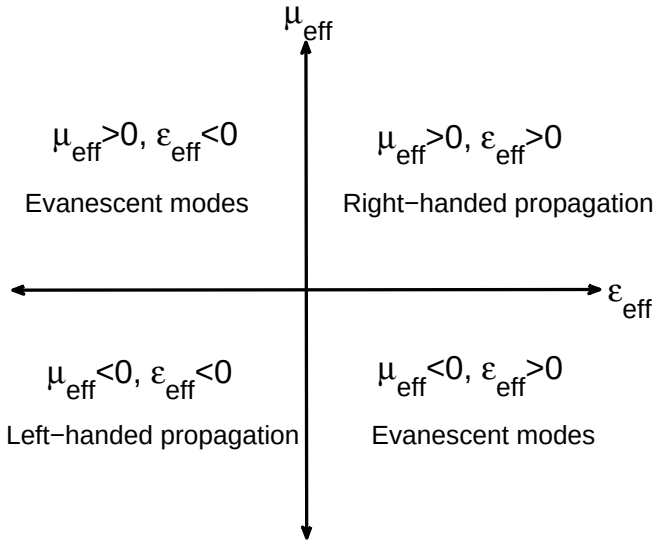

Figure 2.5: Resulting electromagnetic modes depending on signs of ϵ_{eff} and μ_{eff}

wavenumber becomes imaginary:

$$k = j\omega \left|\sqrt{\mu_{eff}\epsilon_{eff}}\right| \tag{2.6}$$

Consequently, the phase-advance term ($e^{j\mathbf{k}.\mathbf{r}}$) of the solution is transformed into an exponential decay term and evanescent wave modes result. Figure 2.5 illustrates the resulting electromagnetic modes depending on signs of effective permittivity and permeability.

An array of periodically arranged split-ring resonators is described as a *single-negative medium* (SNG) for the frequencies between resonant frequency and magnetic plasma frequency because within this band only the effective permeability takes on negative values whereas the permittivity of the medium remains positive. Although it was previously shown by some authors that the SRR can also exhibit an electric response resulting in negative effective permittivity [17]-[19], this effect is rather limited and can be observed at frequencies much higher than the magnetic resonance frequency. Therefore, it is not possible to observe negative effective μ and ϵ simultaneously over the same frequency band using only an arrangement of SRRs.

Consequently, the SRR medium is expected to exhibit a transmission gap in its frequency response between its resonance and magnetic plasma frequencies. By just commenting on the behavior of effective permeability depicted in Figure 2.4, it can be expected that the transmission gap due to the resonance of the SRRs will have very sharp transition edges. This band-reject effect has been shown experimentally in [7]-[10].

2.2.4 SRR-Based Applications Encountered in Literature

SRR-Loaded Hollow Waveguides

Hollow waveguides loaded with split-ring resonators are the first remarkable applications of the SRR to microwave devices. It is well known that hollow waveguides can support TE and TM modes satisfying the general dispersion relation provided in (2.5) where μ_{eff} is identical to the permeability of free space and the effective permittivity is given by:

$$\epsilon_{eff} = \epsilon_0 \left(1 - \frac{\omega_0^2}{\omega^2}\right) \tag{2.7}$$

In (2.7), ω_0 denotes the cut-off frequency of the mode of interest. This equation implies that if the frequency of the excitation is less than the cut-off frequency of the considered mode, the effective permittivity inside the waveguide becomes negative and evanescent modes result.

Considering that the relation given in (2.7) is identical to that of a lossless plasma with plasma frequency ω_0, a hollow metallic waveguide can be regarded as a one-dimensional plasma [12],[14]. Marqués *et al.* experimentally demonstrated for the first time that when an array of SRRs is placed inside such a hollow waveguide provided that the SRRs' resonant frequency is less than the cut-off

frequency (ω_0) of the excited mode, a left-handed passband is observed in the vicinity of the resonant frequency of the SRRs [12].

By means of the enhancement of evanescent waveguide modes observed at frequencies below cut-off, the above result opened the door to the design of hollow waveguides which are both miniaturized in cross-sectional area and usable at relatively low frequencies [13].

Filters Based on Coplanar Waveguides Loaded with SRRs

Waveguide structures are generally preferred only in some high-power and very high frequency applications (*e.g.,* antenna feed of a radar transmitter). Modern microwave systems depend heavily on planar circuit technologies such as stripline, suspended stripline, coplanar waveguide, and microstrip transmission line. This is because the designs of many fundamental microwave devices like filters, couplers, power divider/combiners are based on planar circuit technologies.

Therefore, for the success of SRR-based microwave devices, many researchers have recently investigated the printed circuit board (PCB) and monolithic microwave integrated circuit (MMIC)-compatible applications of the SRR. The impact of the SRR medium on microstrip transmission lines and coplanar waveguides has been examined.

First application of the SRR compatible with PCB or MMIC fabrication technologies was introduced by Martín *et al.* [20]. The microwave device proposed in this work is a band-reject filter based on a coplanar waveguide (without a ground plane on the back substrate side) loaded with SRRs as depicted in Figure 2.6 (a). In this design, the SRRs are aligned with the CPW slots but they are placed on the back side of the substrate. Therefore, no extra circuit space needs to be allocated. It has been shown that suppression levels reaching a few tens of dBs can be obtained with a few stages of SRRs within a narrow

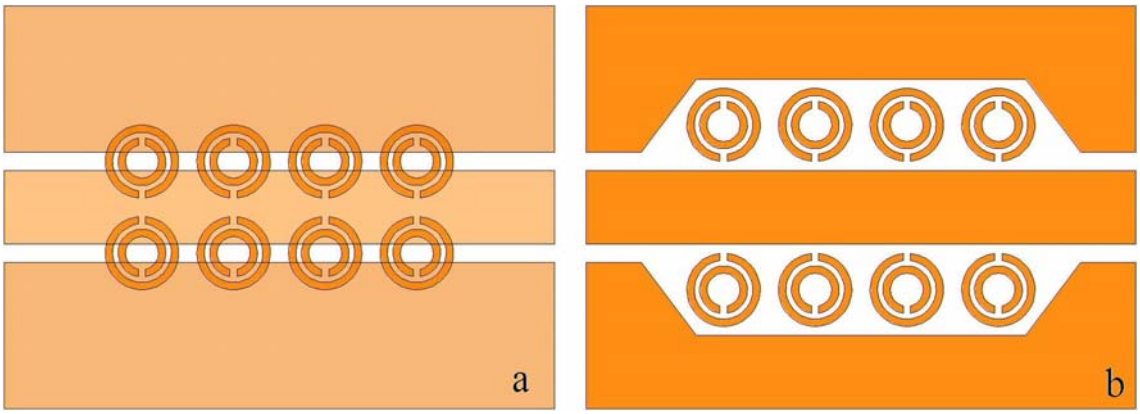

Figure 2.6: Coplanar waveguide topologies loaded with circular SRRs

band near the resonance frequency. The width of the rejection band can be manipulated by employing SRRs with slightly changing radii.

It was also shown that significant levels of rejection can be obtained in a uniplanar design where SRRs share the same plane as the central conductor and are placed in the slots between the central conductor and the ground plane [21] as illustrated in Figure 2.6 (b). Although this topology requires only a single metal level simplifying the fabrication process, CPW slots need to be widened to accommodate the SRRs. This modification increases the characteristic impedance of the line to extreme values resulting in degraded return loss performance and significant ripple in the passband insertion loss. Therefore, extra matching networks should be cascaded at the input and output ports which will increase the device size.

Later, in a paper published by Falcone *et al.* [22], it was shown that the CPW of Figure 2.6 (a) can be modified to a band-pass filter with left-handed wave propagation over the passband by loading the CPW with narrow metallic wires as shown in Figure 2.7. The metallic wires are placed periodically between the central conductor and ground plane. CPW loaded with metallic wires can be considered as an artificial plasma with negative permittivity up to the plasma frequency. If the periodicity of the wires is adjusted such that the plasma frequency is well above the resonant frequency of the rings, a narrow left-handed

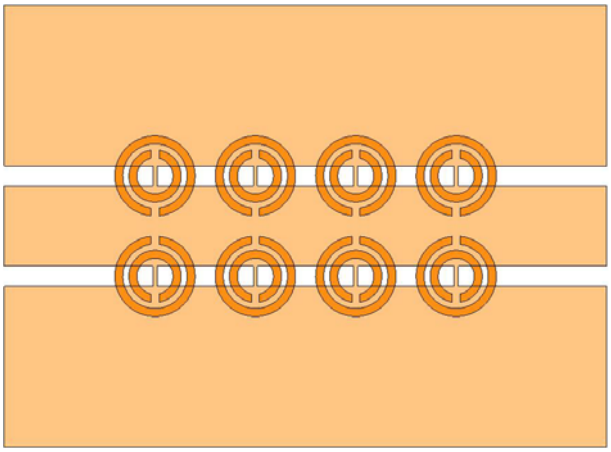

Figure 2.7: Split ring resonator-based left-handed coplanar waveguide

passband is expected over which the negative-μ and -ϵ regions overlap. This structure can be used as a backward-wave band-pass filter with good frequency selectivity.

Microstrip Lines Loaded with SRRs and Their Comparison to EBGs

Electromagnetic band-gaps (EBG) are periodic structures that are able to inhibit signal propagation over certain frequency bands [29]. They have been used for harmonic suppression of broadband amplifiers, suppression of spurious passbands in planar filters, and suppression of surface waves in planar antennas. Their rejection frequency is determined by their periods. Periodicity of the structure is implemented either by periodically defecting the ground plane or by periodically modulating the line width. It can sometimes cause the modulation of the wave impedance, which may cause problems. EBGs can be integrated with the device, avoiding the need for any extra space. However, the rejection level increases with the number of EBG periods and several stages can be needed for significant rejection and good frequency selectivity. Due to the Bragg condition (scaling of period with wavelength), dimensions of the structure can be very large at low or moderate frequencies. They also introduce passband ripple and significant insertion loss which can degrade circuit performance [30].

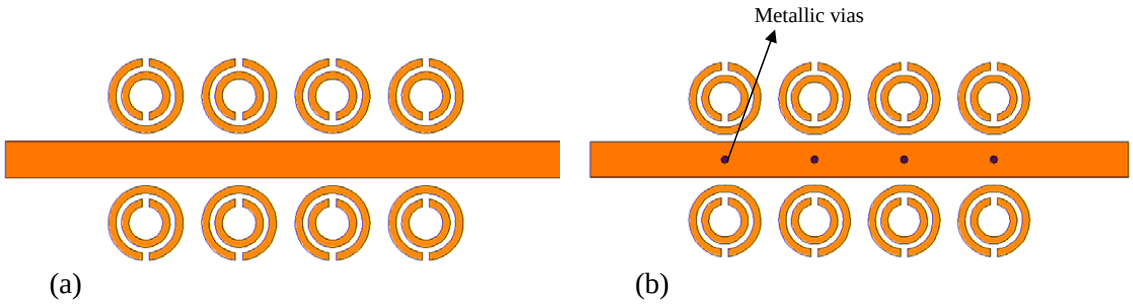

Figure 2.8: Microstrip topologies loaded with circular SRRs

Considering all these mentioned above, authors of [23] and [24] offered SRR-loaded microstrip lines as an alternative to EBGs. In this design, SRR particles are placed adjacent to the central conductor of a microstrip line as depicted in Figure 2.8 (a). Since SRRs are sub-wavelength devices, very compact designs can be achieved. Furthermore, it has been observed that significant rejection levels, although not as strong as those obtained with CPWs, can be obtained by employing a few SRR stages. The rejection frequency can be easily tuned by optimizing the dimensions of the rings. Moreover, SRRs do not alter the characteristics of the line out of their stop band; hence, they do not introduce any insertion loss or ripple over the passband. It has also been demonstrated that by first designing an SRR pair having a resonant frequency set at the center of the desired stop-band and by putting other SRR pairs with slightly increased or decreased dimensions, the rejection band can be narrowed or widened. A detailed investigation of SRR-loaded microstrip lines is presented in Section 3.2.

Microstrip lines loaded with SRRs were also used for suppression of undesired spurious bands of microwave coupled-line filters [24],[25]. It was observed that by properly tuning the dimensions of the SRRs such that they resonate at the center frequencies of the spurious passbands, undesired emissions can be prevented. SRRs can be placed either at both ends of the 50-Ω access lines or in the active filter region to avoid the need for extra space.

Microstrip lines capable of left-handed wave transmission were first designed by Gil *et al.* [27],[28]. In their design, a periodic arrangement of metallic vias extending from the central conductor to the ground plane is introduced to the SRR-loaded microstrip line as illustrated in Figure 2.8 (b). These metallic vias behave as a microwave plasma with negative effective ϵ up to a plasma frequency. If the resonant frequency of the SRRs is kept below this plasma frequency, left-handed wave propagation is observed over a narrow band in the vicinity of the resonant frequency of the SRRs. This structure can be used as a narrow-band bandpass filter with negative phase and positive group velocities.

2.3 Complementary Split-Ring Resonator

The idea of etching the ground plane was first introduced with the advent of Bragg-effect-related EBG concept. It was discovered that EBG devices obtained by etching holes or periodic patterns in the ground plane exhibited wide and deep stop-bands [31]. This technique can be used to design circuits with improved performance such as, harmonic tuning in amplifiers, oscillators, mixers and also reducing spurious content in microwave filters. EBGs designed by etching patterns on the ground plane require no extra circuit area. This feature enables the design of very compact devices.

After the introduction of the split-ring resonator and its applications to planar band-gap structures, some authors thought that the response of the SRR-loaded planar transmission lines (either microstrip line or coplanar waveguide) was rather limited due to the poor coupling between the SRRs and the central conductor. Therefore, they proposed a new structure with enhanced coupling that could be a counter part of the conventional SRR [5],[32]. This new structure was called the *complementary split-ring resonator* (CSRR).

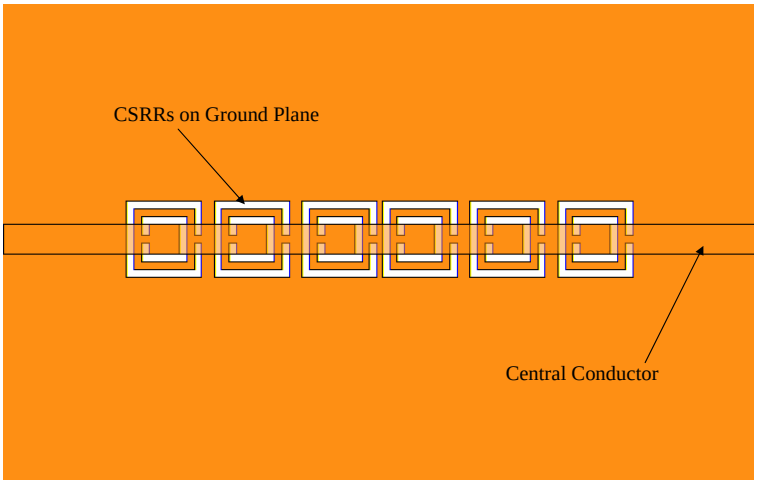

Figure 2.9: CSRRs etched on the ground plane of a microstrip line

CSRRs are SRR-shaped apertures which are etched on the ground plane of a planar transmission line as illustrated in Figure 2.9. The basic concepts behind the design of CSRR are duality, complementarity and also the Babinet's principle. It is well known from electromagnetic theory that the complement of a planar metallic structure can be obtained by replacing the metal parts of the original structure with apertures, and the apertures with metal plates (Babinet's Principle). If the metal plate is infinitesimally thin and perfectly conducting, then the apertures behave as perfect magnetic conductors. Therefore, the original structure and its complement are effectively dual. As a consequence of this duality, if the field $F = (E, H)$ is a solution for the original structure, then F', as expressed in (2.8), is the field solution for the complementary structure where the electric and magnetic field components are interchanged and scaled with an intrinsic impedance factor [5].

$$F' = (E', H') = \left(-\sqrt{\frac{\mu}{\epsilon}} H, \sqrt{\frac{\epsilon}{\mu}} E \right) \tag{2.8}$$

Therefore, it can be said that CSRRs are negative images and dual counterparts of conventional SRRs. Based on the above explanations, the CSRR differs from the conventional SRR in a number of aspects:

- Instead of having metallic SRR patterns, SRR-shaped apertures are employed on the ground plane.

- As (2.8) implies, instead of a magnetic field, the CSRRs must be excited with an electric field having a strong component which is parallel to rings' axes in order to have a resonance. The coupling of the electric field in a CSRR-loaded microstrip structure is explained in more detail in Section 3.3.

- When arranged in a periodic manner, the structure is expected to yield an effective medium with negative effective permittivity in vicinity of the resonant frequency, in contrast to the conventional SRR.

The enhanced electric coupling mechanism between CSRRs and the central conductor of a microstrip transmission line will be investigated in more detail in Section 3.3.

In contrast to the usual quarter- or half-wavelength transmission line resonators, CSRRs are sub-wavelength structures as in the case of SRRs. Therefore, high level of miniaturization can be accomplished by using these particles. Moreover, since CSRRs are etched on the ground plane, they do not need the allocation of any extra space facilitating even more compactness.

When designing a CSRR-based structure, the design formulas for the resonant frequency of the conventional SRR can be a good starting point. However, for some reasons which will be discussed in more detail in Section 3.4.1, the CSRR is not rigorously the dual of the SRR, hence the resonant frequencies may differ accordingly.

In literature, the first application of the CSRR to practical circuits is a microstrip band-reject filter [5] (See Figure 2.9). It has been shown that the band-reject filter based on CSRRs produces very high rejection with sharp cut-offs. Also, the CSRR particles are almost invisible over the passband of

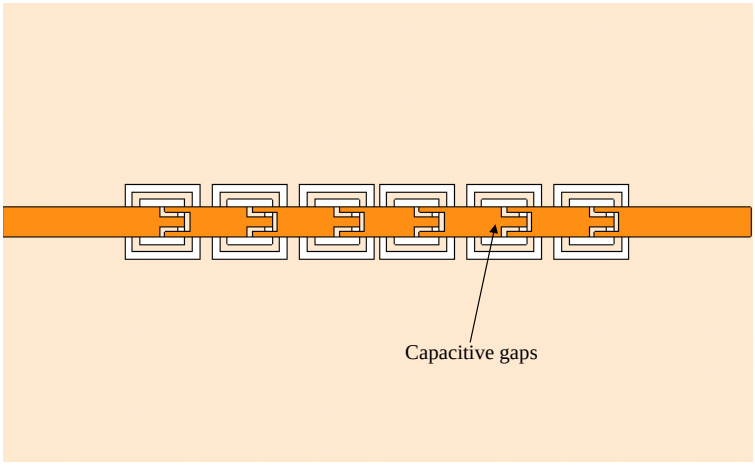

Figure 2.10: Microstrip line loaded with both CSRRs and series capacitive gaps

the frequency response with very good impedance matching as the filter exhibits a flat, low-loss, and low-ripple passband. From an effective medium point of view, this behavior has been interpreted as being due to the presence of negative-valued permittivity. It has been demonstrated that the center frequency and the width of the rejection band can be tuned by tailoring CSRR dimensions.

Since periodic CSRR medium is believed to provide negative effective ϵ, for the realization of LHM using the CSRR, some negative μ effect must also be introduced. By applying the duality principle to the microstrip LHM design given in Figure 2.8 (b), authors of [33] loaded the the central conductor of the CSRR-loaded microstrip line with series capacitive gaps instead of shunt wires as illustrated in Figure 2.10. The microstrip line whose central conductor is interrupted by small capacitive gaps is believed to be a negative effective permeability medium from DC up to a plasma frequency at which the series impedance is no longer capacitive. In a narrow band over which effective values of ϵ and μ are simultaneously negative, transmission with left-handed characteristics is observed. This was the first time left-handed propagation through a CSRR-based structure had ever been observed. Later, in [34] and [35], the possibility of the design of bandpass filters with good frequency selectivity and controllable bandwidth using this methodology was also demonstrated.

Chapter 3

A Comparative Investigation of SRR- and CSRR-Based Band-Reject Filters

3.1 Introduction

In this chapter, a comparative investigation of split-ring resonator (SRR)- and complementary split-ring resonator (CSRR)-based band-reject filters is performed by examining their stopband characteristics in a detailed manner. Two very simple band-reject filter topologies, one for SRR and the other for CSRR, with exactly the same SRR and CSRR dimensions are chosen so that simulation- and fabrication-based errors can be minimized and a fair comparison of their stopband characteristics can be performed. It has been observed that with both topologies significant attenuation levels can be obtained using a few SRR or CSRR stages in the vicinity of a microstrip line. Therefore, both topologies offer very compact band-reject filters with high-Q responses as mentioned in previous studies [5],[20],[21],[23]-[25],[32]. However, some important

stopband characteristics of SRR-based band-reject filters significantly differ from their CSRR-based counterparts. Bandwidth, sharpness of the transition from passband region to stopband region (and vice versa) and effects of number of SRR and CSRR stages on the amount of attenuation in the stopband region are among these characteristics.

In Section 3.2 and Section 3.3, SRR- and CSRR-based band-reject filter designs are given together with simulations supported by measurement results, respectively. Section 3.4 provides a detailed comparison of the stopband characteristics of the designed SRR- and CSRR-based band-reject filters in terms of the frequency of operation (resonant frequency), bandwidth, sharpness of the transition from passband to stopband and vice versa. The section also discusses the amount of rejection level in the stopband and how this level varies with the number of SRR and CSRR stages. A large portion of the contents of this chapter have been published in [36].

3.2 SRR-Based Band-Reject Filter

3.2.1 Theory of Filter Operation

Before explaining the design of the SRR-based band-reject filter, it would be helpful to present a brief review of microstrip structures. Microstrip line is a kind of microwave transmission line which can easily be fabricated using planar circuit technologies such as mechanical, chemical etching or photolithographic processes. Its popularity is not only because of the ease of its fabrication but also its potential for integration with other passive or active microwave devices. A microstrip line is composed of a conducting strip separated from a ground plane by a dielectric substrate. The characteristic impedance of the microstrip line is desired to be kept close to 50 Ω for low-reflection transmission and it is

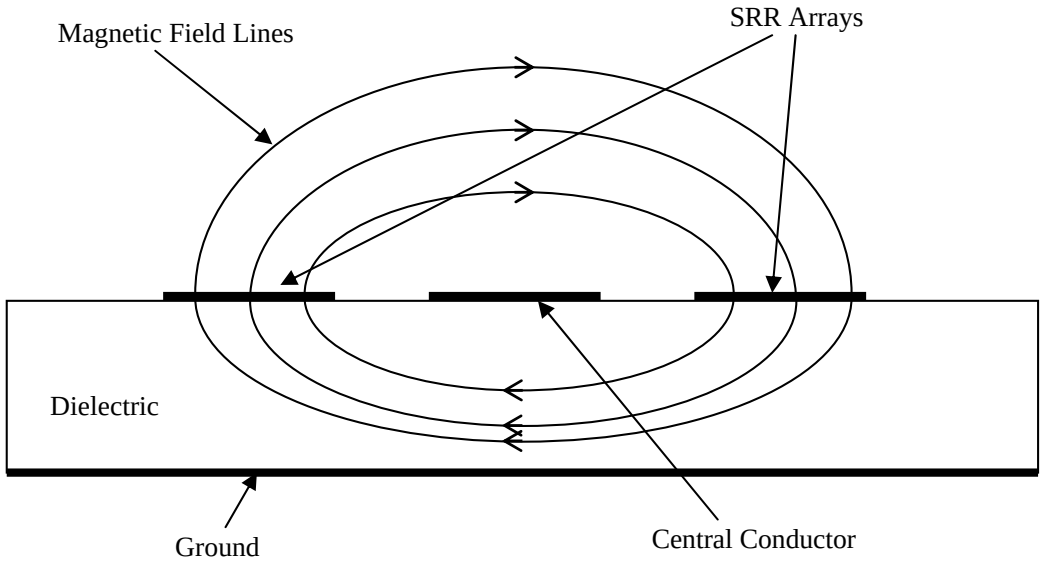

Figure 3.1: Cross-section view and magnetic field lines of a SRR-loaded microstrip line

determined by dielectric thickness, relative permittivity, and the width of the conducting strip [1].

Due to the presence of dielectric substrate and ground plane, the electromagnetic modes supported by microstrip lines are not pure transverse electromagnetic (TEM) waves. Instead, microstrip lines allow the propagation of so called quasi-TEM modes with very small electric and magnetic field components in the direction of propagation. The magnetic field lines induced by the waves propagating along a microstrip line close upon themselves around the central conductor. Because of the quasi-TEM nature of the line, incident waves propagate in a non-uniform medium. Some part of the fields propagate in the air whereas the rest is confined into the dielectric substrate. As a result, the magnetic field lines are not perfect circles and get denser between the central strip and ground plane. Likewise, the electric field lines tend to concentrate in the region just below the central conductor.

Having a strongly anisotropic electromagnetic nature, the SRR is able to inhibit signal propagation in a narrow band in the vicinity of its resonant frequency, provided that it is illuminated by a time-varying magnetic field with an

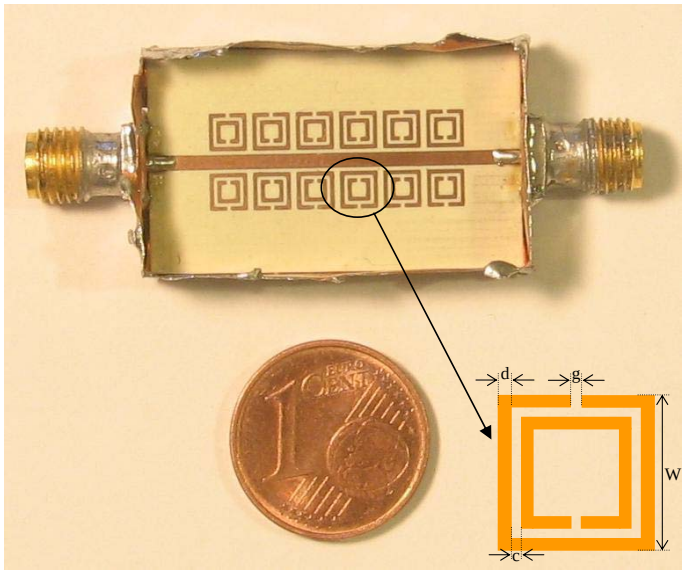

Figure 3.2: Fabricated SRR-based microstrip band-reject filter; Relevant dimensions: $W = 3$ mm, $c = d = g = 0.3$ mm.

appreciable component in its axial direction. If two arrays of SRRs exist closely at both sides of the host microstrip line as shown in Figure 2.8 (a), a significant portion of the magnetic fields induced by the line is expected to cross the SRRs with the desired polarization. This mechanism is illustrated in Figure 3.1. These arrays of SRRs, under the illumination of the time-varying magnetic field with the desired polarization, constitute an effective SNG medium with negative μ_{eff} within a frequency band in the vicinity of the resonant frequency. Thus, previously propagating waves in the absence of SRRs become evanescent waves. Consequently, the signal propagation is inhibited.

3.2.2 Fabricated Prototype

Based on this explanation, an SRR-based band-reject microstrip filter has been designed and fabricated as shown in Figure 3.2. In this initial design, 6 SRR pairs (*i.e.,* a total of 12 SRRs forming 6 stages) have been employed. The topology and the relevant dimensions of these SRRs are also given in the inset and captions of Figure 3.2, respectively. The width of the central strip is set to 1.15 mm so that

Figure 3.3: LPKF ProtoMat H100® circuit board plotting machine

its characteristic impedance is approximately 50 Ω and low out-of-band return loss levels are obtained at both port sides. The concentration of H-field lines decrease quickly away from the central conductor. Therefore, to enhance the coupling of the SRR structures to the central line, the rings must be placed as close to the central conductor as possible. Hence, square-shaped SRRs rather than originally proposed circular ones have been used.

In the fabrication process, a mechanical etching technique has been employed using LPKF ProtoMat H100® circuit board plotting machine, a photo of which is shown in Figure 3.3. The filter has been implemented on a RO4003C® high-frequency laminate, which is commercially available from Rogers Corporation. The properties possessed by this laminate, especially low dielectric loss, facilitate its use in many applications where higher operating frequencies limit the use of conventional circuit board laminates [41]:

- Relative dielectric constant, $\epsilon_r = 3.38$
- Substrate height: 20 mil (≈ 0.508 mm)
- Thickness of the copper cladding: 1 oz (≈ 35 μm)
- Loss tangent, $\tan\delta = 0.0027$

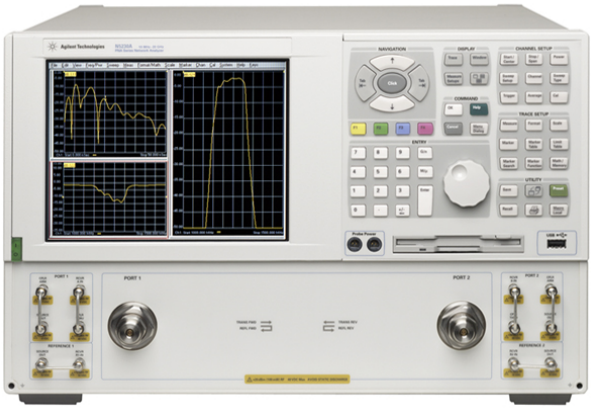

Figure 3.4: Agilent Technologies PNA series N5230A vector network analyzer

The manufacturer's datasheet of RO4003C® laminate is also given in Appendix A.

The magnetic coupling between the SRRs and the central conductor could have been further improved by minimizing the distance between the line and the rings. However, mechanical etching techniques available at hand lose their accuracies for separations less than about one-fifth of a millimeter and cause significant discrepancies between the measured and simulated results. Therefore, the distance between the rings and the line is set to 0.3 mm.

3.2.3 Measurements & Simulations

After soldering 3.5-mm SMA female connectors at both ports, scattering parameters have been measured using an Agilent Technologies PNA series N5230A vector network analyzer, which is capable of making measurements at frequencies up to 40 GHz (See Figure 3.4). Since the filter is completely planar, numerical calculations of the scattering parameters have been performed using the *Method of Moments* (MoM)-based electromagnetic solver of Ansoft Designer^{TM} commercial software [44], which is a 2-D solver and requires noticeably less computational effort than many 3-D solvers. Measured and

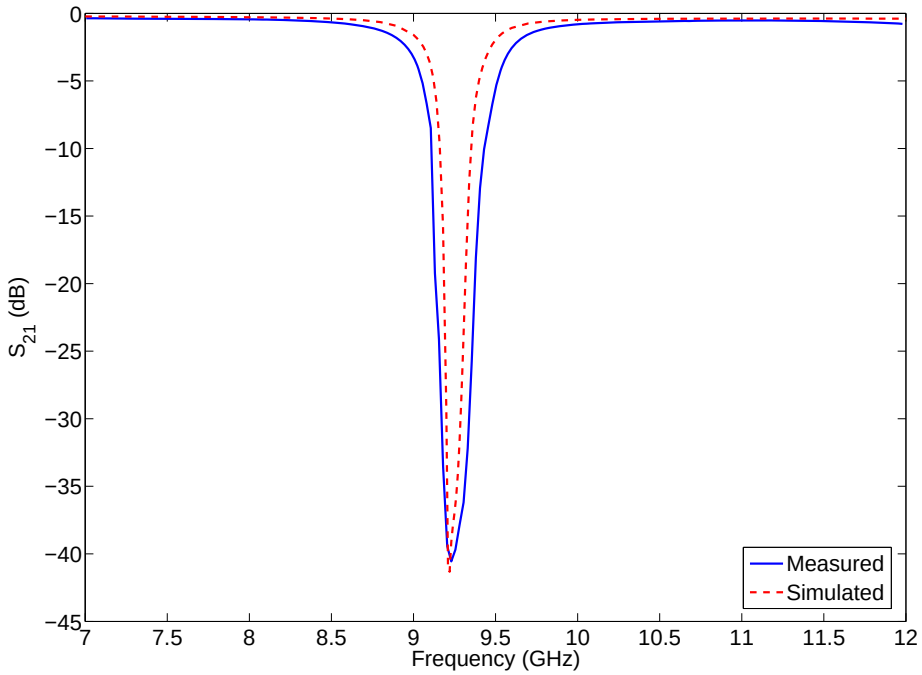

Figure 3.5: Measured (solid) and simulated (dashed) insertion loss of the SRR-based band-reject filter

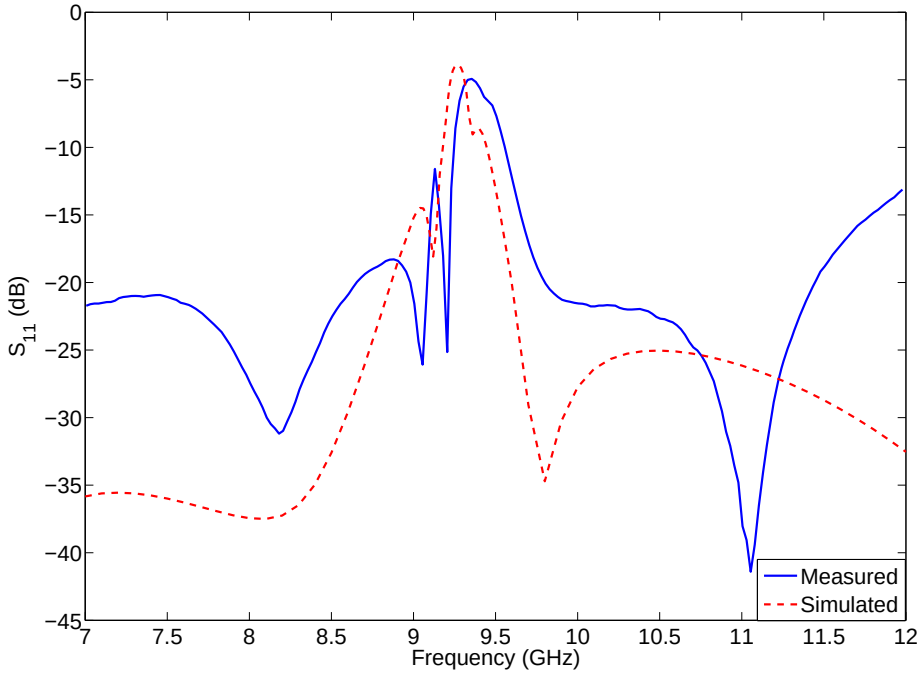

Figure 3.6: Measured (solid) and simulated (dashed) return loss of the SRR-based band-reject filter

simulated insertion and return losses are presented in Figure 3.5 and Figure 3.6, respectively.

Band-reject nature of the fabricated prototype is obvious from the behavior of the S_{21} parameter which displays a dip at about 9.25 GHz. It is evident from Figure 3.5 that quite good agreement is achieved between the numerical and experimental results. Especially, the center frequency of the stopband and also the depth of rejection band ($\approx$ 40 dB) perfectly coincide for the experimental and numerical cases. The rejection band obtained from measurements is slightly wider than that obtained from electromagnetic simulation. Minor discrepancies between the measured and simulated return loss values (Figure 3.6) can be attributed to possible impedance mismatches as a result of coaxial-to-microstrip line transitions at both connector sides and also to imperfections in the fabrication process.

3.2.4 Other Observations on SRR-Based Band-Reject Filters

Some further observations have also been made on the SRR-based band-reject filter design based on full-wave electromagnetic simulations carried on using Ansoft Designer^{TM}.

Firstly, the surface current densities of the fabricated filter have been calculated. A color-map of these distributions is given in Figure 3.7. Current density distributions for two different cases are presented. Figure 3.7 (a) shows the current density at the resonance frequency (9.25 GHz) whereas Figure 3.7 (b) shows the current density at an arbitrary off-resonance frequency (7 GHz). It must be noted that the color-map is scaled logarithmically to accommodate a wider range of current densities. It is observed that the currents induced on the rings are much stronger in magnitude for an excitation near the resonant

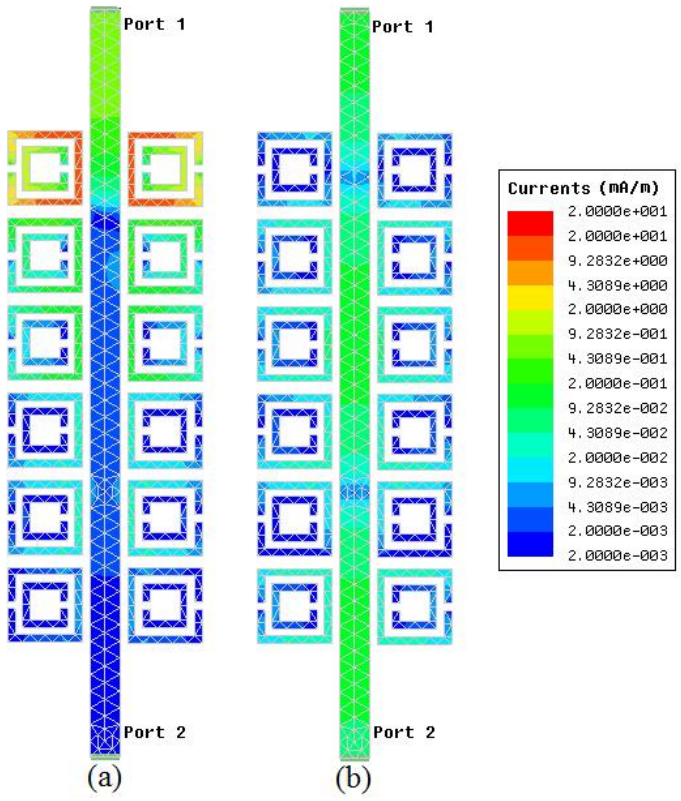

Figure 3.7: Simulated surface current distribution of the SRR-based filter for resonance (a) and off-resonance (b) cases

frequency of the rings. This definitely proves that the notch at 9.25 GHz of Figure 3.5 is really due to the resonance of the SRRs.

At resonant frequency, highest currents are induced over the rings that are closest to the input port and the current density drops as the wave progresses towards the end of the line. This can be explained in the following manner. When the wave enters the SRR medium, it will experience its first reflection at the first SRR pair and the attenuated wave will be transmitted to the subsequent SRR pair. However, having been reflected, it will have less power, hence can induce less current over the rings. Again reflection, attenuation, and transmission; the wave will propagate along the line being attenuated (reflected) more and more at each stage, but inducing less and less current over the rings.

Another important observation has been made on the tuning capabilities of the SRR-based band-reject filter. It has been numerically demonstrated that the

Table 3.1: Estimated resonant frequencies for proportionally scaled SRRs

W (mm)	d (mm)	g (mm)	c (mm)	Resonant Frequency (GHz)	
				Simple Calculation	EM Simulation
3	0.3	0.3	0.3	9.09	9.25
3.5	0.35	0.35	0.35	7.79	7.55
4	0.4	0.4	0.4	6.82	6.5
4.5	0.45	0.45	0.45	6.06	6.2
5	0.5	0.5	0.5	5.45	5.5

resonant frequency of the structure can be increased by scaling down the rings and vice versa. If the SRRs are scaled keeping the ratios of all dimensions unchanged, a good estimate of the resonant frequency can be made by taking the width (W) of the SRRs as one-eleventh of the free-space wavelength at resonance. For example, the resonant frequency of an SRR having the dimensions of $W = 5$ mm and $c = g = d = 0.5$ mm can be estimated as:

$$\frac{\lambda}{11} = \frac{c_0}{11 f_0} \approx W \Rightarrow \frac{3 \times 10^8}{11 f_0} \approx 0.005 \Rightarrow f_0 \approx 5.45 \text{ GHz}$$

The estimated resonant frequency of the above case has been found to be 5.5 GHz via electromagnetic simulation. Table 3.1 shows the estimated and numerically evaluated resonant frequencies for 5 different SRR dimensions. It must be noted that the SRR in each row of this table is a scaled version of all the others (*i.e.,* ratios of W, c, d, and g are the same in each case). The agreement in the presented data reveals that the above approach can be a good starting point when designing an SRR-based band-reject filter with a desired center frequency.

It has also been shown that the resonant frequency of the SRR can be adjusted by individually tuning the separation between the inner and outer rings (d) or the slit width (g). According to (2.4), a decrease in the separation causes the inter-ring capacitance to increase resulting in a drop in resonant frequency and vice versa. Although it is not included in (2.4), the slit width (g) also exhibits a similar effect on the resonant frequency of the SRRs. The variations of the

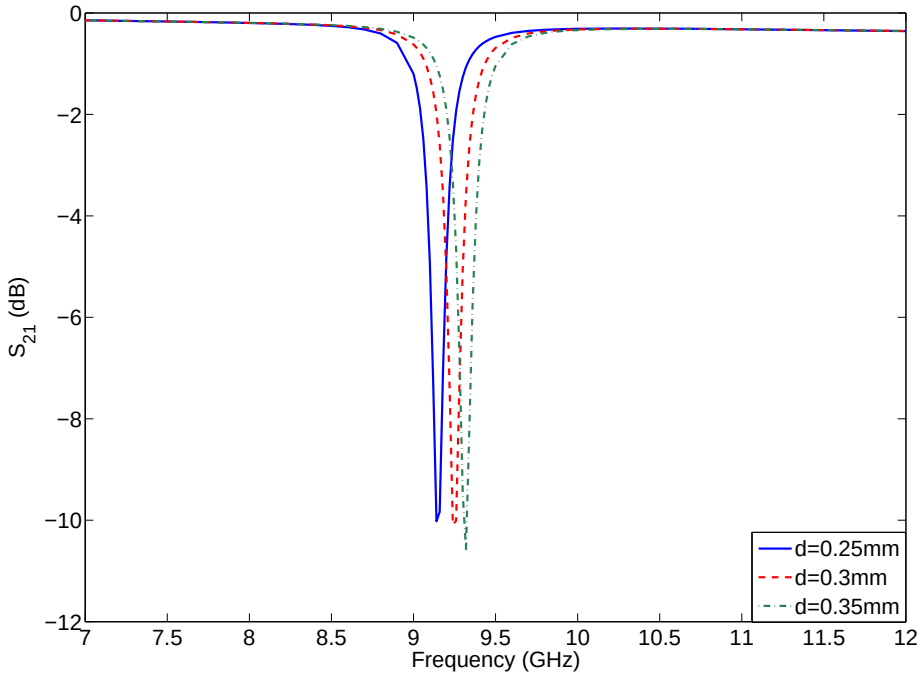

Figure 3.8: Variation of the insertion loss as a function of the separation between the rings (d)

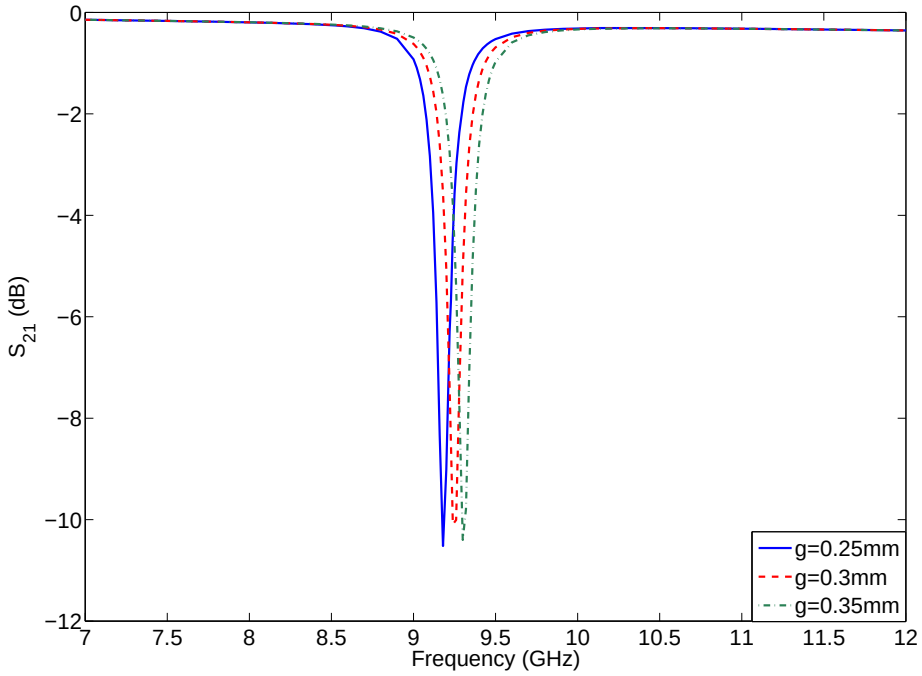

Figure 3.9: Variation of the insertion loss as a function of the slit width (g)

insertion loss for a filter containing a single SRR pair when the d and g parameters are varied are given in Figure 3.8 and Figure 3.9, respectively. It is clear that increasing d or g results in reduced capacitance and increased resonant frequency.

Capabilities of all of these tuning methods are limited only by the resolution of the etching technology utilized in the fabrication process.

3.3 CSRR-Based Band-Reject Filter

3.3.1 Theory of Filter Operation

Being the dual counterpart of the conventional SRR, the CSRR requires the excitation of a time-varying electric field having a strong component parallel to its axis so that it can resonate at some frequencies.

A microstrip transmission line induces electric field lines that originate from the central strip and terminate perpendicularly on the ground plane. Due to the presence of the dielectric substrate and ground plane, field lines are tightly concentrated just below the central conductor, and the electric flux density reaches its maximum value in the vicinity of this region. Hence, if an array of CSRRs is etched on the ground plane just aligned with the microstrip line as illustrated in Figure 3.10, a strong electric coupling with the desired polarization is expected. As a result, a microstrip line loaded with a linear array of CSRRs effectively constitutes a SNG medium with a negative ϵ_{eff} in the vicinity of the resonant frequency of the CSRRs. Therefore, in a similar fashion to the SRR-based case, previously propagating waves in the absence of CSRRs become evanescent waves. Consequently, the signal propagation is again inhibited.

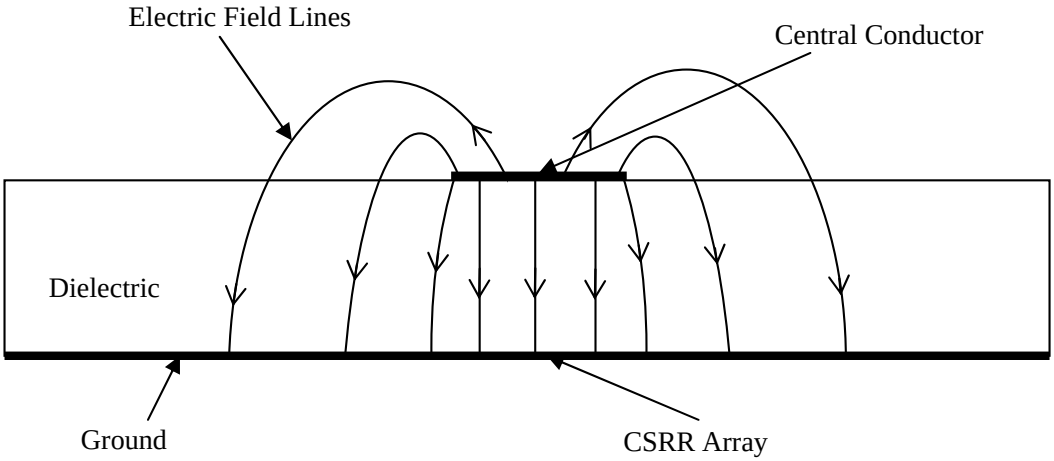

Figure 3.10: Cross-section view and electric field lines of a CSRR-loaded microstrip line

3.3.2 Fabricated Prototype

Considering the abovementioned physical picture, a CSRR-based band-reject filter has been designed and fabricated as illustrated in Figure 3.11. All dimensions of the CSRRs have been selected identical to their counterparts in SRR-based case (dimensions are given in the caption of Figure 3.11) so that the operating frequency of the current filter is around 9.25 GHz, too. Again 6 CSRR stages (note that CSRRs do not appear in pairs) have been employed. During the fabrication process, the filter has been implemented on the same high-frequency laminate. This way a comparative analysis between the two filter types can be performed.

It must be noticed that, because the distance between the microstrip line and the CSRRs is determined by the thickness of the laminate, this configuration does not allow us to adjust the distance between the CSRRs and the line easily unless a laminate with different substrate height is used. Optionally, using a dielectric substrate with a higher permittivity can more effectively confine the electric field lines into the dielectric slab rather than extending into the air and

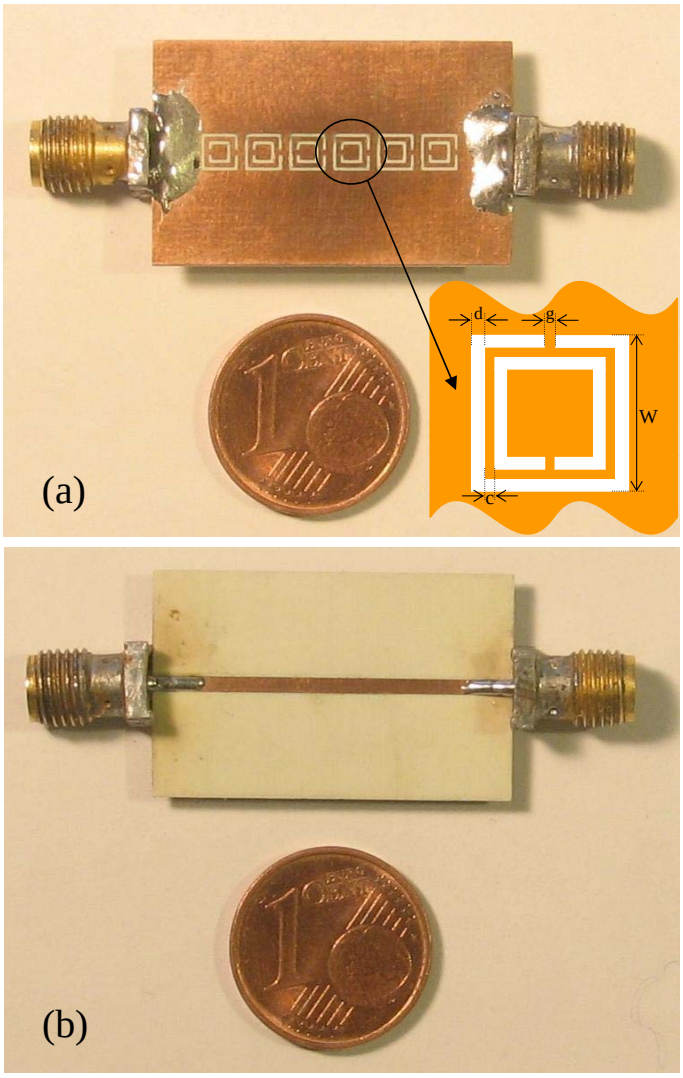

Figure 3.11: Fabricated CSRR-based microstrip band-reject filter; (a) Bottom view: Ground plane, (b) Top view: 50-Ω central conductor; Relevant dimensions: $W = 3$ mm, $c = d = g = 0.3$ mm.

stronger capacitive coupling due to the increased permittivity can be obtained resulting in an enhanced suppression level.

Shape of the CSRRs is not expected to have a drastic effect on the amount of coupling but we have preferred to make use of square CSRRs to be consistent with the topology in the SRR-based case. Therefore, the comparative analysis of the two cases carried out here is expected to depend only on whether the microstrip line is loaded with SRRs or CSRRs and should be independent of all dimensions and material properties.

3.3.3 Measurements & Simulations

The structure has been simulated using the *Finite Element Method* (FEM)-based High-Frequency Structure Simulator^{TM} (HFSS) commercial software of Ansoft Corporation [45]. Since the resonating particles (CSRRs) are etched on the ground plane in this design (*i.e.,* two metalization levels required), it has been necessary to make use of a 3-D solver. Scattering parameters of the fabricated prototype have been measured using the same Agilent Technologies PNA series N5230A vector network analyzer. Also, the analyzer has been operated using the same calibration settings for both cases in order to be consistent in the accuracy of measurements.

Plots of the insertion and return losses for both numerical and experimental cases are presented in Figure 3.12 and Figure 3.13. Very good agreement is obtained between the simulated and measured results. If a minimum rejection level of 20 dB in the stopband is assumed for this filter, the stopband extends from 7.9 GHz to 10.7 GHz yielding a center frequency of approximately 9.3 GHz, which is close to the center frequency of the SRR-based filter. Small discrepancies can be attributed to tolerances in fabrication process and impedance mismatches created by the coax-to-microstrip transitions just like the SRR-based case. Impedance mismatch problem is evident from the return loss level which is quite high even outside of the stopband.

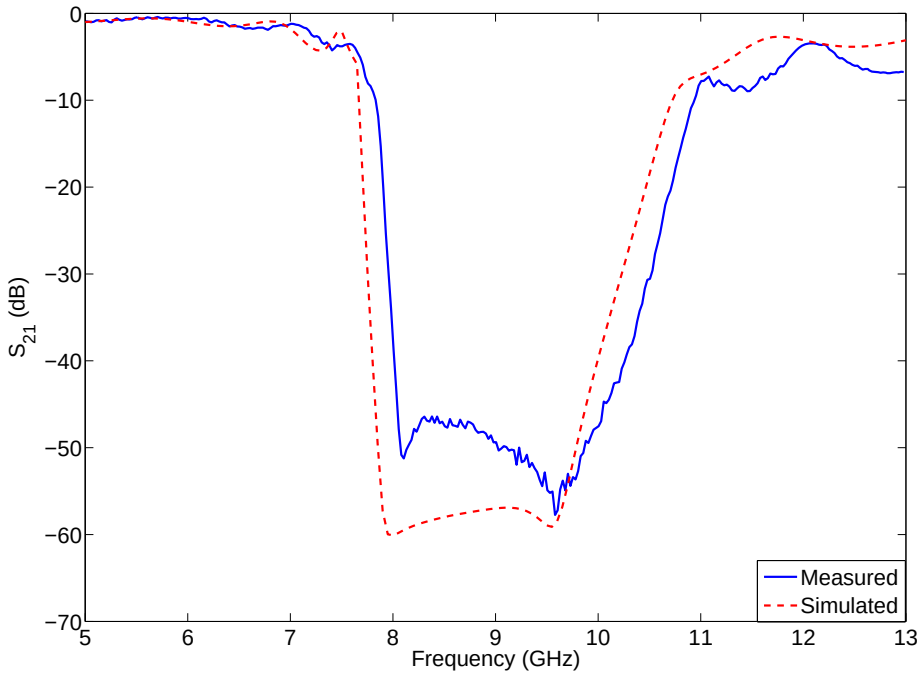

Figure 3.12: Measured (solid) and simulated (dashed) insertion loss of the CSRR-based band-reject filter

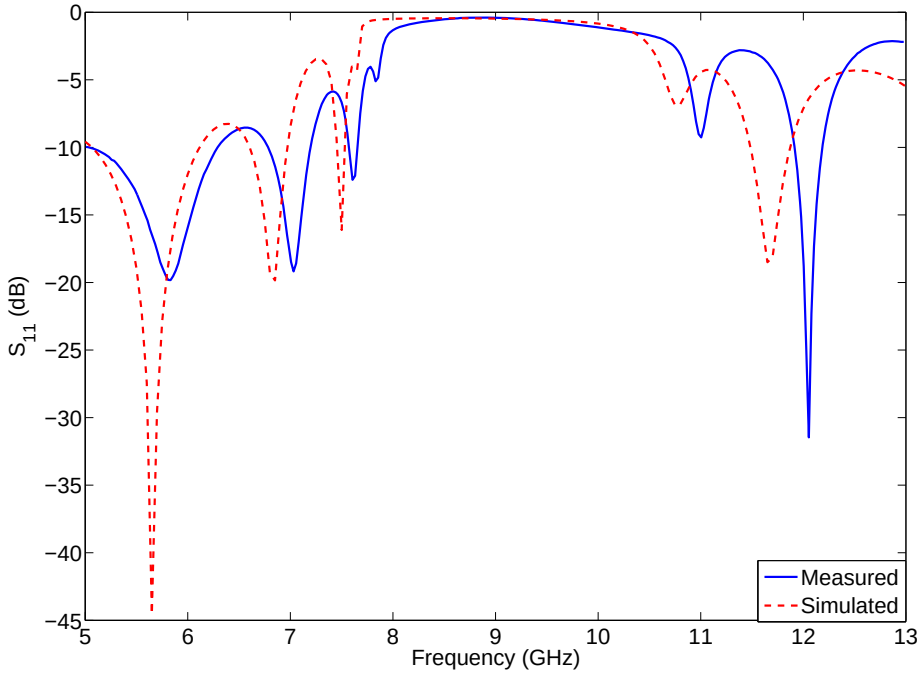

Figure 3.13: Measured (solid) and simulated (dashed) return loss of the CSRR-based band-reject filter

3.4 Discussions on the Filter Responses for the Two Topologies

3.4.1 Resonant (Operating) Frequency

In the case of both SRR- and CSRR-based band-reject filters, the signal propagation is inhibited in the vicinity of structures' resonant frequency. The measured and simulated frequency responses reveal that both SRR-based (9.25 GHz) and CSRR-based (9.3 GHz) filters yield center frequencies very close to each other (based on a minimum rejection level of 20 dB in the stopband).

If these resonating structures are considered as externally driven parallel inductor-capacitor (LC) tank circuits with strong current loops at resonance [11], principle of duality claims that the only difference between the lumped-element models is that the positions of inductors and capacitors are interchanged [26]. The inductance and capacitance values of the lumped-element models are determined from the device dimensions as well as material properties (*e.g.,* dielectric substrate, metal cladding). Since we employ exactly the same dimensions and dielectric laminates for both cases, it is natural that these dual structures would yield approximately the same resonant frequency.

However, it is important to note that due to the presence of the dielectric slab which introduces an additional boundary condition, the CSRR is not a perfect dual of the conventional SRR. In a quasi-static analysis, duality holds between a SRR and a CSRR printed on an infinitely thick substrate. Hence, for relatively thick substrates (compared to c and d parameters depicted in Figure 3.2 and Figure 3.11 (a)), the resonant frequency of both the CSRR and the SRR should be approximately the same [5]. In the case of our fabricated prototypes, the related parameters are $c = d = 0.3$ mm whereas the dielectric thickness is about 0.5 mm. Since the substrate thickness is not much larger than c and d, some

minor discrepancies can be expected between the resonant frequencies of SRR- and CSRR-based cases.

For both cases, the resonant frequency can be varied by individually tuning the d or g parameters depicted in Figure 3.2 and Figure 3.11 (a).

3.4.2 Bandwidth & Sharpness (Filter Selectivity)

One major difference between the SRR- and CSRR-based band-reject filters is the bandwidth of their stopbands as seen clearly in Figure 3.5 and Figure 3.12. The CSRR-based filter provides a much wider stopband in its frequency response whereas the SRR-based filter looks more like a very high-Q notch filter suppressing electromagnetic waves in a very narrow band. The quality factor for filters is conventionally defined as the ratio of the center frequency of the stopband to the rejection bandwidth, and in that sense the CSRR-based filter may be treated as a filter with a lower quality factor compared to the SRR-based filter. However, in fact, the CSRR-based filter is also a very high-Q filter as it exhibits a very sharp transition going from passband to stopband (at the lower edge of the rejection region) and a fairly sharp transition going from stopband to passband (at the higher edge of the rejection region).

Furthermore, as will be discussed in the next subsection, the addition of more CSRR stages improves the sharpness at the higher transition edge unlike the SRR-based filter, which remains the same regardless of the number of SRR stages.

As a result, such different band characteristics encourage the use of SRR- or CSRR-based filters depending on the nature of applications, namely the bandwidth requirement. Finally, as in the case of operating frequency, the bandwidth of both types of filters can be controlled by employing resonators

with slightly changing dimensions [23]. However, in that case, one might have to sacrifice from the rejection level.

3.4.3 Rejection Level & Effects of Number of SRR/CSRR Stages

When the rejection levels presented by both filters are compared, it is observed that the SRR-based filter has a maximum rejection level of approximately 40 dB whereas it is nearly 60 dB for the CSRR-based one. This enhanced rejection level of the CSRR-based filter can be attributed to the very strong capacitive coupling between the microstrip line and the CSRR stages. As stated earlier, the fundamental mode in a microstrip line is quasi-TEM mode. E-field lines are tightly concentrated in the region between the central conductor strip and ground plane (See Figure 3.10), whereas the H-field lines close along the central conductor (See Figure 3.1) which results in the following problems of the H-field [30]:

- SRR particles needs to be placed very close to the central conductor strip for proper excitation.
- Since the field lines are closely bounded to the central conductor strip, SRR particles are asymmetrically excited.

In contrast, E-field lines are highly concentrated between the central conductor strip and the ground plane having very strong vertical polarization. Therefore, the electric field component is more adequate to excite the resonating particles. This is the reason for significantly stronger attenuation of CSRR-based band-reject filters.

As observed in Figure 3.5 and Figure 3.12, a better rejection level is achieved using CSRRs although both filters have the same number of stages. Hence, it

is predicted that the number of SRR or CSRR stages may have different effects on the overall filter response. To verify this claim, the insertion loss responses of both filter types have been investigated by increasing the number of SRR and CSRR stages starting with a single stage as shown in Figure 3.14 and Figure 3.16, respectively. Two additional graphs illustrating the depth of rejection (*i.e.,* the maximum attenuation level) are also presented in Figure 3.15 and Figure 3.17.

For the SRR-based band-reject filter it is observed that with a single SRR pair (single stage), a maximum of 10 dB suppression can be obtained. This amount is close to 30 dB for 2 stages and about 37 dB for 4 stages. Adding more stages (5, 6, etc.) increases the rejection level at most to a level slightly higher than 40 dB and a saturation is observed in the amount of maximum rejection level as seen in Figure 3.14, where Figure 3.15 clearly shows this variation. This behavior has been attributed to the effects of coupling between successive SRR stages and also the direct coupling between the input and output ports. As a result, adding more SRR pairs cannot enhance the performance of an SRR-based band-reject filter indefinitely. Furthermore, upon the addition of excess number of stages, the device loses its compactness and increased device length introduces more passband insertion loss, which is undesired.

On the other hand, unlike the SRR-based band-reject filter, the rejection level of the CSRR-based filter increases almost linearly when the number of CSRR stages is increased as seen in Figure 3.16, particularly in Figure 3.17 where the rejection level versus number of CSRR stages (from 2 stages to 10 stages) is shown. A rejection level over 80 dB is achieved with 10 CSRR stages, which is indeed very deep.

Furthermore, as the number of SRR/CSRR stages is increased, the operating frequency of both filter types is not altered much. However, the stopband characteristics of the CSRR-based filter starts to improve its behavior

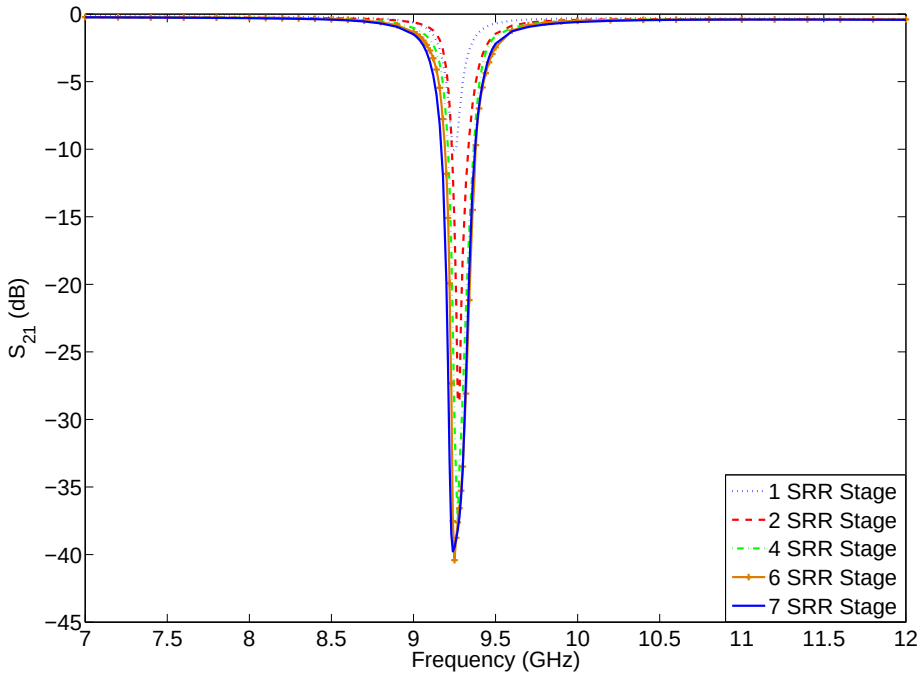

Figure 3.14: Rejection levels for increased number of SRR stages

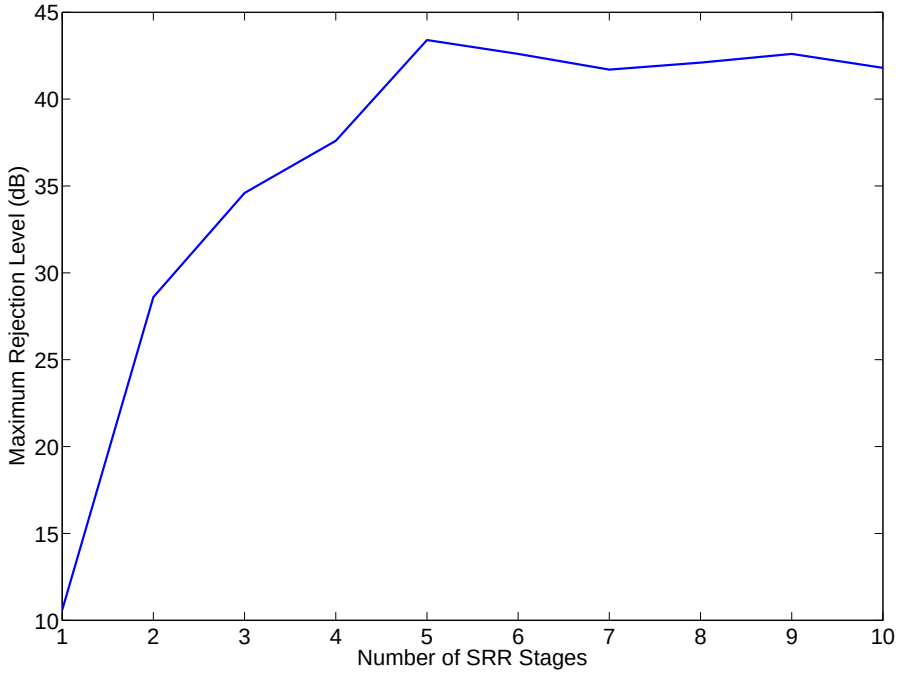

Figure 3.15: Maximum rejection level as a function of the number of SRR stages

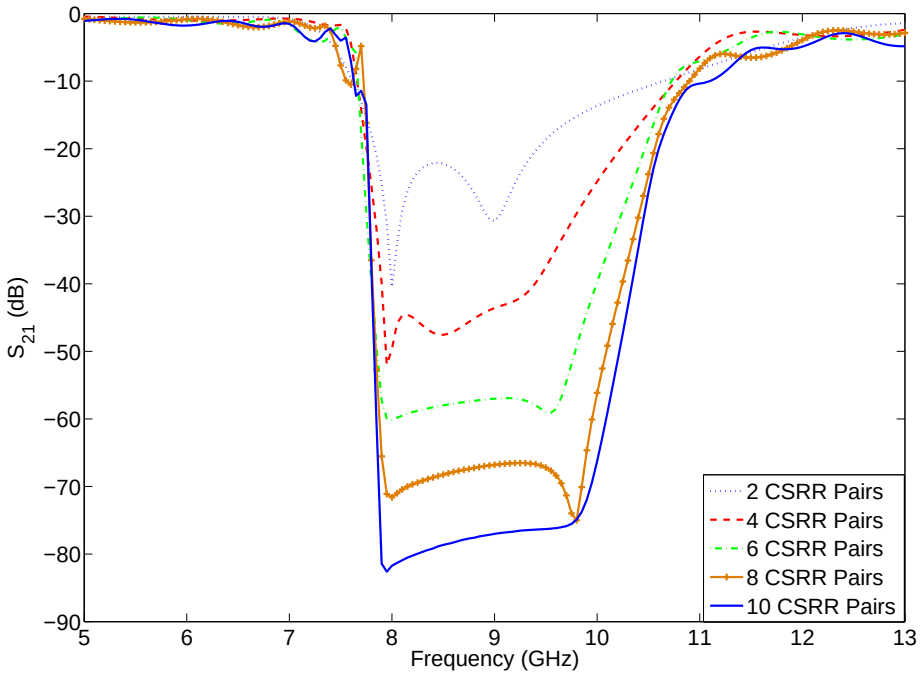

Figure 3.16: Rejection levels for increased number of CSRR stages

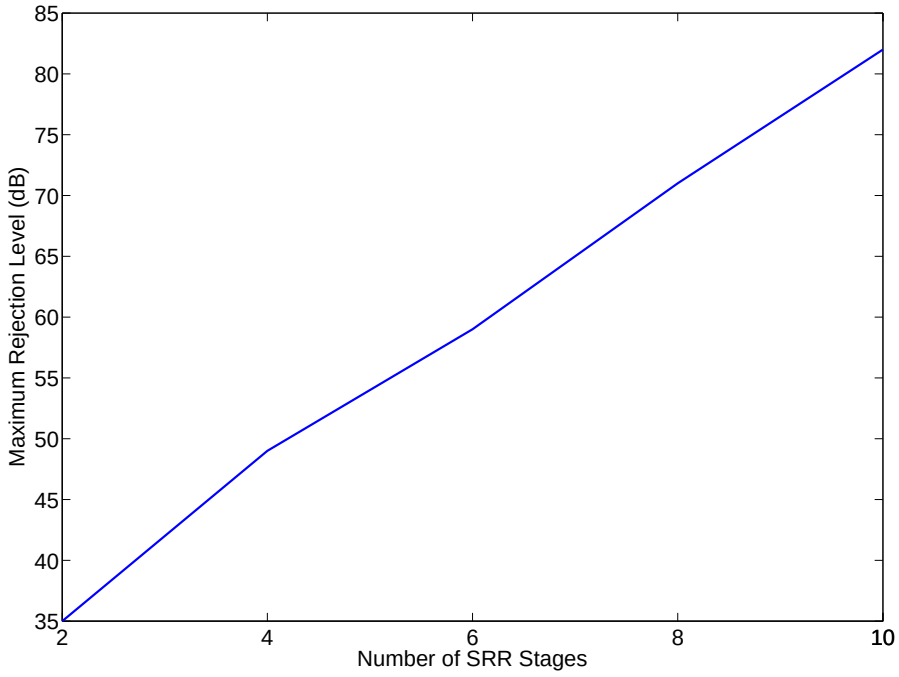

Figure 3.17: Maximum rejection level as a function of the number of CSRR stages

significantly after 4 stages by sharpening the stopband-to-passband transition edge.

Chapter 4

Electronically Switchable Band-Reject Filters Based on PIN Diode-Loaded SRRs

4.1 Introduction

All applications of the SRR mentioned in previous chapters are passive structures which do not incorporate any bias circuitry or any electrical control. Design of active structures using the SRR requires its combination with active components such as diodes and transistors.

The first application of the SRR to active microwave components encountered in literature was realized by loading SRRs with varactor diodes [37]. By placing varactor diodes between the inner and outer rings and changing the bias voltage of the diode, Gil *et al.* showed that the resonant frequency of the individual SRRs could be tuned electronically. In this configuration, the capacitance of the diode is in parallel to the inter-ring capacitance of the SRR. As a result of the variation in the equivalent capacitance between the inner and outer split

rings, the center frequency of the rejection band can be shifted. This idea led to the design of band-stop and band-pass filter structures based on SRRs whose rejection bandwidth and center frequency could be tuned electronically through an analog control voltage [28]. Recently, some authors have also demonstrated the possibility of tunable band-reject and bandpass filters based on complementary split-ring resonators (CSRRs) loaded with varactor diodes [38].

Another application of the SRR to active circuits is the design of microwave oscillators utilizing SRRs as their resonant component. High-Q and narrow-band nature of the SRR makes it possible to design microwave oscillators with low phase noise and good harmonic suppression [39]. It has been recently shown by some authors that inclusion of varactor diodes also enables the design of broadband voltage-controlled oscillators (VCOs) based on SRRs [40].

In this chapter, a new application of the SRR to active microwave components is proposed, in which the magnetic resonances of individual SRRs can be turned on and off electronically. Such a concept may lead to the design of SRR-based electronically switchable filters.

4.2 Idea Behind the Electronically Switchable SRR Concept

Early applications of the SRR to microstrip structures encountered in literature are SRR-based band-reject filters. These filters are designed by etching arrays of SRRs in close proximity to the central conductor on both sides. Due to the shape of field line patterns around the microstrip line, when it is excited by a signal, the magnetic field of the propagating wave illuminates the SRR arrays with a strong component in the axial direction; hence, the polarization requirement for proper SRR operation is automatically satisfied. Therefore, if the frequency of the

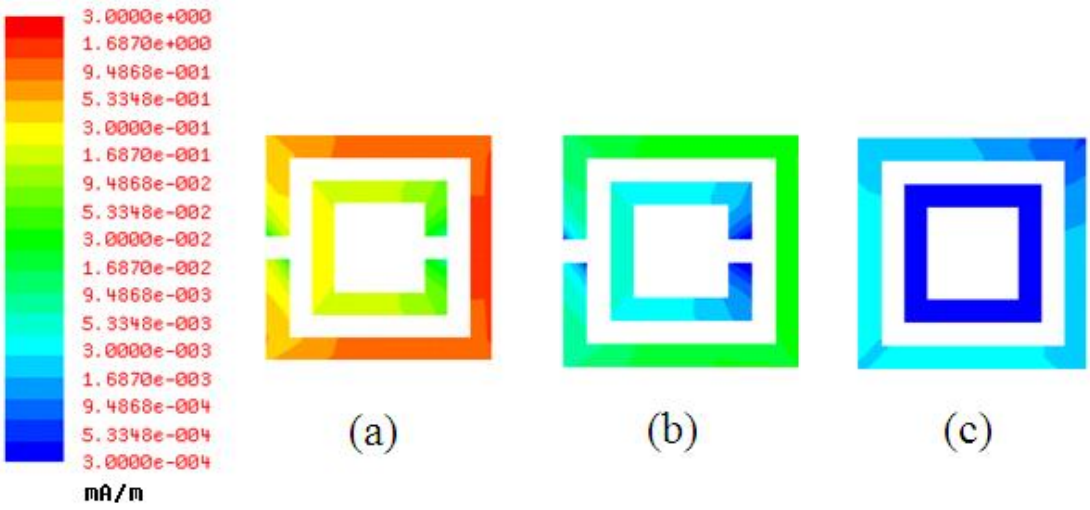

Figure 4.1: Surface current densities for (a) SRR at resonance frequency, (b) SRR at an off-resonance frequency, (c) SRR with slits removed

applied signal is close to the magnetic resonance frequency of the SRRs, strong loop currents are induced around the rings and signal propagation is inhibited due to negative effective permeability.

In order to illustrate the distribution of surface current density for resonance and off-resonance cases, the SRR-loaded microstrip structure examined in Section 3.2 has been simulated using Ansoft Designer^{TM} electromagnetic solver. This structure displays a magnetic resonance at about 9.25 GHz. In the vicinity of this frequency, a narrow rejection band is observed in the transmission spectrum and strong loop currents are expected to be induced over the rings. Figure 4.1 (a) and Figure 4.1 (b) illustrate the surface current densities over a single SRR at the resonant frequency (9.25 GHz) and at a distinct frequency (7 GHz), respectively. The colorbar is scaled logarithmically and the current density drops when moved from the red region to blue region. It is clearly seen that loop currents induced at the resonant frequency are more than 100 times ($\approx$ 40 dB) stronger than those observed when the frequency of the applied signal is away from the negative-μ region (*i.e.,* rejection band).

4.2.1 Removal of Magnetic Response in SRRs

Some previous studies have shown that the periodic SRR medium displays both a magnetic response due to the presence of the slits and an electric response induced by the dipole-like charge distribution along the incident electric field [17],[18]. Therefore, the gaps in the transmission spectrum of the SRR medium can be caused not only by negative effective permeability but also negative effective permittivity.

Authors of [17] have demonstrated that magnetic resonances of SRRs can be killed by removing the slits in the inner and outer rings. If the magnetic response of the SRRs is destroyed by closing the gaps, no negative effective permeability region; hence, no signal inhibition region is expected to be observed in the transmission spectrum of this medium. Since the removal of the gaps destroys only the magnetic response, such a structure can still display an electric response. However, the resonance due to the electric response will occur at much higher frequencies and it is very weak compared to the magnetic resonance. Hence, microstrip structures loaded with closed SRRs will not display a rejection band and act almost like ordinary 50-Ω transmission lines up to very high frequencies.

The elimination of resonating behavior for closed SRRs can also be verified from the surface current density distribution shown in Figure 4.1 (c). This figure illustrates the resulting currents over the rings when the rings of the structure given in Section 3.2 are closed. As seen clearly, regardless of applied frequency, much lower current densities (almost 80 dB) than those of resonating SRRs are induced over the closed rings. Consequently, the rejection band in the transmission spectrum is removed.

The idea behind the design of electronically switchable band-reject filters using SRRs is to achieve the removal of the slits (*i.e.,* closure of the rings) by means of an electrical component. Through the excitation of a control voltage

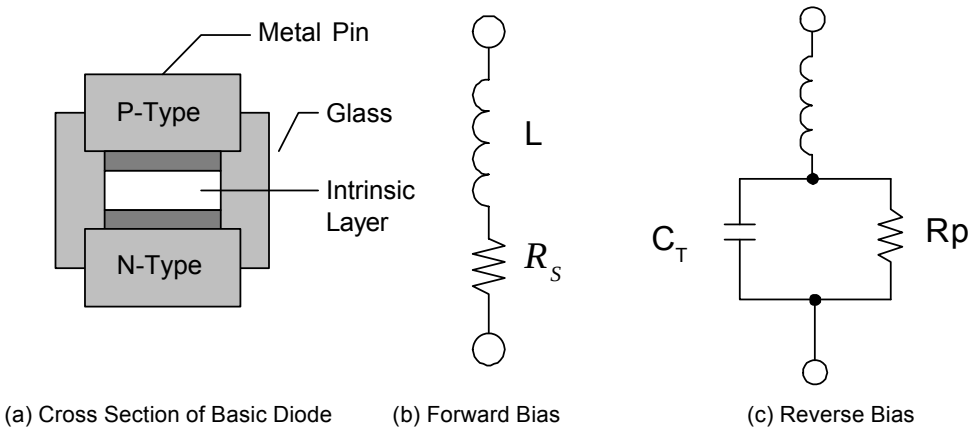

Figure 4.2: PIN diode cross section and equivalent circuits

or current, one should be able to turn the magnetic response of the SRRs on and off. Therefore, a switching microwave component which can electronically short-circuit the SRR gaps is required. However, short-circuits and open-circuits are not very easy to achieve at microwave frequencies. When short-circuited, the switching device must exhibit very low inductance and resistance to completely close the ring. On the other hand, when open-circuited, it must exhibit very low capacitance to display high impedance against RF flow and to avoid disturbing the functioning of the slit.

4.2.2 PIN Diode-Based RF Switching

A good alternative for fulfilling the abovementioned requirements can be the use of a PIN (p-type - intrinsic - n-type) diode. A PIN diode is a semiconductor device that operates as a variable resistor at RF and microwave frequencies. The resistance value of the PIN diode is determined only by the forward-biased DC current. In switch and attenuator applications, the PIN diode should ideally control the RF signal level without introducing distortion which might change the shape of the RF signal. Figure 4.2 (a) illustrates the outline of a PIN diode. The chip is prepared by starting with a wafer of almost intrinsically pure silicon,

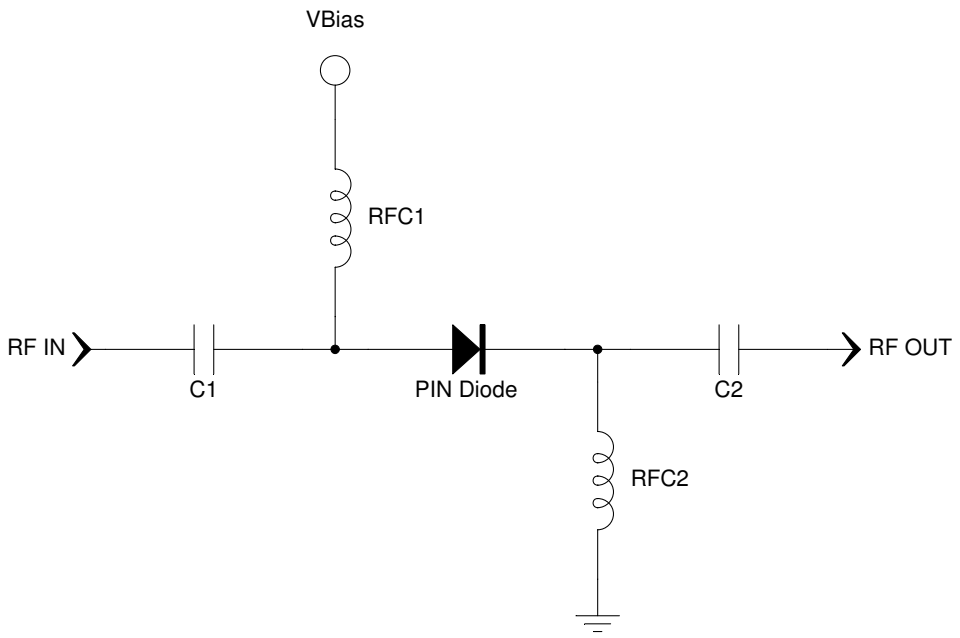

Figure 4.3: Typical PIN diode-based RF switch circuit

having high resistivity and long lifetime. A p-region is then diffused into one diode surface and an n-region is diffused into the other surface [42].

PIN diodes can be used to construct electronic switches that are compatible with planar circuitry and capable of very high frequency and fast switching operation. It holds some i-v characteristics that make it a good choice as an RF switching element. Figure 4.2 (b) and Figure 4.2 (c) show the equivalent circuit models of a PIN diode for forward- and reverse-bias cases, respectively. When reverse biased, it possesses a very small series junction capacitance resulting in a high impedance state blocking the RF signal flow. When forward biased, it displays very small resistance and inductance allowing the propagation of the RF signal.

Figure 4.3 illustrates a typical RF switching mechanism based upon PIN diodes. The circuit consists of a PIN diode, two radio frequency choke coils (RFC), and two capacitors. RFCs are employed to decouple the RF signal from the DC voltage source and DC ground. On the other hand, the capacitors block

the DC bias current from flowing into the source and destination RF devices. The inductance of the RFCs should be sufficiently high to disallow RF leakage into DC path at the frequency of operation. Likewise, the capacitance of DC blocking elements should be sufficiently high to reduce the insertion loss of the device. If very high values for RFCs and capacitors are chosen, they might become useless at the intended frequencies due to lumped parasitic effects. Therefore, some trade-off should be made.

When a positive DC control voltage is applied to this circuit, some bias current flows through the RFCs and the diode. If this current is strong enough to turn the diode on, the RF power is transferred from the input port to the cascaded stage following the switch. Conversely, if a negative DC voltage is applied to the control pin, the diode is in the off state and propagation of RF power is inhibited.

PIN diodes can be turned on even under the excitation of very low voltages. Therefore, when the switch is desired to be off, it is strongly recommended that the diode is reverse-biased rather than being left under zero bias. Otherwise, excitation of a strong RF signal can turn the switch on causing the malfunction of the device.

4.3 PIN Diode-Loaded Split-Ring Resonator

4.3.1 Modifications in Conventional SRR Structure

The original idea to construct electronically switchable SRRs is to connect PIN diodes across the split gaps of the concentric rings as illustrated in Figure 4.4. When a forward bias voltage is applied, the diodes will be in conduction short-circuiting the splits of the concentric rings. Therefore, each split ring will

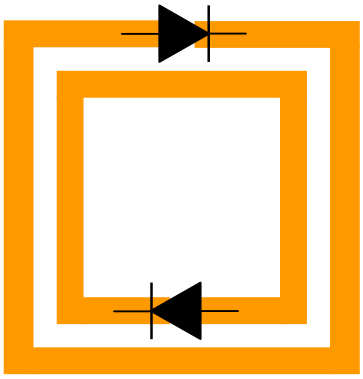

Figure 4.4: SRR Loaded with PIN Diodes

be converted to a closed ring and the magnetic response of the overall SRR structure will be eliminated. If a band-reject microstrip filter is built based on these SRR structures, excitation of forward bias will remove the rejection band resulting from the magnetic resonance of the rings and a filter with electronic switching capability will be obtained.

However, the conventional square-shaped SRR structure depicted in Figure 4.4 is not very convenient for operation when loaded with PIN diodes. The first difficulty is encountered in biasing the diodes. Using such a topology, it is not possible to apply the required bias voltage to switch the diodes on since the anode and cathode terminals of the diodes are already short-circuited by the metallic rings. Hence, some sort of DC blocking mechanism must be incorporated into the design to DC-wise isolate the two terminals of the diode from each other. The second difficulty encountered in this structure is that the access of the DC bias current to the diode installed across the slit of the inner ring is not very easy and can only be achieved by the use of long bond wires or metallic vias which are not desirable as they can disturb the response of the SRR. Therefore, some modifications have been made in the conventional SRR structure to make it convenient for use with an active component.

The first modification is the removal of the inner ring from the original topology. It is clearly seen in Figure 4.1 (a) and Figure 4.1 (b) that the currents

induced over the outer ring are much stronger than the currents induced over the inner one. For that reason, it can be predicted that the electromagnetic behavior of the outer ring will dominate that of the inner one and the overall magnetic response of the SRR will be primarily determined by the outer split ring.

In order to verify this claim, SRR-based single-stage band-reject structures depicted in Figure 4.5 (a) and Figure 4.5 (b) have been simulated using Ansoft Designer software. Figure 4.5 (a) represents a filter based on the conventional SRR whereas Figure 4.5 (b) represents a filter with the inner ring of the SRRs removed. In the graph, a comparison of the insertion loss responses of the two topologies is illustrated. It is observed that the double- (solid line) and single-ring (dashed line) SRR structures yield resonances at 5.46 GHz and 5.51 GHz, respectively. The rejection level of the filter at resonance is almost identical for both cases. It is apparent that the removal of the inner ring from the SRR structure does not disturb the overall response significantly. This modification causes only to a slight shift in the overall magnetic response but also appreciably simplifies the structure.

Having been left with a single ring, the PIN diode-loaded SRR still has the problem of short-circuited diode terminals which obstructs the proper biasing of the diode. Since the diode is short-circuited by the metallic ring itself, it will always have zero bias voltage and can never be turned on. In order to overcome this problem, a second slit has been introduced to the SRR as depicted in Figure 4.6 (b). This additional gap can be thought of as a second capacitance which is in series to the original gap capacitance reducing the equivalent capacitance value. The reduction in the gap capacitance is expected to cause an increase in the resonant frequency of the overall structure. The simulated insertion loss response of the double-slit structure is also shown in Figure 4.6 in comparison to the single-slit ring resonator case. Indeed, the

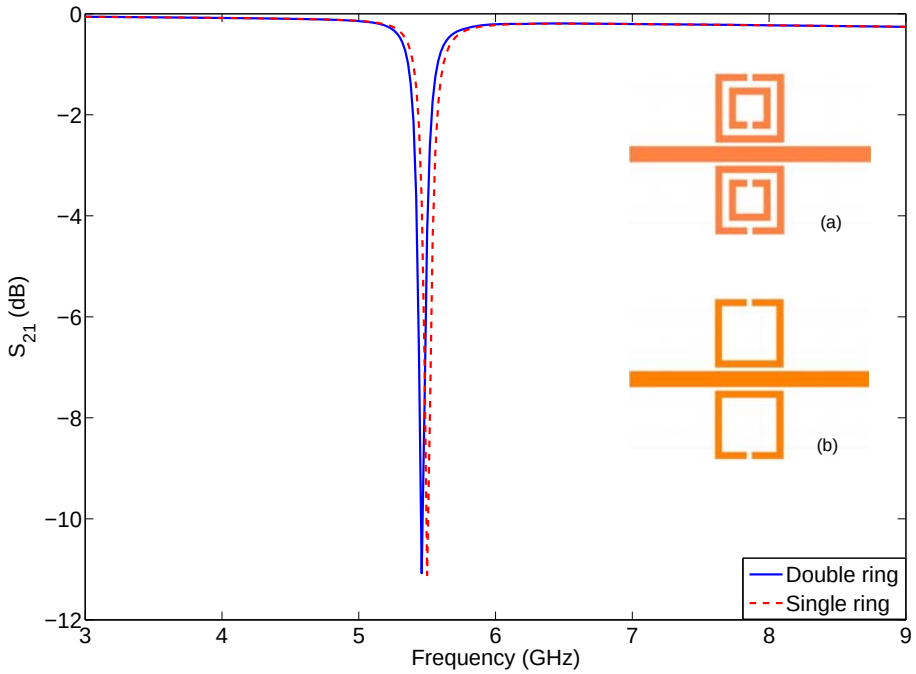

Figure 4.5: Simulated insertion losses for SRRs with single (dashed) and double rings (solid)

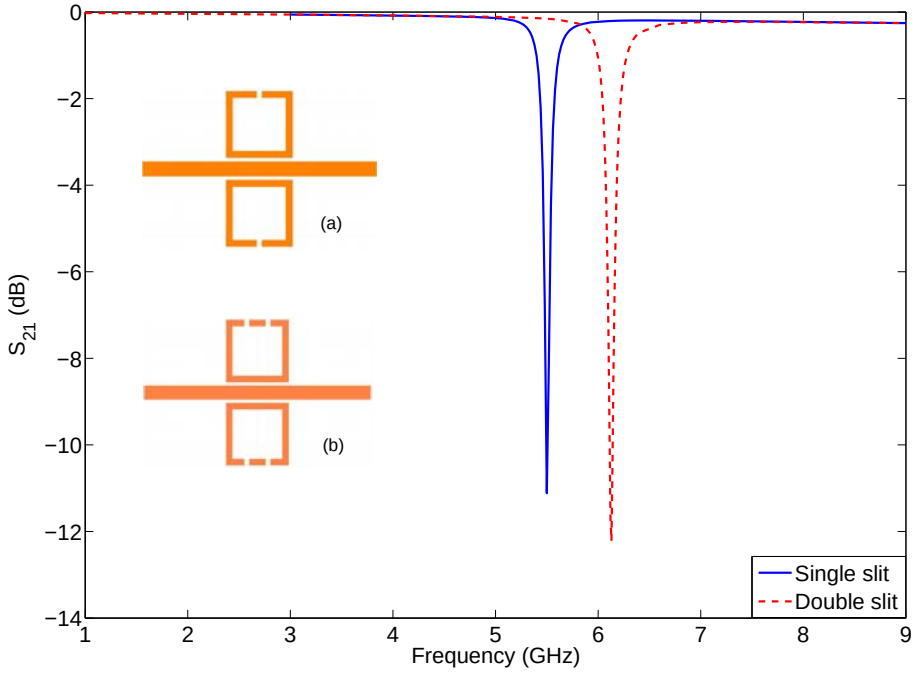

Figure 4.6: Simulated insertion losses for SRRs with single (solid) and double slits (dashed)

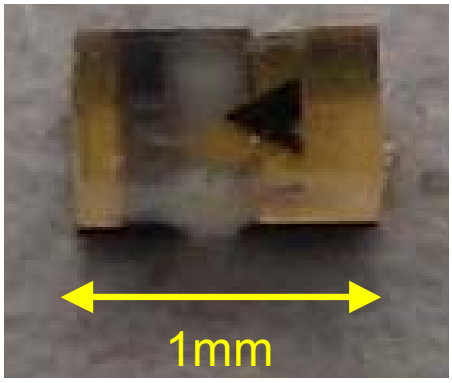

Figure 4.7: MPP4204-206 PIN diode

introduction of the second slit causes a shift in the resonant frequency of the SRR from 5.51 GHz to 6.14 GHz as expected.

4.3.2 Fabricated PIN Diode-Loaded Prototype

Choice of PIN Diodes

The diodes which have been employed in the fabrication of the PIN diode-loaded SRR prototype are manufactured by Microsemi Corporation with part number MPP4204-206, especially for high-speed microwave switch applications. A photo of MPP4204-206 PIN diode is presented in Figure 4.7. Small black arrow on the package points the cathode terminal. The package dimensions are 40 mil×20 mil ($\approx$ 1 mm×0.5 mm).

These diodes utilize the new monolithic microwave surface mount (MMSM) technology which provides them with very low parasitic effects:

- Less than 200 pH of series inductance
- Typical 75 fF of parasitic capacitance
- Maximum 2 Ω of series on resistance under 10mA of bias current

The technology is a package/device integration accomplished at the wafer fabrication level. Since the cathode and anode interconnections utilize precision photolithographic techniques rather than wire bonds, parasitic package effects are tightly controlled. These superior electrical characteristics facilitate the diodes' functionality up to frequencies above 12 GHz [43].

The manufacturer's datasheet of MPP4204-206 PIN diodes is given in Appendix B.

Design Details

To obtain the final form of PIN diode-loaded SRR design, two of these PIN diodes are mounted across the split gaps of the abovementioned modified SRR structure in a back-to-back configuration which is illustrated in Figure 4.8. This design allows the proper biasing of the diodes by isolating the anode and cathode terminals from each other.

It is also possible to load only one of the slits with a PIN diode. In this case, when a forward bias is applied, there will still be a capacitance which can give rise to a resonance and the rejection band will not be completely removed. It is expected that the resonance frequency is slightly shifted down since one of the series slit capacitances is eliminated, causing an increase in the equivalent capacitance.

The small metallic part between the diodes is used as the common anode and the rest of the metallic ring is used as the common cathode terminal as shown in Figure 4.8. Therefore, DC-wise, the structure consists of two PIN diodes connected in parallel.

Related SRR dimensions as shown in Figure 4.8 are chosen as follows; the width (W) of the SRR is 5 mm, the ring thickness (d) is 0.5 mm and the width

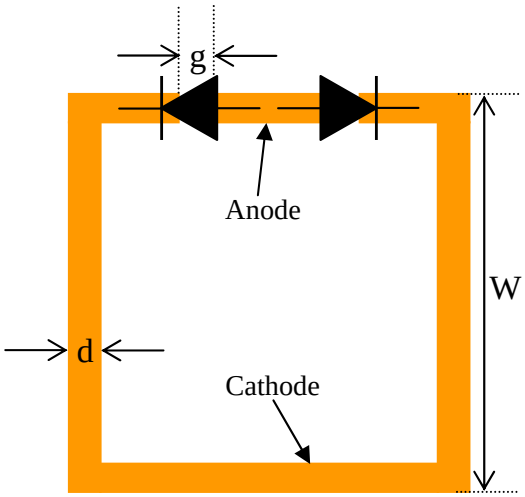

Figure 4.8: PIN Diode-Loaded Split-Ring Resonator. Relevant dimensions are: $d = 0.5$ mm, $g = 0.4$ mm, and $W = 5$ mm

of the split gap (g) is 0.4 mm. The g and d parameters have been chosen based on the pad layout dimensions of the MPP4204-206 diodes. The width of the central conductor of the microstrip structure is designed as 1.15 mm to obtain a characteristic impedance of approximately 50 Ω. Square-shaped SRR structure rather than a circular one enhances the coupling between the rings and the microstrip line and also helps create suitable pads for connecting the diodes.

The fabricated single-stage PIN diode-loaded SRR-based band reject filter is depicted in Figure 4.9. This prototype has been fabricated on a RO4003C high frequency laminate commercially available from Rogers Corporation. The height of the dielectric is 20 mil (≈ 0.51 mm), the permittivity is 3.38 relative to that of vacuum and the thickness of the copper cladding is 1 oz (35 μm). Especially, the fabrication of the printed inductor in this design is very challenging and cannot be realized using a mechanical etching technique as in previous filters. Therefore, a laser structuring technique using the LPKF ProtoLaser 200 machine has been employed to fabricate the circuit board.

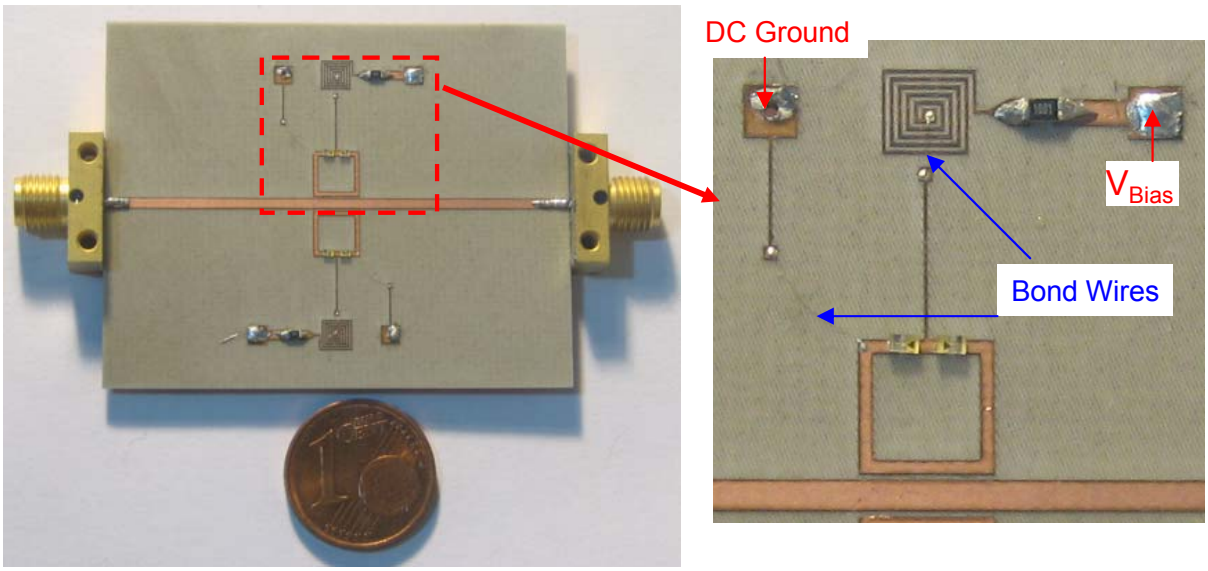

Figure 4.9: Fabricated single-stage PIN diode-loaded SRR-based band-reject filter

Since the diodes might not withstand the high temperature reflow profile required by ordinary solder, they have been mounted on the PCB by using a silver-filled conductive epoxy cured at 150 °C.

The details of the design can be seen from the magnified picture in Figure 4.9. A DC ground pad and a positive voltage pad have been employed as the starting and ending points of the bias current path. The connection of these pads to the diode terminals on the SRR has been achieved by utilizing gold bond wires having a thickness of 1 mil ($\approx$ 25.4 μm). Connection of bond wires has been accomplished using some clean-room techniques. Thin and relatively long ($\approx$ 7 mm) bond wires used in this design are expected to exhibit significant inductance at the frequencies of interest and behave as radio frequency chokes (RFCs) which prevent RF leakage into the DC path. To further improve the RF isolation from the DC path, a spiral inductor has also been employed. Since the SRRs do not have any metallic connection to the microstrip line, there is a natural isolation of DC current from RF signal path. Therefore, no extra mechanism such as a coupling capacitor is necessary to prevent DC current leakage into the RF path.

In order to prevent the diodes from burning out, 0603 package chip resistors have been employed. These resistors limit the current flowing through the diodes. When the diodes are on, there is approximately 0.8 V of voltage between the anode and cathode terminals of each diode. Intending a DC bias current of 10 mA through each diode and a control voltage of 5 V, the value of this current limiting resistor has been set to 200 Ω:

$$\text{Voltage across the resistor: } 5\text{ V} - 0.8\text{ V} = 4.2\text{ V}$$

$$i_{Total} = \frac{4.2\text{ V}}{200\ \Omega} = 21\text{ mA for a single SRR unit}$$

which yields 10.5 mA through each diode.

A single-stage filter will then draw 42 mA of current from the 5-V supply which corresponds to a power dissipation of about 0.2 W which might seem a little big. It has been observed during the measurements that decreasing the bias current to 1 mA may also suffice to turn the diodes on. This change reduces the power dissipation to 20 mW. However, it must be kept in mind that the power dissipation occurs only when the rejection band is electronically removed.

Measurements and Simulations

After soldering 3.5-mm SMA connectors at both port sides, the prototype was tested using an Agilent N5230A vector network analyzer. Figure 4.10 illustrates the insertion loss response of the filter for three different cases:

- Diodes are not present (Dashed-dotted line)
- Diodes are installed but not biased (Solid line)
- Diodes are installed and forward biased (Dashed Line)

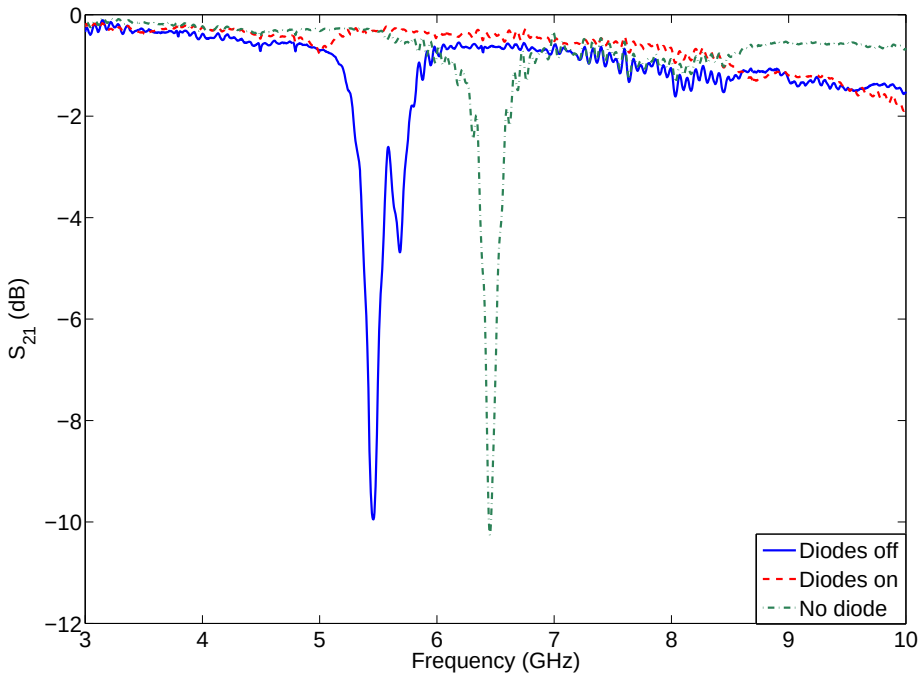

Figure 4.10: Measured insertion loss responses of the fabricated PIN diode-loaded filter

The filter exhibits a rejection dip at 6.46 GHz before the diodes are connected across the split gaps. This response is represented by a dotted-dashed line in the graph. Since the filter consists of a single stage, its rejection level can reach only 10 dB. When the diodes are present but no bias current is applied, the diodes are not in conduction. Since the PIN diodes in this configuration are not placed on the main RF path, which is the central conductor of the microstrip, flow of very strong RF currents is not expected through the diodes. Hence, it is not necessary to apply a reverse-bias voltage to keep the diodes off. Instead, the V_{Bias} pad shown in Figure 4.9 is connected to the ground to apply zero DC bias. In this diodes-off case, what is observed in the frequency response is the effect of diodes' parasitic capacitance. The junction capacitance of diodes, which is typically 75 fF, acts as an additional capacitance which appears in parallel to the already available gap capacitance of the split ring. This slight increase in the equivalent capacitance causes a slight decrease in the resonant frequency of the overall structure. The solid line in the graph clearly shows this effect. Rejection

band is shifted by about 1 GHz to lower frequencies compared to the case where diodes are not present.

In order to check the electronic switching mechanism of the filter, the V_{Bias} pad shown in Figure 4.9 is connected to 5 V. In this case, about 10 mA of forward bias current flows through each diode. Due to the presence of forward bias, the diodes starts conducting and the split gaps are RF-wise short-circuited eliminating the magnetic response of the SRRs. The response of the filter for this case is represented by the dashed line in Figure 4.10. It is observed that the previously seen rejection band is completely removed from the frequency response and the filter acts as a through transmission line with low insertion loss. Low insertion loss proves that when a positive control voltage is applied, the line is acting as if no rings were placed around the central conductor, that is, the rings are invisible to the RF flow.

An interesting aspect of the diodes-off case compared to the case where diodes are not present is that the rejection band of the filter is not only shifted to lower frequencies but also slightly widened and also a second but not-so-deep transmission gap appears as a result of the installation of the PIN diodes. The presence of this second dip can be attributed to the manufacturing tolerances of the PIN diodes. Although the manufacturer claims a junction capacitance of about 75 fF for each diode, it is expected that there can be small variations in these parasitic values. Different diode capacitances can cause SRRs resonating at different frequencies and as a result, the rejection band can be widened and even multiple transmission dips can be observed.

In order to illustrate the abovementioned effect of PIN diodes, a hybrid computer simulation combining electromagnetic and lumped-circuit simulation tools has been set up. Initially, an electromagnetic simulation of the single-stage SRR-based filter has been performed. However, when making the simulation setup, besides the input and output ports (P1 and P2) of the filter, eight

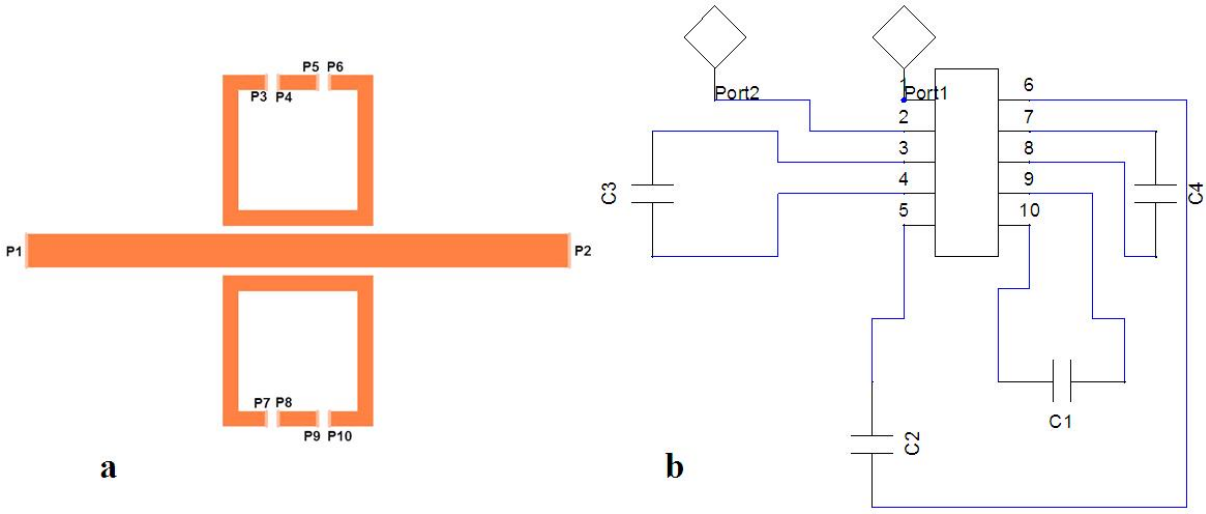

Figure 4.11: Simulated model of the PIN diode-loaded SRR-based filter

additional ports (P3 through P10) have been placed at the slit openings of the rings as illustrated in Figure 4.11 (a). Therefore, the output of the electromagnetic simulation is the scattering parameters of a device with 10 ports. For the no-bias case, the PIN diodes have been modeled as 75-fF capacitors and for the forward bias-case, the diodes have been modeled as 2-Ω resistors. Finally, a model of the overall structure has been obtained including the effects of the PIN diodes as shown in Figure 4.11 (b).

Simulated insertion loss responses of the filter are illustrated in Figure 4.12. In this graph, the frequency responses for three different cases are presented; two of them correspond to the case when the diodes are not biased, and the third one corresponds to the case when a forward-bias current is passed through the diodes. In the first graph, it is assumed that all the diodes are perfectly identical and have the same parasitic junction capacitance of 75-fF (dashed line). In this case, a single and narrow rejection band is observed in the overall transmission spectrum. For all diodes being identical, the shape and the width of the rejection band are well preserved since all diodes produce the same amount of shift in the frequency response.

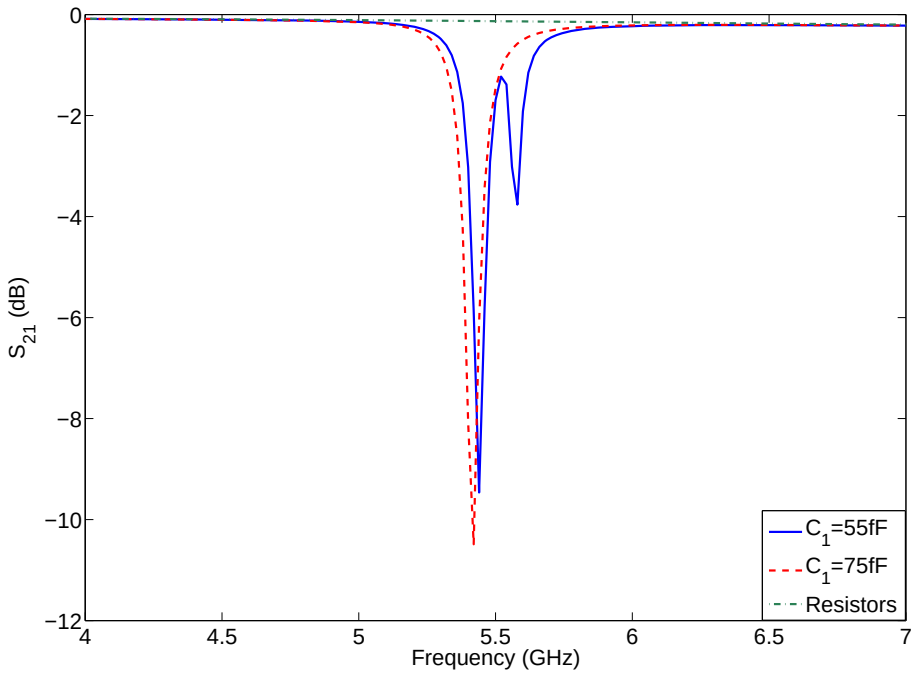

Figure 4.12: Simulated insertion loss responses for diodes-off case

As an alternative possibility, the junction capacitance of one of the capacitors, namely the one labeled as C1 in Figure 4.11 (b), is changed to 55 fF while the rest is still maintained at 75 fF. This modification imitates the case when one of the diodes possesses a slightly smaller junction capacitance as a result of manufacturing tolerances. The solid line of Figure 4.12 clearly demonstrates the effect of this change. The bandgap in the transmission spectrum is slightly widened and also a second but weaker dip appears over the rejection band. This graph broadly matches the case obtained during the measurements as shown by the solid line of Figure 4.10 in terms of both shape of the response and the center frequency of the rejection band. The resemblance of the measured and simulated cases can be more obviously seen from Figure 4.13. In this graph, the frequency of the rejection dip perfectly coincides for simulated and measured responses whereas the rejection band of the experimental result is slightly wider than the simulated case. It can be concluded that:

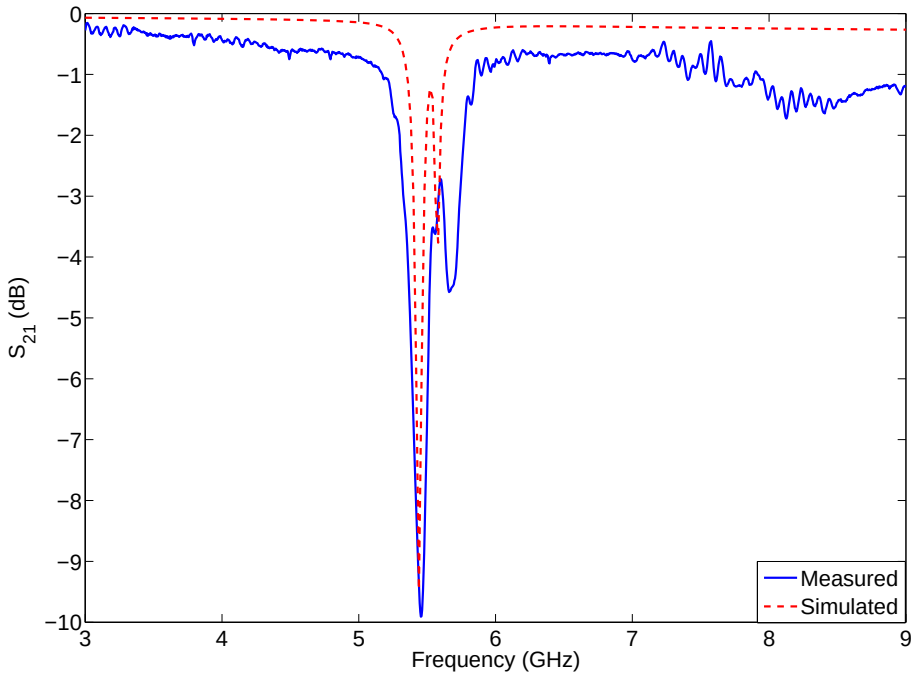

Figure 4.13: Measured (solid) and simulated (dashed) insertion loss responses for the diodes-off case when one of the diodes is modeled as a 55-fF capacitor

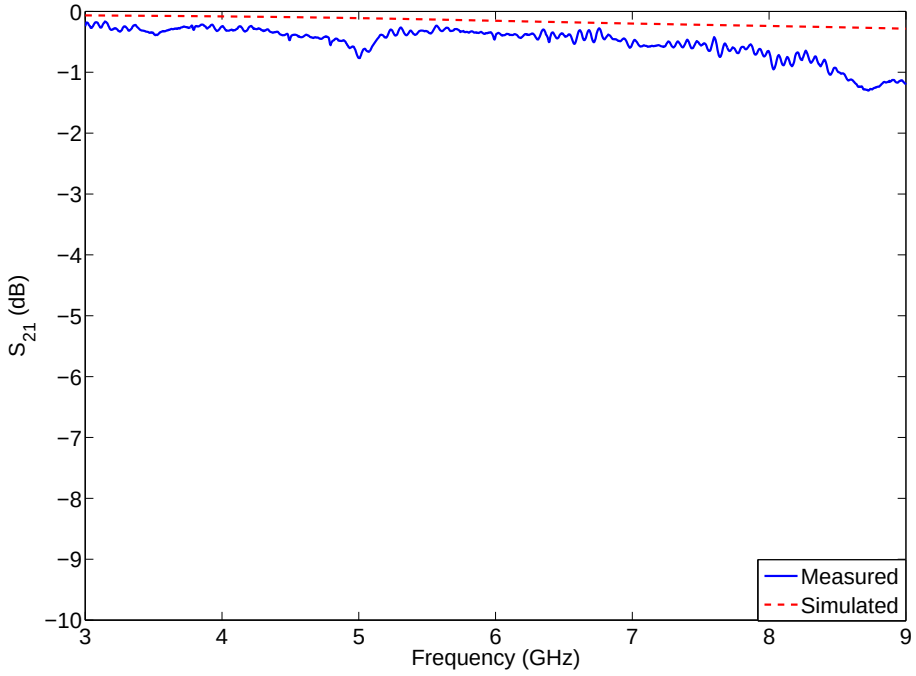

Figure 4.14: Measured (solid) and simulated (dashed) insertion loss responses for the diodes-on case when one of the diodes is modeled as a 2-Ω resistor

- If a very narrow rejection band is required, the choice of diodes is very crucial. Parasitic effects are not tolerable.

- If a filter with relatively wider band is desired, diodes with slightly varying junction capacitances must be employed. Alternatively, choosing perfectly identical diodes, SRRs with slightly changing dimensions can be used to widen the rejection band.

To simulate the case when the diodes are forward-biased, all the capacitors of Figure 4.11 (a) have been replaced with 2-Ω resistors. The frequency response of this forward-bias model is represented by the dotted-dashed line in Figure 4.12. It is observed that the bandgap in the frequency response is eliminated and the filter acts like a transmission line. Comparison of simulated and measured responses for the diodes-on case can be more clearly seen in Figure 4.14.

4.4 Multi-Stage Switchable Filter Design

The single-stage band-reject filter introduced in the previous section provides a low level of rejection. However, this prototype is a good starting point since it reveals the ability of the PIN diode-loaded SRR to create electronically switchable rejection bands. Design of filters with improved suppression levels requires the employment of multiple SRR stages.

4.4.1 Four-Stage Band-Reject Filter

To obtain a frequency response with enhanced suppression characteristics, firstly, a four-stage band-reject filter as depicted in Figure 4.15 has been fabricated on RO4003C dielectric substrate and tested. All SRRs have the same dimensions as the previous single-stage prototype as shown in Figure 4.8.

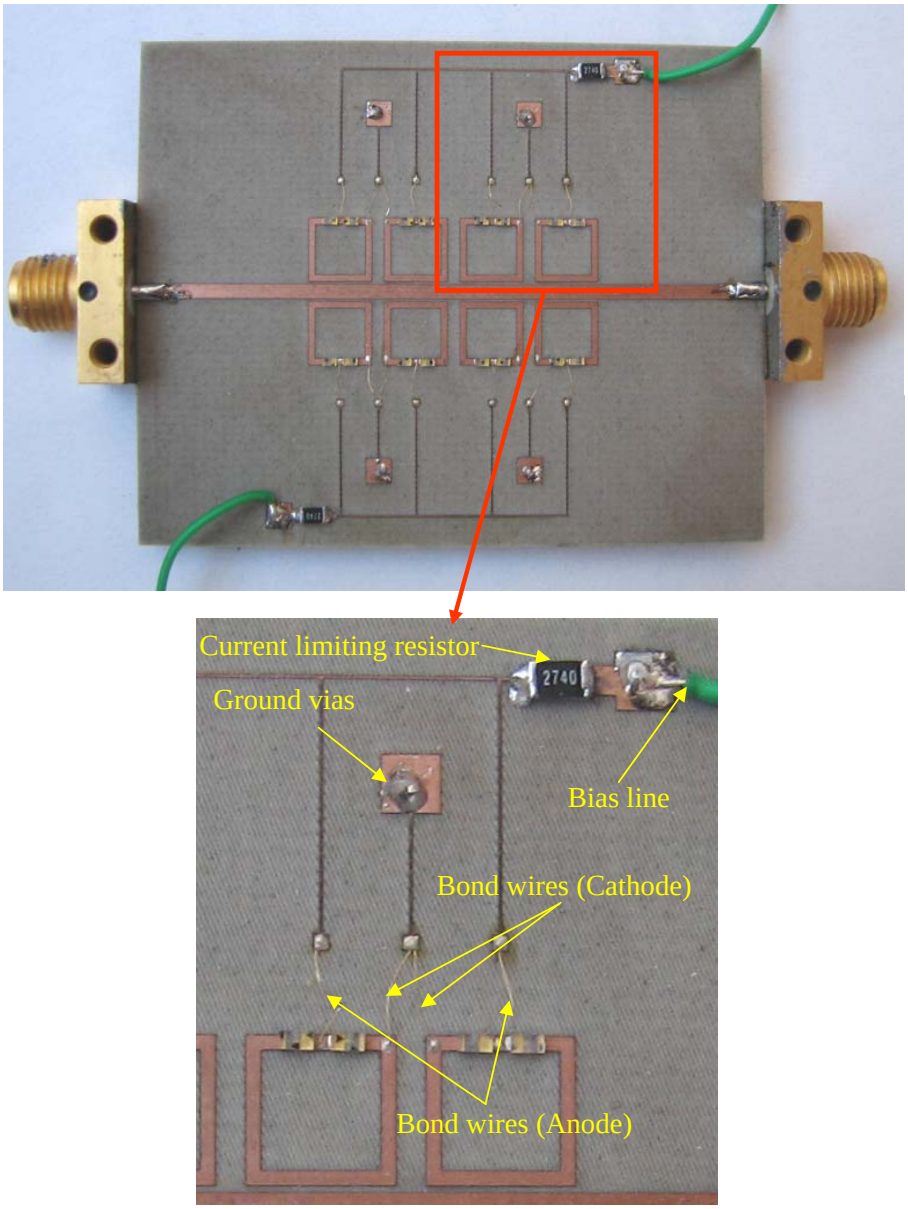

Figure 4.15: Fabricated four-stage PIN diode-loaded SRR-based band-reject filter

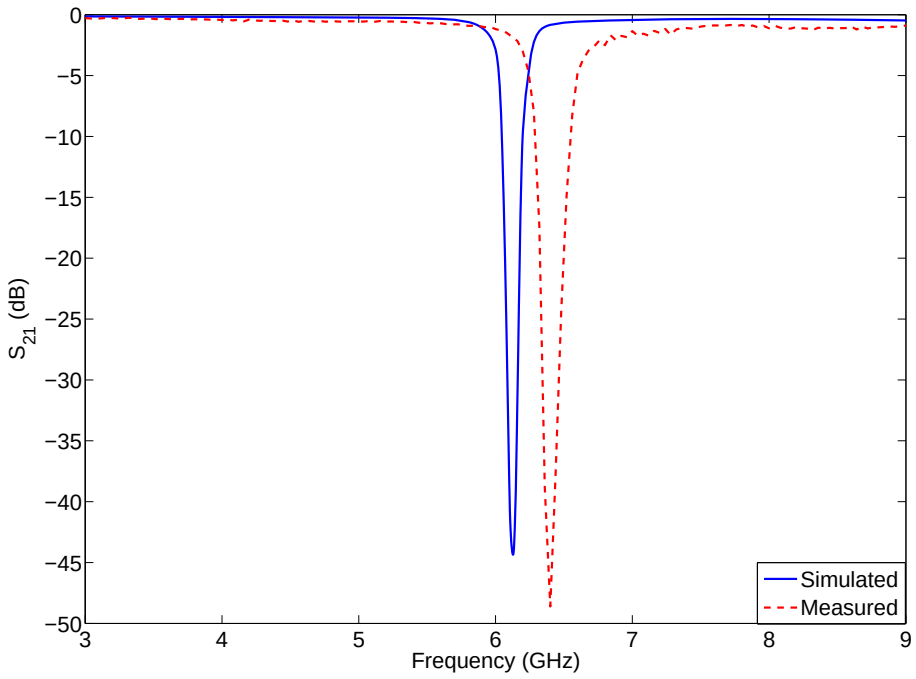

Figure 4.16: Simulated (solid) and measured (dashed) insertion loss responses for 4-stage filter with no diodes installed

As a first step, the scattering parameters of the prototype have been measured before the diodes are mounted. The insertion loss performance of this structure can be seen from Figure 4.16. There is a relatively good agreement between the measured (dashed) and simulated (solid) responses except a slight shift in center frequency which can be attributed to manufacturing tolerances. The measured center frequency of the rejection band perfectly coincides with the one observed in single-stage case (See dashed-dotted line of Figure 4.10) as expected. The depth of rejection notch exceeds 40 dB which is not more than 10 dB for the single-stage filter.

The next step is the installation of diodes and bond wires. Due to their problematic fabrication, the spiral inductors of the previous design have not been used in this filter. Furthermore, it has been found out that the inductance-per-mm of a bond wire of 1-mil diameter is about 1 nH. In the current

design, the bond wires have a length of approximately 8 mm. At the resonant frequency ($\approx$ 6 GHz), this corresponds to a reactance of about:

$$X_L = 2\pi f L = 2\pi \times 6 \times 10^9 \times 8 \times 10^{-9} \approx 302\ \Omega$$

which is quite sufficient to choke the RF signal, hence there is no need to employ an additional RFC inductor.

The details of this design can be seen form the magnified picture in Figure 4.15. The diodes are again connected in a back-to-back configuration sharing a common anode and a common cathode as in Figure 4.8. Each SRR unit has two bond-wire connections; one for the anode, another for the cathode terminal of the PIN diodes. Anode terminals are fed by the same DC bias line through a 0603-package chip resistor. Cathode terminals of two successive SRRs are connected to the same pad which is connected to the device ground through a metallic via hole.

The scattering parameters of the fabricated four-stage prototype are plotted in Figure 4.17. The solid line represents the case when no bias voltage is applied to the diodes. A rejection band is observed near the expected frequency region. The observed band is much wider than that of the single-stage prototype. However, the level of suppression is quite nonuniform over the rejection band. There are two obvious dips reaching 15 dB and at the peak point, the suppression is only around 7 dB. This widened band and multiple rejection dips can again be attributed to the junction capacitances of the PIN diodes which has also been demonstrated via simulation in previous section.

The dashed line of Figure 4.17 shows the variation of the insertion loss when the diodes are forward biased with 5 V. It is observed that the rejection band is completely removed and the frequency response displays transmission with low insertion loss, that is, the SRR particles are invisible to the microstrip line.

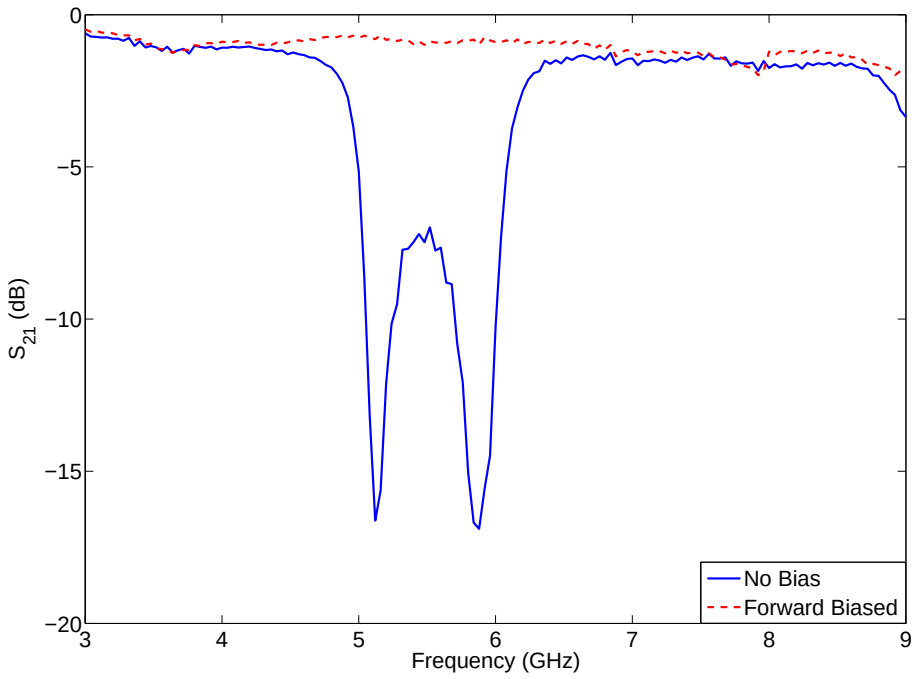

Figure 4.17: Measured insertion loss responses for four-stage PIN diode-loaded band-reject filter for forward-bias (dashed) and no-bias (solid) cases

4.4.2 Eight-Stage Band-Reject Filter with Independent SRR Switching

Design of a filter with a narrow and deep rejection band, especially with a single transmission dip requires the knowledge of diode junction capacitances before fabrication. Due to the lack of a precise measurement device which can measure the capacitances of the PIN diodes, a different structure which allows the individual characterization of the diodes has been designed as shown in Figure 4.18 (a) and Figure 4.18 (b).

This time 8 stages of PIN diode-loaded SRR (*i.e.,* a total of 16 SRRs) have been employed. However, the most crucial property of this design which distinguishes it from the previous four-stage filter is that each SRR particle can be turned on and off independently from all the others. This is accomplished through the use of two single-pole single-throw (SPST) switch arrays as depicted

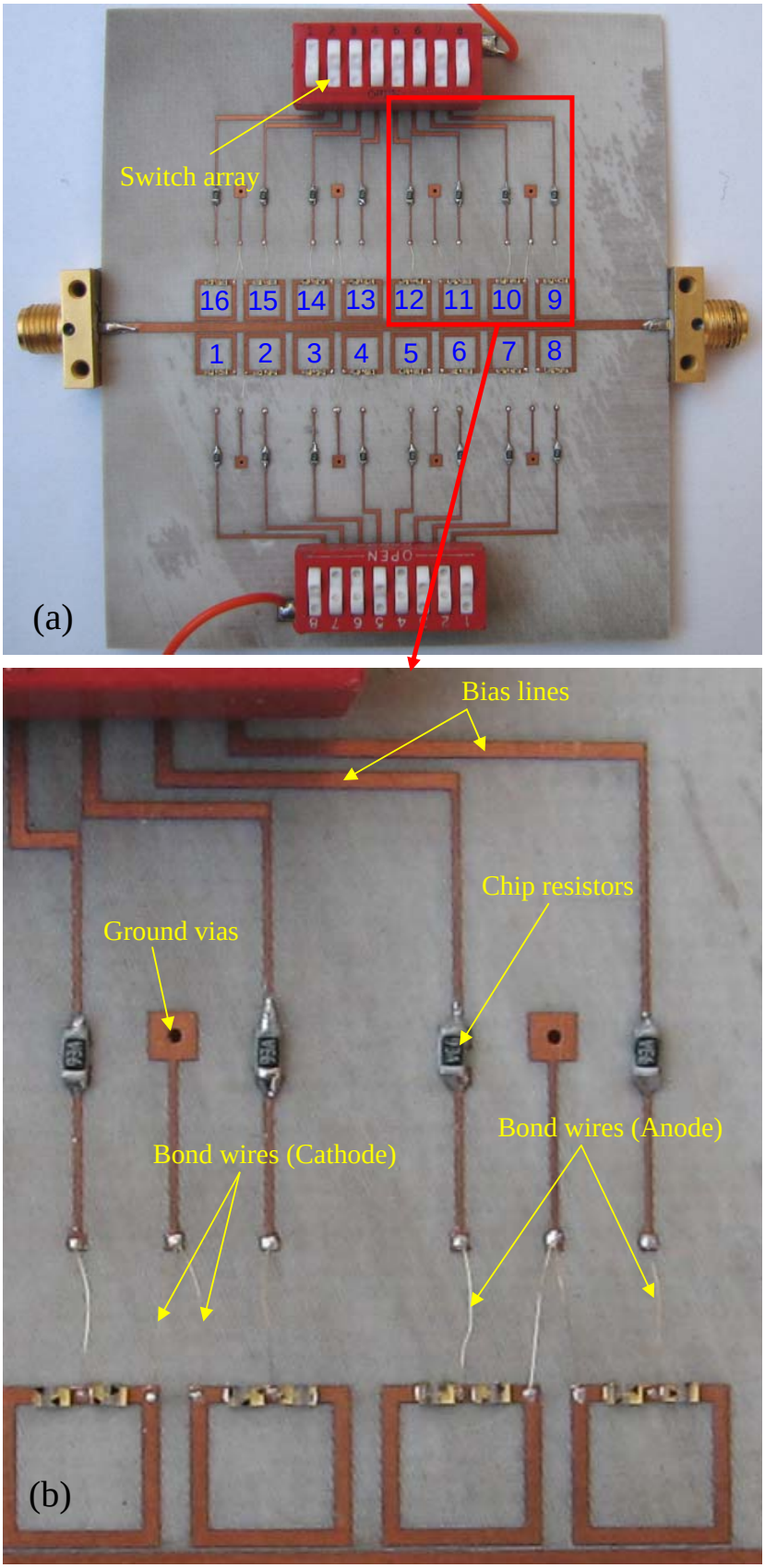

Figure 4.18: Fabricated eight-stage PIN diode-loaded SRR-based band-reject filter

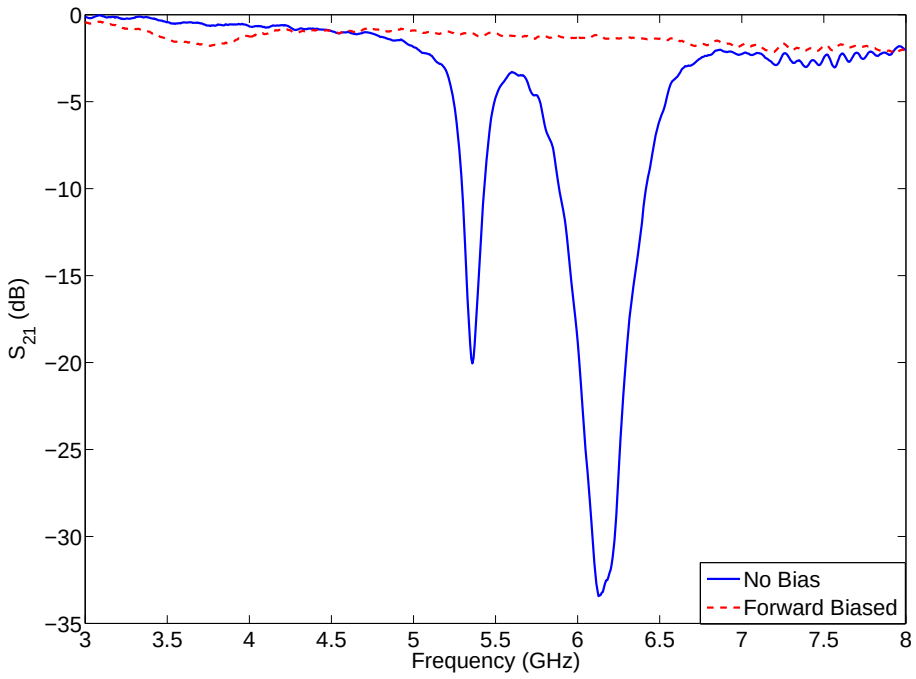

Figure 4.19: Measured insertion loss responses for eight-stage PIN diode-loaded band-reject filter for forward-bias (dashed) and no-bias (solid) cases

in Figure 4.18 (a). Each switch array accommodates 8 independent SPST switches. Therefore, a total of 16 switches provide independent bias current paths for each SRR particle. When an arbitrary switch is closed, the PIN diodes of the associated SRR particle are forward biased and the magnetic response of this SRR is removed. Hence, the filter will behave as if this SRR were not there at all. Keeping one of the switches open and all the others closed, the frequency response of an individual SRR unit can be determined.

Considering the possibility of high current levels that might be drawn from the DC supply by 32 PIN diodes, separate limiting resistors have been employed for each SRR unit. Configurations of bond wires and DC bias paths are identical to those explained in previous section. The details of the design can be seen from the magnified image in Figure 4.18 (b).

Initially, the insertion loss response of the filter has been tested for the cases when all diodes are under no bias and when all of them are forward biased. These

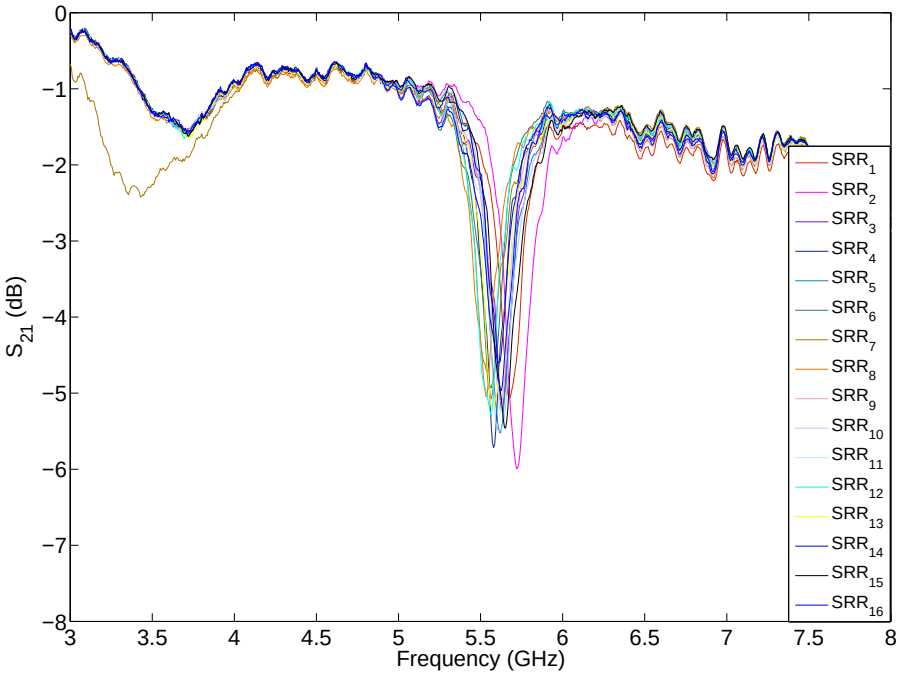

Figure 4.20: Insertion loss responses due to the individual SRRs of the eight-stage filter

responses are plotted in Figure 4.19. It is seen that when all of the switches are open and no bias current is passed through the diodes, a wide rejection band and two deep rejection notches are displayed just as in the case of four-stage filter (solid line). Although the transition edges of the rejection band are very sharp, the nonuniformity in the suppression level reduces the usefulness of the filter. However, the suppression of this band is stronger than the case of four-stage filter. As expected, the filter acts as a well-matched microstrip line with low insertion loss when all switches are closed and all diodes are forward biased (dashed line).

The configuration explained above allows the observation of the effect of each SRR unit on the overall filter response. By measuring the resonance frequency of each individual SRR, the diodes with similar junction capacitances can be discriminated.

Table 4.1: Individual resonant frequencies for the SRRs of the eight-stage filter

SRR Label	1	2	3	4	5	6	7	8
Frequency (GHz)	5.673	5.720	5.633	5.579	5.619	5.566	5.566	5.539
SRR Label	9	10	11	12	13	14	15	16
Frequency (GHz)	5.617	5.610	5.613	5.566	5.573	5.613	5.653	5.626

Using this approach, each SRR in the current filter has been switched one-by-one and their contributions to the overall insertion loss response have been measured. These responses are presented in Figure 4.20. Due to the big crowd of SRR units, individual frequency responses are not clearly seen from this plot. Therefore, a tabular representation of individual resonance frequencies (*i.e.,* the frequencies with strongest attenuation) of the SRRs is also provided in Table 4.1. In the legend of Figure 4.20 and in Table 4.1, the SRR particles are referred to according to the labels given in Figure 4.18 (a). It is observed that the variations in diode capacitances cause individual SRRs to resonate at different frequencies ranging from 5.56 GHz to 5.72 GHz. The inhomogeneity of the PIN diode-loaded SRR units results in the widened rejection band and quite nonuniform in-band response of the filter.

The aim of individual characterization of SRR particles given in Table 4.1 is, to some extent, to categorize the PIN diodes based on their capacitances. If the SRRs having resonances close to 5.58 GHz are considered, those labeled as 1, 2, 3, 15, and 16 in Figure 4.18 (a) can be said to have diodes with intolerable capacitance variations. Therefore, these PIN diodes must be avoided if a filter with a narrow and deep rejection band is desired, that is, the switches associated with these SRR units must be closed so that a bias current flows and their magnetic responses are eliminated. These PIN diodes and associated SRR units will be useless for the rest of this design.

Figure 4.21 demonstrates the insertion loss of the filter when the switches of SRRs labeled as 4, 5, 6, 7, 8, 9, 10, 11, 12, and 13 are open and the rest are

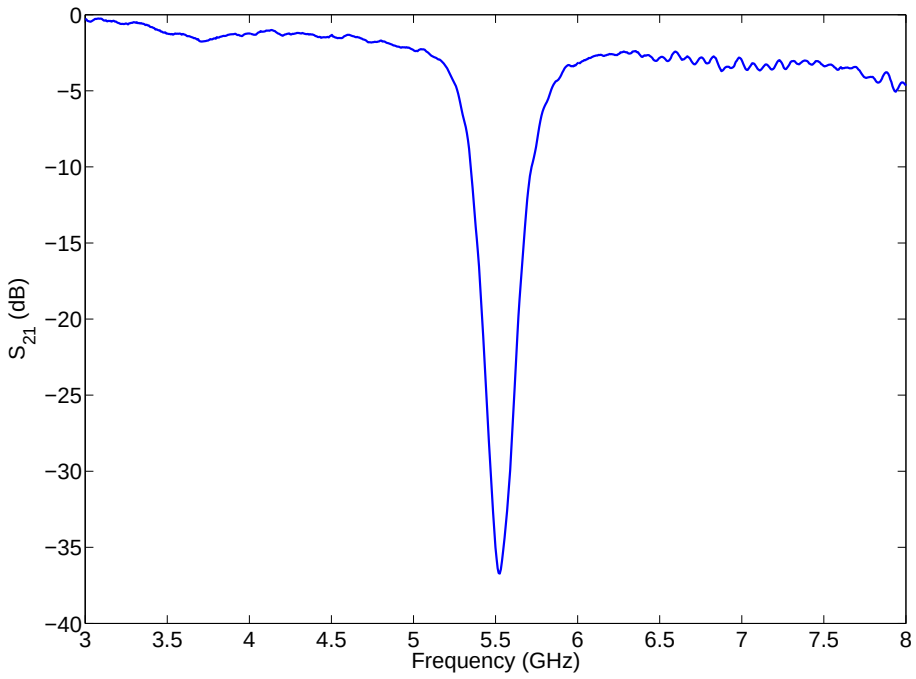

Figure 4.21: Overall insertion loss response of SRRs with close resonant frequencies

closed. It is observed that a narrow rejection band with a single transmission dip is displayed in the frequency response. Furthermore, the rejection level of this configuration, which reaches about 37 dB, is much stronger than all previously observed responses. The center frequency of the rejection band is about 5.55 GHz. This is expected because only the magnetic responses of SRRs with resonant frequencies close to 5.58 GHz are exploited. Consequently, a band-reject filter with strong suppression and good frequency selectivity is obtained.

Although the design procedure seems a little bit peculiar and some SRRs and diodes seem to be wasted, this result is important in that it demonstrates the possibility of the designs of electronically switchable filters with good frequency selectivities if the characteristics of the PIN diodes are precisely determined before fabrication. Alternatively, diodes with guaranteed low manufacturing tolerances can be preferred.

Chapter 5

Conclusions

In this thesis, two types of sub-wavelength resonators, namely split-ring resonator (SRR) and its dual complementary split-ring resonator (CSRR); in particular, their applications to microstrip band-reject filters have been studied extensively. These structures have been recently attracting the attention of many researchers as they provide high-Q and good frequency-selective characteristics in compact dimensions.

In Chapter 3, microstrip band-reject filters based on both SRRs and CSRRs using the same ring dimensions and the same substrates have been fabricated and their performances have been tested and compared. Good agreement has been achieved between numerical and experimental results. It has been observed that SRRs and CSRRs of the same geometry and sizes yield resonances around nearly the same center frequency. Frequency responses reveal that filters of both types exhibit very sharp transitions between the passband and stopband which shows their high-Q characteristics. However, much wider rejection bands and deeper rejection levels of CSRR-based filters attract attention. This difference is believed to be a consequence of the enhanced electric coupling between the microstrip line and the rings in the CSRR-based configuration. The resonators in both of these

two designs have dimensions in the order of one-eleventh of the wavelength at their resonant frequencies. Moreover, these filter structures are fully planar. Therefore, they can easily be fabricated using planar circuit technologies, such as mechanical and photo etching techniques. This feature enables the design of very compact, promising devices for printed-circuit board (PCB) and in even more compact dimensions for monolithic microwave integrated circuit (MMIC) technologies. Especially, in the case of CSRR, the resonators are placed on the ground plane; therefore, no extra circuit area needs to be allocated and even more compactness can be accomplished. The differences between the SRR- and CSRR-based filters in terms of their bandwidths and rejection capabilities can make them preferable for different applications.

In Chapter 4, electronically switchable SRR concept has been introduced for the first time. The proposed structure is obtained by loading SRRs' slits with microwave PIN diodes. Some modifications have been made on the conventional SRR to make it appropriate for use with PIN diodes. Based on the designed SRR structure, single- and multi-stage electronically switchable band-reject filter prototypes have been fabricated, tested, and also simulated. Good agreement has been achieved between the numerical and experimental results. It has been demonstrated that the rejection bands of these filters can be removed when a forward-bias current is passed through the PIN diodes by eliminating the magnetic responses of the SRRs. Also, it has been shown that the shape of the rejection band of these structures depends significantly on the characteristics of the diodes. By proper choice of PIN diodes, filters with good frequency selectivity and deep rejection bands can be designed.

This work pioneers the designs where rejection bands due to magnetic response and negative effective μ bands are desired to be switched electronically. As a future work, it can be extended to the designs of filters with wide and uniform rejection band. Also, by employing SRRs at different resonant

frequencies, designs of switched multiplexers can be achieved. Moreover, by combining these negative-μ structures with negative-ϵ ones, electronically controllable left-handed materials can be designed.

Appendix A

RO4003C High-Frequency Laminate Datasheet

ROGERS CORPORATION

Advanced Circuit Materials

Advanced Circuit Materials Division
100 S. Roosevelt Avenue
Chandler, AZ 85226
Tel: 480-961-1382, Fax: 480-961-4533
www.rogerscorporation.com

Data Sheet

RO4000® Series High Frequency Circuit Materials

Features:

- Not-PTFE
- Excellent high frequency performance due to low dielectric tolerance and loss
- Stable electrical properties versus frequency
- Low thermal coefficient of dielectric constant
- Low Z-Axis expansion
- Low in-plane expansion coefficient
- Excellent dimensional stability
- Volume manufacturing process

Some Typical Applications:

- LNB's for Direct Broadcast Satellites
- Microstrip and Cellular Base Station Antennas and Power Amplifiers
- Spread Spectrum Communications Systems
- RF Identifications Tags

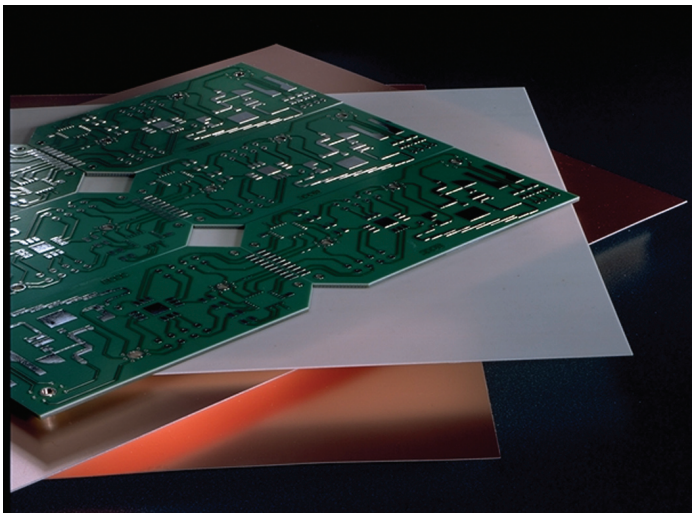

RO4000® Series High Frequency Circuit Materials are glass reinforced hydrocarbon/ceramic laminates (**Not PTFE**) designed for performance sensitive, high volume commercial applications.

RO4000 laminates are designed to offer superior high frequency performance and low cost circuit fabrication. The result is a low loss material which can be fabricated using standard epoxy/glass (FR4) processes offered at competitive prices.

The selection of laminates typically available to designers is significantly reduced once operational frequencies increase to 500 MHz and above. RO4000 material possesses the properties needed by designers of RF microwave circuits and allows for repeatable design of filters, matching networks and controlled impedance transmission lines. Low dielectric loss allows RO4000 series material to be used in many applications where higher operating frequencies limit the use of conventional circuit board laminates. The temperature coefficient of dielectric constant is among the lowest of any circuit board material (Chart 1), and the dielectric constant is stable over a broad frequency range (Chart 2). This makes it an ideal substrate for broadband applications.

RO4000 material's thermal coefficient of expansion (CTE) provides several key benefits to the circuit designer. The expansion coefficient of RO4000 material is similar to that of copper which allows the material to exhibit excellent dimensional stability, a property needed for mixed dielectric multilayer boards constructions. The low Z-axis CTE of RO4000 laminates provides reliable plated through-hole quality, even in severe thermal shock applications. RO4000 series material has a Tg of >280°C (536°F) so its expansion characteristics remain stable over the entire range of circuit processing temperatures.

RO4000 series laminates can easily be fabricated into printed circuit boards using standard FR4 circuit board processing techniques. Unlike PTFE based high performance materials, RO4000 series laminates do not require specialized via preparation processes such as sodium etch. This material is a rigid, thermoset laminate that is capable of being processed by automated handling systems and scrubbing equipment used for copper surface preparation.

RO4003™ laminates are currently offered in various configurations utilizing both 1080 and 1674 glass fabric styles, with all configurations meeting the same laminate electrical performance specification. Specifically designed as a drop-in replacement for the RO4350 material, RO4350B laminates utilize RoHS compliant flame-retardant technology for applications requiring UL 94V-0 certification. These materials conform to the requirements of IPC-4103, slash sheet /10 for RO4003C and /11 for RO4350B.

Chart 1: RO4000 Series Materials
Dielectric Constant vs. Temperature

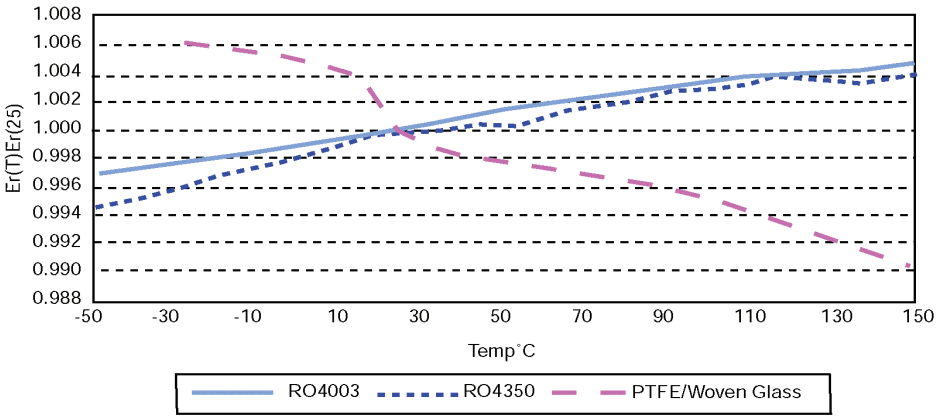

Chart 2: RO4000 Series Materials
Dielectric Constant vs. Frequency

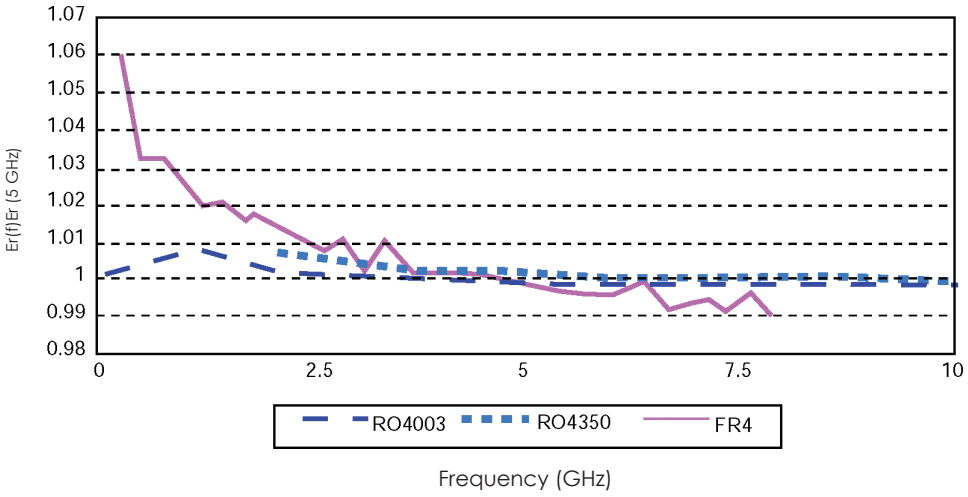

Chart 3: Microstrip Insertion Loss
(0.030" Dielectric Thickness)

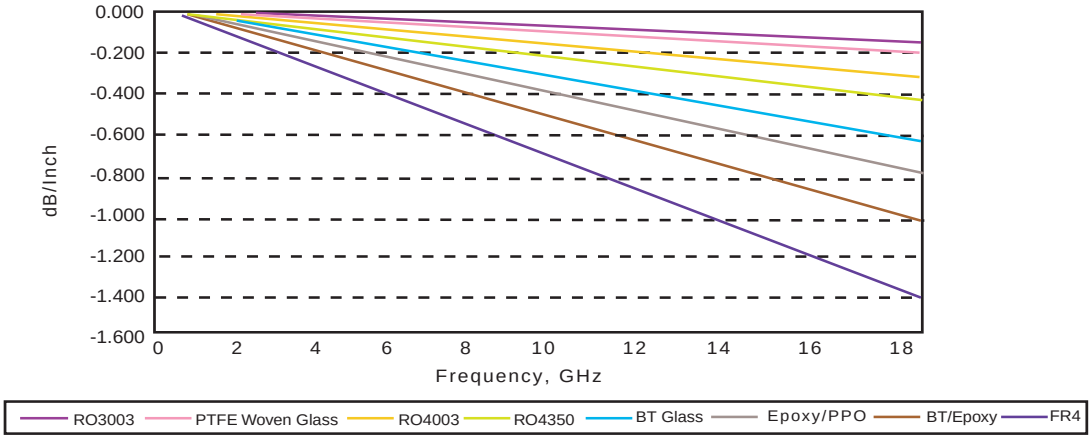

Property	Typical Value		Direction	Units	Condition	Test Method
	RO4003C™	RO4350B™				
Dielectric Constant, ε_r (Process specification)	3.38 ± 0.05	(1) 3.48 ± 0.05	Z	--	10 GHz/23°C	IPC-TM-650 2.5.5.5 (2)Clamped Stripline
(3) Dielectric Constant, ε_r (Recommended for use in circuit design)	3.55	3.66	Z	--	FSR/23°C	IPC-TM-650 2.5.5.6 Full Sheet Resonance
Dissipation Factor tan, δ	0.0027 0.0021	0.0037 0.0031	Z	--	10 GHz/23°C 2.5 GHz/23°C	IPC-TM-650 2.5.5.5
Thermal Coefficient of ε_r	+40	+50	Z	ppm/°C	-100°C to 250°C	IPC-TM-650 2.5.5.5
Volume Resistivity	1.7 X 10^{10}	1.2 X 10^{10}		MΩ•cm	COND A	IPC-TM-650 2.5.17.1
Surface Resistivity	4.2 X 10^{9}	5.7 X 10^{9}		MΩ	COND A	IPC-TM-650 2.5.17.1
Electrical Strength	31.2 (780)	31.2 (780)	Z	KV/mm (V/mil)	0.51mm (0.020")	IPC-TM-650 2.5.6.2
Tensile Modulus	26,889 (3900)	11,473 (1664)	Y	MPa (kpsi)	RT	ASTM D638
Tensile Strength	141 (20.4)	175 (25.4)	Y	MPa (kpsi)	RT	ASTM D638
Flexural Strength	276 (40)	255 (37)		MPa (kpsi)		IPC-TM-650 2.4.4
Dimensional Stability	<0.3	<0.5	X,Y	mm/m (mils/inch)	after etch +E2/150°C	IPC-TM-650 2.4.39A
Coefficient of Thermal Expansion	11 14 46	14 16 35	X Y Z	ppm/°C	-55 to 288°C	IPC-TM-650 2.1.41
Tg	>280	>280		°C DSC	A	IPC-TM-650 2.4.24
Td	425	390		°C TGA		ASTM D3850
Thermal Conductivity	0.64	0.62		W/m/°K	100°C	ASTM F433
Moisture Absorption	0.06	0.06		%	48 hrs immersion 0.060" sample Temperature 50°C	ASTM D570
Density	1.79	1.86		gm/cm^3	23°C	ASTM D792
Copper Peel Strength	1.05 (6.0)	0.88 (5.0)		N/mm (pli)	after solder float 1 oz. EDC Foil	IPC-TM-650 2.4.8
Flammability	N/A	94V-0				UL
Lead-Free Process Compatible	Yes	Yes				

(1) Dielectric constant typical value does not apply to 0.004" (0.101mm) laminates. Dielectric constant specification value for 0.004 RO4350B material is 3.36.
(2) Clamped stripline method can potentially lower the actual dielectric constant due to presence of airgap. Dielectric constant in practice may be higher than the values listed.
(3) Typical values are a representation of an average value for the population of the property. For specification values contact Rogers Corporation.

Prolonged exposure in an oxidative environment may cause changes to the dielectric properties of hydrocarbon based materials. The rate of change increases at higher temperatures and is highly dependent on the circuit design. Although Rogers' high frequency materials have been used successfully in innumerable applications and reports of oxidation resulting in performance problems are extremely rare, Rogers recommends that the customer evaluate each material and design combination to determine fitness for use over the entire life of the end product.

Standard Thickness	Standard Panel Size	Standard Copper Cladding
RO4003C: 0.008" (0.203mm), 0.012 (0.305mm), 0.016" (0.406mm), 0.020" (0.508mm) 0.032" (0.813mm), 0.060" (1.524mm) **RO4350B**: *0.004" (0.101mm), 0.0066" (0.168mm) 0.010" (0.254mm), 0.0133 (0.338mm), 0.0166 (0.422mm), 0.020" (0.508mm) 0.030" (0.762mm), 0.060" (1.524mm)	12" X 18" (305 X457 mm) 24" X 18" (610 X 457 mm) 24" X 36" (610 X 915 mm) 48" X 36" (1.224 m X 915 mm) *0. 004" material in not available in panel sizes larger than 24"x18" (610 X 457mm).	½ oz. (17μm), 1 oz. (35μm) and 2 oz. (70μm) electrodeposited copper foil.

Fabrication Guidelines for RO4000® Series High Frequency Circuit Materials

RO4000® High Frequency Circuit Materials were developed to provide high frequency performance comparable to woven glass PTFE substrates with the ease of fabrication associated with epoxy/glass laminates. RO4000 material is a glass reinforced hydrocarbon/ceramic filled thermoset material with a very high glass transition temperature (Tg >280°C). Unlike PTFE based microwave materials, no special through-hole treatments or handling procedures are required. Therefore, RO4000 material circuit processing and assembly costs are comparable to epoxy/glass laminates.

Some basic guidelines for processing double sided RO4000 panels are provided below. In general, process parameters and procedures used for epoxy/glass boards can be used to process RO4000 boards.

DRILLING:

ENTRY/EXIT MATERIAL:

Entry and exit materials should be flat and rigid to minimize copper burrs. Recommended entry materials include aluminum and rigid composite board (0.010" to 0.025" (0.254 0.635mm)). Most conventional exit materials with or without aluminum cladding are suitable.

MAXIMUM STACK HEIGHT:

The thickness of material being drilled should not be greater than 70% of the flute length. This includes the thickness of entry material and penetration into the backer material.
For example:

Flute Length:	0.300" (7.62mm)
Entry Material:	0.015" (0.381mm)
Backer Penetration:	0.030" (0.762mm)
Material Thickness:	0.020" (0.508mm)⇒(0.023"(0.584mm) with 1 oz Cu on 2 sides)

Maximum Stack Height = 0.70 x 0.300"(7.62mm) = 0.210" (5.33mm) (available flute length)
-0.015" (0.381mm) (entry)
-0.030" (0.762mm) (backer penetration)
0.165"(4.19mm) (available for PCBs)

$$\text{Maximum Boards per Stack} = \frac{0.165" \text{ (4.19mm) (available for PCBs)}}{0.023" \text{ (0.58mm) (thickness per board)}} = 7.2 = 7 \text{ boards/stack (round down)}$$

DRILLING CONDITIONS:

Surface speeds greater than 500 SFM and chip loads less than 0.002" (0.05mm) should be avoided, whenever possible.

Recommended Ranges:

Surface Speed:	300 - 500 SFM (90 to 150 m/mm)
Chip Load:	0.002" - 0.004"/rev. (0.05-0.10 mm/rev)
Retract Rate:	500 - 1000 IPM 500 IPM (12.7 m/min) for tool less than 0.0135" (0.343 mm),1000 IPM (25.4 m/min) for all others.
Tool Type:	Standard Carbide
Tool life:	2000-3000 hits

Hole quality should be used to determine the effective tool life rather than tool wear. The RO4003™ material will yield good hole quality when drilled with bits which are considered worn by epoxy/glass standards. Unlike epoxy/glass, RO4003 material hole roughness does not increase significantly with tool wear. Typical values range from 8-25 um regardless of hit count (evaluated up to 8000 hits). The roughness is directly related to the ceramic filler size and provides topography that is beneficial for hole-wall adhesion. Drilling conditions used for epoxy/glass boards have been found to yield good hole quality with hit counts in excess of 2000.

CALCULATING SPINDLE SPEED AND INFEED:

$$\text{Spindle Speed (RPM)} = \frac{12 \times [\text{Surface Speed (SFM)}]}{\pi \times [\text{Tool Diam. (in.)}]}$$

Feed Rate (IPM) = [Spindle Speed (RPM)] x [Chip Load (in/rev.)]

Example:

Desired Surface Speed:	400 SFM
Desired Chip Load:	0.003"(0.08 mm)/rev.
Tool Diameter:	0.0295"(0.75 mm)

$$\text{Spindle Speed} = \frac{12 \times [400]}{3.14 \times [0.0295]} = 51{,}800 \text{ RPM}$$

Infeed Rate = [51,800] x [0.003] = 155 IPM

***QUICK REFERENCE TABLE*:**

Tool Diameter	Spindle Speed (kRPM)	Infeed Rate (IPM)
0.0100" (0.254mm)*	95.5	190
0.0135" (0.343mm)*	70.7	141
0.0160" (0.406mm)*	95.5	190
0.0197" (0.500mm)*	77.6	190
0.0256" (0.650mm)	60.0	180
0.0258" (0.655mm)	60.0	180
0.0295" (0.749mm)	51.8	155
0.0354" (0.899mm)	43.2	130
0.0394" (1.001mm)	38.8	116
0.0453" (1.151mm)	33.7	101
0.0492" (1.257mm)	31.1	93
0.0531" (1.349mm)	28.8	86
0.0625" (1.588mm)	24.5	74
0.0925" (2.350mm)	16.5	50
0.1250" (3.175mm)	15.0	45

* *Conditions stated are tapered from 200SFM and 0.002 chip load up to 400 SFM and 0.003" chip.*

DEBURRING:

RO4000 material can be deburred using conventional nylon brush scrubbers.

COPPER PLATING:

No special treatments are required prior to electroless copper plating. Board should be processed using conventional epoxy/glass procedures. Desmear of drilled holes is not typically required, as the high Tg (280°C+ [536°F]) resin system is not prone to smearing during drill. Resin can be removed using a standard CF4/O2 plasma cycle or a double pass through an alkaline permanganate process should smear result from aggressive drilling practices.

IMAGING/ETCHING:

Panel surfaces may be mechanically and/or chemically prepared for photoresist. Standard aqueous or semi-aqueous photoresists are recommended. Any of the commercially available copper etchants can be used.

SOLDERMASK:

Any screenable or photoimageable solder masks typically used on epoxy/glass laminates bond very well to the surface of RO4003. Mechanical scrubbing of the exposed dielectric surface prior to solder mask application should be avoided as an "as etched" surface provides for optimum bonding.

HASL and REFLOW:

RO4000 material baking requirements are comparable to epoxy/glass. In general, facilities which do not bake epoxy/glass boards will not need to bake RO4000 boards. For facilities that do bake epoxy/glass as part of their normal process, we recommend at 1-2 hour bake at 250°F-300°F (121°C-149°C).

Warning: RO4003 *does not contain fire retardant(s). We understand boards trapped in an infrared (IR) unit or run at very slow conveyor speeds can reach temperatures well in excess of 700°F (371°C). RO4003 may begin to burn at these high temperatures. Facilities which still use IR reflow units or other equipment which can reach these high temperatures should take the necessary precautions to assure that there are no hazards.*

SHELF LIFE:

Rogers' High Frequency laminates can be stored indefinitely under ambient room temperatures (55-85°F, 13-30°C) and humidity levels. At room temperature, the dielectric materials are inert to high humidity. However, metal claddings such as copper can be oxidized during exposure to high humidity. Standard PWB pre-exposure cleaning procedures can readily remove traces of corrosion from properly stored materials.

ROUTING:

RO4000 material can be machined using carbide tools and conditions typically used for epoxy/glass. Copper foil should be etched away from the routing channels to prevent burring.

MAXIMUM STACK HEIGHT:

The maximum stack height should be based on 70% of the actual flute length to allow for debris removal.

Example:

Flute Length:	0.300" x 0.70 =		0.210"(5.33 mm)
Backer Penetration:		–	0.030"(0.762mm)
Max. Stack Height:			0.180"(4.572mm)

TOOL TYPE:

Carbide multifluted spiral chip breakers or diamond cut router bits.

ROUTING CONDITIONS:

Surface speeds below 500 SFM should be used whenever possible to maximize tool life. Tool life is generally greater than 50 linear feet when routing the maximum allowable stack height.

Chip Load:	0.0010-0.0015"(0.0254-0.0381mm)/rev
Surface Speed:	300 - SFM

QUICK REFERENCE TABLE:

Tool Diameter	Spindle Speed	Lateral Feed Rate
1/32	40 k RPM	50 IPM
1/16	25 k RPM	31 IPM
3/32	20 k RPM	25 IPM
1/8	15 k RPM	19 IPM

World Class Performance

Rogers Corporation (NYSE:ROG), headquartered in Rogers, Conn., is a global technology leader in the development and manufacture of high performance, specialty material-based products for a variety of applications in diverse markets including: portable communications, communications infrastructure, computer and office equipment, consumer products, ground transportation, aerospace and defense. In an ever-changing world, where product design and manufacturing often take place on different sides of the planet, Rogers has the global reach to meet customer needs. Rogers operates facilities in the United States, Europe and Asia. The world runs better with Rogers.®

CONTACT INFORMATION:

USA:	Rogers Advanced Circuit Materials, ISO 9002 Certified	Tel: 480-961-1382	Fax: 480-917-5256
Belgium:	Rogers N.V. - Gent	Tel: +32-9-2353611	Fax: +32-9-2353658
Japan:	Rogers Japan Inc.	Tel: 81-3-5200-2700	Fax: 81-3-5200-0571
Taiwan:	Rogers Taiwan Inc.	Tel: 886-2-86609056	Fax: 886-2-86609057
Korea:	Rogers Korea Inc.	Tel: 82-31-716-6112	Fax: 82-31-716-6208
Singapore:	Rogers Technologies Singapore Inc.	Tel: 65-747-3521	Fax: 65-747-7425
China:	Rogers (Shanghai)	Tel: 86-21-63916088	Fax: 86-21-63915060
China:	Rogers (Shenzhen)	Tel: 86-755-8236 6060	Fax: 86-755-8236 6123

Revised 11/02/2007-1107-0.5CC
Publication #92-004

Appendix B

MPP4204-206 PIN Diode Datasheet

75 Technology Drive
Lowell, MA 01851
PH: (978) 442-5600
FAX: (978) 937-3748

MPP4201 - MPP4204
MPL4700
MPV1965
MPV2100

MONOLITHIC MICROWAVE SURFACE MOUNT MICRO-PAK PIN AND VARACTOR DIODES

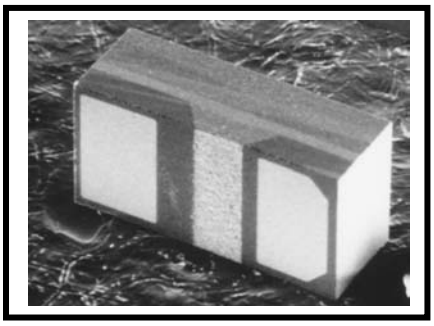

Features:

- Tape and Reeled for Automatic Assembly
- Low Series Inductance (<0.2nH typical)
- Low Parasitic Capacitance (0.06 pf typical)
- Optimized for PCS products
- Meets All Commercial Qualification Requirements
- 0204 Outline
- Very low thermal resistance

Description:

This series of surface mount PIN and Varactor diodes utilize new and unique monolithic MMSM technology. The technology is a package/device integration accomplished at the wafer fabrication level. Since the cathode and anode interconnections utilize precision photolithographic techniques rather than wire bonds, parasitic package inductance is tightly controlled. The package parasitics provide smooth non-resonant functionality through 12 GHz.

ELECTRICAL CHARACTERISTICS

Part #	Vb @10uA (min) Volts	Ct@10V pf	Rs @ .01mA Ohms	Rs @ 1mA Ohms	Rs @ 10mA Ohms	Rs @ 20mA Ohms	TL (typ) Nsec	Outline	APPLICATION
MPP4201	70	0.20				2.5	150	206	High Power Switch
MPP4202	50	0.15				2.8	50	206	Magnetic Resonance Imaging
MPP4203	50	0.10				3.0	50	206	High Isolation Switch and Attenuator
MPP4204	25	0.15			2.0		30	206	High Speed Switch
MPP4205	70	0.15	250	7-16	5.0		150	206	Attenuator
MPL4700	25	0.15		2.0	2.0		10	206	Amplifier Protection

Part #	Vb@10uA (min) (volts)	Ct @1V (pf)	Ct 1V/ Ct 3V (pf)	Ct 1V/ Ct 6V (pf)	Q (min/4v/ 50MHz)	Outline Dwg Number	APPLICATION
MPV1965	15	2.6-3.8	1.4-2.2	2.6-3.6	1500	206	Low Voltage VCO
Part #	**Vb@10uA (min) (volts)**	**Ct@4V (pf)**	**Ct @ 0V (typ) (pf)**	**Ct @ 20V (pf)**	**Q (min/4v/ 50MHz)**	**Outline Dwg Number**	**APPLICATION**
MPV2100	22	0.9-1.5	3.25	0.2-0.5	1500	206	Wide Bandwidth VCO

DIMENSIONS

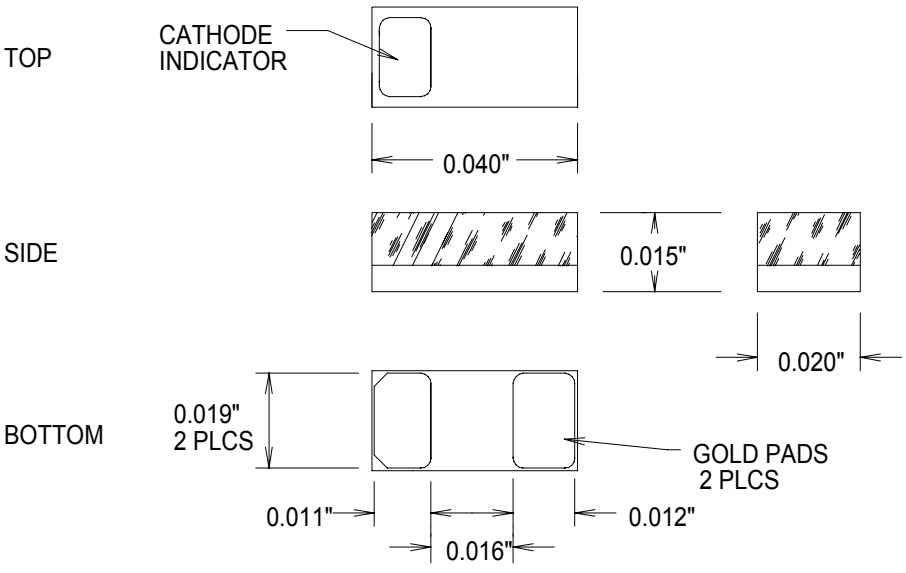

ALL DIMENSION TOLERANCES ARE +- .002"

Bibliography

[1] D.M. Pozar, *Microwave Engineering*. John & Wiley Sons, New York, 1998.

[2] J.-S. Hong and M.J. Lancaster, *Microstrip Filters for RF/Microwave Applications*. John & Wiley Sons, New York, 2001.

[3] D.K. Cheng, *Field and Wave Electromagnetics*. Addison-Wesley, California, 1983.

[4] J.B. Pendry, A.J. Holden, D.J. Robbins, and W.J. Stewart, "Magnetism from Conductors and Enhanced Nonlinear Phenomena," *IEEE Trans. Microwave Theory Tech.*, vol. 47, no. 11, pp. 2075–2084, 1999.

[5] F. Falcone, T. Lopetegi, J.D. Baena, R. Marqués, F. Martín, and M. Sorolla, "Effective Negative-ϵ Stopband Microstrip Lines Based on Complementary Split-Ring Resonators," *IEEE Microwave Wireless Comp. Lett.*, vol. 14, no. 6, pp. 280–282, 2004.

[6] V.G. Veselago, "The Electrodynamics of Substances with Simultaneously Negative Values of ϵ and μ," *Sov. Phys. Uspekhi*, vol. 10, pp. 509–514, 1968.

[7] D.R. Smith, W.J. Padilla, D.C. Vier, S.C. Nemat-Nasser, and S. Schultz, "Composite Medium with Simultaneously Negative Permeability and Permittivity," *Phys. Rev. Lett.*, vol. 84, pp. 4184–4187, 2000.

[8] R.A. Shelby, D.R. Smith, S.C. Nemat-Nasser, and S. Schultz, "Microwave Transmission Through a Two-Dimensional, Isotropic, Left-Handed Metamaterial," *Appl. Phys. Lett.*, vol. 78, pp. 489–491, 2001.

[9] M. Bayindir, K. Aydin, E. Ozbay, P. Markos, and M. Soukoulis, "Transmission Properties of Composite Metamaterials in Free Space," *Appl. Phys. Lett.*, vol. 81, pp. 120–122, 2002.

[10] E. Ozbay, K. Aydin, E. Cubukcu, and M. Bayindir, "Transmission and Reflection Properties of Composite Double Negative Metamaterials in Free-Space," *IEEE Trans. Antennas Propag.*, vol. 51, pp. 2592–2595, 2003.

[11] R. Marqués, F. Mesa, J. Martel, and F. Medina, "Comparative Analysis of Edge- and Broadside-Coupled Split-ring Resonators for Metamaterial Design - Theory and Experiments," *IEEE Trans. Antennas Propagat.*, vol. 51, no. 10, pp. 2572–2581, 2003.

[12] R. Marqués, J. Martel, F. Mesa, and F. Medina, "Left-Handed Media Simulation and Transmission of EM Waves in Subwavelength Split-Ring-Resonator-Loaded Metallic Waveguides," *Phys. Rev. Lett.*, vol. 89, no. 18, 183901, 2002.

[13] S. Hrabar, J. Bartolic, and Z. Sipus, "Waveguide Miniaturization Using Uniaxial Negative Permeability Metamaterial," *IEEE Trans. Antennas Propagat.*, vol. 53, no. 1, pp. 110–119, 2005.

[14] J. Esteban, C. Camacho-Penalosa, J.E. Page, T.M. Martin-Guerrero, and E. Marquez-Segura, "Simulation of Negative Permittivity and Negative Permeability by Means of Evanescent Waveguide Modes - Theory and Experiment," *IEEE Trans. Microwave Theory Tech.*, vol. 53, no. 4, pp. 1506–1514, 2005.

[15] J.B. Pendry, A.J. Holden, W.J. Stewart, and I. Youngs, "Extremely Low-Frequency Plasmons in Metallic Mesostructures," *Phys. Rev. Lett.*, vol. 76, pp. 4773–4776, 1996.

[16] J.B. Pendry, A.J. Holden, D.J. Robbins, and W.J. Stewart, "Low-Frequency Plasmons in Thin-Wire Structures," *J. Phys. Condens. Matter*, vol. 10, pp. 4785–4809, 1998.

[17] T. Koschny, M. Kafesaki, E. N. Economou, and C. M. Soukoulis, "Effective Medium Theory of Left-Handed Materials," *Phys. Rev. Lett.*, vol. 93, no. 10, 107402, 2004.

[18] K. Aydin, K.Guven, M. Kafesaki, L. Zhang, C.M. Soukoulis, and E. Ozbay, "Experimental Observation of True Left-Handed Transmission Peaks in Metamaterials," *Optics Lett.*, vol. 29, no. 22, pp. 2623–2625, 2004.

[19] N. Katsarakis, T. Koschny, M. Kafesaki, E. N. Economou, and C. M. Soukoulis, "Electric Coupling to the Magnetic Resonance of Split-Ring Resonators," *Appl. Phys. Lett.*, vol. 84, no. 15, pp. 2943–2945, 2004.

[20] F. Martín, F. Falcone, J. Bonache, R. Marqués, and M. Sorolla, "Miniaturized Coplanar Waveguide Stop Band Filters Based on Multiple Tuned Split Ring Resonators," *IEEE Microwave Wireless Comp. Lett.*, vol. 13, no. 12, pp. 511–513, 2003.

[21] F. Falcone, F. Martín, J. Bonache, R. Marqués, and M. Sorolla, "Coplanar Waveguide Structures Loaded with Split-Ring Resonators," *Microwave and Opt. Tech. Lett.*, vol. 40, no. 1, pp. 3–6, 2004.

[22] F. Falcone, F. Martín, J. Bonache, R. Marqués, T. Lopetegi, and M. Sorolla, "Left-Handed Coplanar Waveguide Band Pass Filters Based on Bi-Layer Split Ring Resonators," *IEEE Microwave Wireless Comp. Lett.*, vol. 14, no. 1, pp. 10–12, 2004.

[23] J. García-García, J. Bonache, I. Gil, F. Martín, R. Marqués, F. Falcone, T. Lopetegi, M.A.G. Laso, and M. Sorolla, "Comparison of Electromagnetic Band Gap and Split-Ring Resonator Microstrip Lines as Stop Band Structures," *Microwave and Opt. Tech. Lett.*, vol. 44, no. 4, pp. 376–379, 2005.

[24] J. García-García, F. Martín, F. Falcone, J.D. Baena, I. Gil, E. Amat, T. Lopetegi, M.A.G. Laso, J.A.M. Iturmendi, M. Sorolla, and R. Marqués, "Microwave Filters with Improved Stopband Based on Sub-Wavelength Resonators," *IEEE Trans. Microwave Theory Tech.*, vol. 53, no. 6, pp. 1997–2006, 2005.

[25] J. García-García, F. Martín, F. Falcone, J. Bonache, I. Gil, T. Lopetegi, M.A.G. Laso, M. Sorolla, and R. Marqués, "Spurious Passband Suppression in Microstrip Coupled Line Band Pass Filters by Means of Split Ring Resonators," *IEEE Microwave Wireless Comp. Lett.*, vol. 14, no. 9, pp. 416–418, 2004.

[26] J.D. Baena, J. Bonache, F. Martín, R. M. Sillero, F. Falcone, T. Lopetegi, M.A.G. Laso, J. García-García, I. Gil, M.F. Portillo, and M. Sorolla, "Equivalent-Circuit Models for Split-Ring Resonators and Complementary Split-Ring Resonators Coupled to Planar Transmission Lines," *IEEE Trans. Microwave Theory Tech.*, vol. 53, no. 4, pp. 1451–1461, 2005.

[27] I. Gil, J. Bonache, J. García-García, F. Falcone, and F. Martín, "Metamaterials in Microstrip Technology for Filter Applications," *IEEE Antennas and Propagation Society International Symposium*, vol. 1A, pp. 668–671, 2005.

[28] I. Gil, J. Bonache, J. García-García, and F. Martín, "Tunable Metamaterial Transmission Lines Based on Varactor-Loaded Split-Ring Resonators," *IEEE Trans. Microwave Theory Tech.*, vol. 54, no. 6, pp. 2665–2674, 2006.

[29] Y. Yablonovitch, "Photonic Bandgap Structures," *J. Opt. Soc. Amer. B.*, vol. 10, pp. 283–295, 1993.

[30] F. Falcone, *Synthesis and applications of microwave metamaterials in planar circuit technology: From electromagnetic bandgaps to left handed materials,* PhD dissertation, Public University of Navarre Dept. of Electrical and Electronics Engineering, Navarre, Spain, 2005.

[31] F.R. Yang, K.P. Ma, Y. Qian, and T. Itoh, "A Uniplanar Compact Photonic-Bandgap (UC-PBG) Structure and Its Applications for Microwave Circuits," *IEEE Trans. Microwave Theory Tech.*, vol. 47, pp. 1509, 1999.

[32] S.N. Burokur, M. Latrach, and S. Toutain, "Study of the Effect of Dielectric Split-Ring Resonators on Microstrip-Line Transmission," *Microwave and Opt. Tech. Lett.*, vol. 44, no. 5, pp. 445–448, 2005.

[33] F. Falcone, T. Lopetegi, M.A.G. Laso, J.D. Baena, J. Bonache, M. Beruete, R. Marqués, F. Martín, and M. Sorolla, "Babinet Principle Applied to the Design of Metasurfaces and Metamaterials," *Phys. Rev. Lett.*, vol. 93, no. 19, pp. 197401, 2004.

[34] J. Bonache, F. Martín, J.D. Baena, T. Lopetegui, J. García-García, M.A.G. Laso,I. Gil, A. Marcotegui, R. Marqués, and M. Sorolla, "Application of Complementary Split-Ring Resonators to the Design of Compact Narrow Band-Pass Structures in Microstrip Technology," *Microwave and Opt. Tech. Lett.*, vol. 46, no. 5, pp. 508–512, 2005.

[35] J. Bonache, I. Gil, J. García-García, and F. Martín "Novel Microstrip Bandpass Filters Based on Complementary Split-Ring Resonators," *IEEE Trans. Microwave Theory Tech.*, vol. 54, no. 1, pp. 265–271, 2006.

[36] V. Öznazlı and V.B. Ertürk, "A Comparative Investigation of SRR- and CSRR-Based Band-Reject Filters: Simulations, Experiments, and

Discussions," *Microwave and Opt. Tech. Lett.*, vol. 50, no. 2, pp. 519–523, 2008.

[37] I. Gil, J. García-García, J. Bonache, F. Martín, and R. Marqués, "Varactor-Loaded Split Ring Resonators for Tunable Notch Filters at Microwave Frequencies," *Electron. Lett.*, vol. 40, no. 21, 2004.

[38] A. Vélez, J. Bonache, and F. Martín, "Varactor-Loaded Complementary Split Ring Resonators (VLCSRR) and Their Application to Tunable Metamaterial Transmission Lines," *IEEE Microwave Wireless Comp. Lett.*, vol. 18, no. 1, pp. 28–30, 2008.

[39] C.G. Hwang and N.H. Myung, "An Oscillator with Low Phase Noise and Superior Harmonic Suppression Characteristics Based on Uniplanar Compact Split Ring Resonators," *Microwave and Opt. Tech. Lett.*, vol. 48, no. 5, pp. 938–940, 2006.

[40] J. Choi and C. Seo, "Broadband VCO Using Electronically Controlled Metamaterial Transmission Line Based on Varactor-Loaded Split-Ring Resonator," *Microwave and Opt. Tech. Lett.*, vol. 50, no. 4, pp. 1078–1082, 2008.

[41] RO4003C High Frequency Laminate Datasheet - http://www.rogerscorporation.com/mwu/pdf/RO4000data_ fab_ 10_ 07.pdf, Rogers Corporation, Chandler, AZ.

[42] Application Notes on RF and PIN Diodes - http://www.microsemi.com/micnotes/701.pdf, Microsemi Corporation, Irvine, CA.

[43] MPP4204 PIN Diode Datasheet - http://www.microsemi.com/datasheets/mmsm%207%20041.pdf, Microsemi Corporation, Irvine, CA.

[44] Ansoft Designer(TM) v2.0 - http://www.ansoft.com/products/hf/ansoft_ designer, Ansoft Corporation, Pittsburgh, PA.

[45] Ansoft High Frequency Structure Simulator, Ansoft HFSS(TM) v9.2.1 - http://www.ansoft.com/products/hf/hfss, Ansoft Corporation, Pittsburgh, PA.